Visualització sísmica mitjançant tècniques tomogràfiques

Isaac Flecha Lacalle

Visualització sísmica mitjançant tècniques tomogràfiques

Isaac Flecha Lacalle

Director: Ramon Carbonell i Bertran
Institut Jaume Almera (CSIC)

Programa: Ciències de la Terra
Bieni: 2001/2003

Agraïments

Una tesi doctoral és un treball ampli i elaborat en que hi intervé tot un conjunt de persones que, en més o menys grau, fan possible que aquest treball es pugui dur a terme. El meu cas no és cap excepció i ara que enllesteixo aquesta tasca crec que és un bon moment per recapitular i agraïr la seva col·laboració a tots els que d'una manera o altra han estat partíceps del treball que tens entre les mans.

Per començar voldria donar les gràcies als meus pares, sempre em van motivar per tirar endevant amb els estudis i em van recolzar en els moments que calia, malgrat que en molts casos no entenguèssin ni perquè estudiava el que estudiava ni per a que serviria, aquest treball té un dels seus pilars en la vostra paciència i comprensió. També vull donar les gràcies al meu germà Ruben, ell també ha tingut molta paciència com a germà i com a amic, i en certs moments m'ha ajudat aportant el seu punt de vista estrictament matemàtic.

En els meus inicis en això de la geofísica vaig tenir l'oportunitat de treballar a l'àrea de geologia de l'Institut Cartogràfic de Catalunya. Guardo molt bon record d'aquella època i en general de tot el personal amb qui vaig conviure, de totes maneres voldria fer una menció especial a les tres persones amb qui més directament vaig treballar a l'àrea de geofísica aplicada. En geofísica, una part important és l'adquisició de dades, sovint, els petits detalls són els que determinen la qualitat de les dades i en aquest sentit en Pere Valls em va ensenyar el que cal saber per fer treball de camp. A la Teresa Teixidó, peculiar com ningú, li haig d'agraïr bona part del poc que sé de sísmica, va ser ella la que em va despertar l'interès per aquesta branca de la física i la que en certa manera em va obrir les portes al doctorat. En aquest sentit podria dir que ella és la meva "mare científica". També agraïr la confiança d'en Pere Martínez, que era l'encarregat de posar ordre en l'aparent caos de l'àrea de geofísica aplicada.

Si hi ha una "mare científica" també hi ha "pare científic" i aquest és en Ramon Carbonell, el meu director. A tu et dec aquesta tesi doctoral. Resumir en quatre línies tot el que has fet per mi seria demanar massa, de totes maneres voldria donar-te les gràcies per confiar en mi i animar-me en moments delicats, la veritat és que el teu il·limitat optimisme i la teva capacitat de treball són contagioses i aconsegueixes il·lusionar a la gent que t'envolta. Sempre has buscat el millor per als teus estudiants i has fet el possible perquè ens obrim pas en el món científic, sovint a batzegades, però sempre pensant en nosaltres. Si has estat bon director, crec que encara ets millor persona, sempre has tingut molt clar que darrera de cada estudiant hi ha una persona i has obrat en conseqüència. Vull que sàpigues que sempre tindré un record especial d'aquesta etapa de la meva vida, ha estat un plaer aprendre al teu costat, gràcies per tot.

A Andrés Pèrez le tengo que agradecer su preocupación por los estudiantes, gracias

también por tus comentarios, correcciones y valoraciones y por hacer de la geologia una novela interesante y comprensible para los profanos como yo.

En la meva peregrinació per l'Institut Jaume Almera he tingut oportunitat de compartir molts moments agradables amb molta gent. Al departament de geofísica i tectònica voldria recordar al David, el meu predecessor, per aconsellar-me en els meus inicis i ensenyar-me a veure les coses des d'un punt de vista pràctic, al Rafa per la seva paciència davant les meves insistents preguntes sobre Linux, al Mario que també va tenir la seva part en aquella tasca tot i que amb el temps l'alumne ha superat al mestre (je,je) gràcies per aguantar-me en general, al Manu per aportar la seva visió com a geòleg i per *fer pinya* per afrontar la vida a la capital penedesenca, a la Leire pel seu indomable esperit, al Javier per les disquisicions sobre el mon de la ciència, a l'Oriol per aportar un toc rural al departament, al Martin per estar sempre disponible a resoldre qualsevol dubte, a la Imma per estar sempre disponible a plantejar qualsevol dubte, al Sergio, una màquina programant llàstima que t'hagis equivocat de s.o., a la Bea una màquina preguntant. També vull mostrar la meva gratitud a companys/es i excompanys/es de despatx amb els quals he compartit el dia a dia: vull recordar al Percha i els seus coneixements sobre material multimedia, al Sergio per la seva actitud i hospitalitat, a la Natàlia, la reina mare, per mantenir un bon ambient al despatx, a la Mar per les nostres converses sobre la vida en general, al Tobias per aportar la visió pragmàtica de les coses, al Miguel, sempre disposat a provocar, a la Mari Cruz, sempre disposada a respondre les provocacions, al Madriles per les seves constants visites i a la Mapi i al Jorge per aguantar tot aquest enrenou amb bon humor. Al Josep Elvira li haig d'agraïr els seus coneixements d'un s.o. "de cuyo nombre no quiero acordarme" i al Ramón Cuscó per resoldre alguns dubtes sobre programació en C. A l'Amèlia, al Xavi i a la Pepi per la seva simpatia i en general a tot el personal científic i administratiu de l'Institut per la seva col·laboració.

A Hermann Zeyen por su rigor (plenamente justificado) en las correcciones y por sus comentarios siempre constructivos. A Fernando Simancas por compartir sus conocimientos sobre la geología ibérica. To Immo Trinks for the training in the use of TTT. To Richard Hobbs for providing useful ideas and interensting, fun and non-conventional points of view about some issues, thank you and your family for a very warm welcome in such a cold castle.

La major part d'aquest treball s'ha dut a terme utilitzant software lliure, desde el mateix sistema operatiu fins als programes d'inversió tomogràfica passant per l'editor de text i els programes per generar imatges. Voldria reconèixer aqui la tasca que han dut a terme els desenvolupadors d'aquest software i en general la comunitat del software lliure, persones que, sovint desinteressadament, fan possible que aquestes eines estiguin disponibles per al públic.

Tampoc vull oblidar a la Gemma Guilera per la seva amabilitat en un moment tan important i per proporcionar material per la portada d'aquesta tesis.

No puc acabar sense esmentar a la Natàlia que és qui més mereix la meva gratitud. Sempre m'has recolzat en tots el projectes en que m'he embrancat (per esbojarrats que semblin) i aquesta tesi no ha estat cap excepció. Si estic enllestint aquest treball és principalment gràcies a tú. Amiga, confessora i amant, has estat al meu costat per gaudir en els moments feliços, per patir en els moments difícils i per aguantar-me sempre. Fa un temps em vas portar la Clara i després el Guillem, dues meravelles que juntament amb tú fan que tingui una família fantàstica. Moltes gràcies per fer la vida tan fàcil, gràcies de tot cor.

ÍNDEX

ÍNDEX DE FIGURES

ÍNDEX DE TAULES

1. INTRODUCCIÓ

El coneixement del subsòl sempre ha estat objecte d'interès per part de l'home. Per una banda és en els primers metres de la superfície terrestre on es desenvolupa la major part de l'activitat humana però també d'on s'extreuen bona part dels recursos que proporciona la natura (minerals, aigua, hidrocarburs ...). L'obra civil, el disseny d'infraestructures o la gestió de residus perillosos són exemples d'activitats per a les quals és fonamental un coneixement previ i acurat del medi, tant per dur a terme possibles actuacions com per a preveure'n les conseqüències. Per altra banda també cal conèixer l'escorça terrestre en fondària, no només per el seu interès científic i acadèmic sinó perquè molts aspectes que s'observen en superfície com ara el relleu, la distribució de jaciments minerals, el vulcanisme o la sismicitat troben la seva explicació en l'estructura a gran escala de l'escorça terrestre.

La forma més eficient per obtenir informació del subsòl de forma indirecta és mitjançant tècniques de prospecció geofísica. Aquestes tècniques són mètodes no destructius, cosa que fa molt útil la seva utilització en estudis superficials on és prioritari no alterar la zona d'estudi. Per als estudis profunds no només són útils, sinó que es pot dir que aquestes tècniques són gairebé les úniques disponibles, ja que els sondejos mecànics, tot i que proporcionen informació molt detallada, només la proporcionen en el punt concret on s'ha emplaçat el sondeig, fent difícil la extrapolació lateral de la informació, i a més impliquen un cost econòmic molt elevat. Els mètodes de prospecció geofísica es basen en els mateixos principis físics independentment de les peculiaritats de la zona d'estudi i de la fondària que vulguem assolir, això sí, depenent del nostre objectiu hi hauran factors que variaran enormement d'un cas a un altre com ara els paràmetres d'adquisició, el dispositiu experimental i fins i tot la instrumentació a utilitzar.

En aquest treball es tracten diverses aplicacions d'un d'aquests mètodes, a saber, la tomografia sísmica. Així doncs, en aquest treball es presenten diferents estudis duts a terme a diferents escales i en diferents condicions geològiques. A priori, es podria pensar que els cinc estudis que conformen el cos d'aquest treball no tenen cap interconnexió degut a que no tracten la mateixa zona, ni el mateix context geològic i ni tan sols l'escala dels treballs és la mateixa, de totes maneres, en tots ells s'ha utilitzat com a eina fonamental la tomografia sísmica, esdevenint així el fil conductor d'aquesta tesis. Mitjançant aquesta

tècnica obtindrem un model de velocitats del subsòl, cosa que per ella mateixa ja proporciona informació valuosa. També es pot utilitzar la tomografia sísmica com a punt de partida per a la implementació d'altres tècniques més sofisticades que requereixen d'un control exhaustiu de les velocitats en el medi, com poden ser correccions estàtiques o migracions en fondària. Per aplicar tècniques tomogràfiques es poden dissenyar experiments específics, però un dels grans avantatges d'aquesta metodologia és que la podem utilitzar en qualsevol conjunt de dades sísmiques, en particular en dades sísmiques d'incidència vertical i en dades de gran angle. En aquest treball s'han fet servir també en alguns casos dades de sísmica de reflexió que han proporcionat informació complementària de gran utilitat per determinar l'estructura de la zona d'estudi.

Els capítols que integren aquesta tesis representen cinc estudis diferents que, malgrat la seva rellevància a nivell teòric, en la majoria dels casos responen a qüestions pràctiques plantejades en l'àmbit de la prospecció sísmica. Per tant els resultats obtinguts i les conclusions que se n'extreuen es poden considerar d'interès tant des d'un punt de vista acadèmic com industrial.

1.1 Simulacions sintètiques

En quatre dels cinc estudis desenvolupats, s'han utilitzat en més o menys grau simulacions sintètiques. El fet de treballar amb dades sintètiques presenta un seguit d'avantatges:

- Rapidesa: en poques hores i des del despatx es poden simular conjunts de dades que en la realitat trigarien dies a ser adquirits.

- Flexibilitat en l'implementació: es té una gran flexibilitat per a dissenyar el dispositiu experimental, geòfons i fonts es poden situar en qualsevol punt del model.

- Control de les dades: en tot moment es pot determinar la qualitat de les dades i es poden modificar fàcilment paràmetres propis del senyal com ara la freqüència, el tipus de font, l'interval de mostreig i el soroll.

- Costos reduïts: avui en dia qualsevol ordinador capaç de realitzar aquesta tasca és, com a mínim, varis ordres de magnitud més econòmic que l'adquisició real d'un perfil de sísmica.

Malgrat això, treballar amb sismogrames sintètics no està absent de limitacions. Per començar estem suposant que les dades que hem creat són equivalents a unes dades reals, per tant implícitament suposem que els algoritmes que utilitzem per crear-les poden reproduir exactament el comportament de la natura, cosa que no és del tot certa per què el

propi fet de matematitzar el problema ja representa una aproximació a la realitat. A més en els casos aquí tractats, s'ha treballat amb dades creades sobre un model bidimensional, fet que només possibilita una visió parcial del problema, ja que a la realitat el subsòl sempre és tridimensional.

Sovint és molt útil realitzar simulacions sintètiques prèvies a un experiment real per tal de discriminar dispositius experimentals poc favorables o poc resolutius. De totes maneres no és recomanable treure de context el significat dels resultats obtinguts amb simulacions numèriques, ja que difícilment podrem assegurar l'èxit rotund d'un experiment basant-nos en tests sintètics, doncs sempre la natura té la última paraula. Cal tenir present que en un problema real les millors condicions experimentals que es poden donar són, de lluny, pitjors que qualsevol experiment sintètic. Les condicions climàtiques, les limitacions dels instruments d'adquisició, l'orografia del terreny o la presència de soroll ambiental són efectes molt difícils de neutralitzar que de ben segur quedaran reflectits en la qualitat de les dades. Tot i així, un balanç dels pros i els contres d'aquesta forma de procedir, la fa recomanable com ho demostra el fet de que actualment la simulació numèrica sigui una pràctica àmpliament extesa en molts àmbits de la ciència.

En la generació de dades sintètiques s'han utilitzat dos softwares diferents depenent de l'aproximació escollida: acústica o elàstica. Per al cas acústic s'ha utilitzat un programa integrat en el paquet de processat Seismic Unix (SU) de Colorado School of Mines que resol la propagació d'ones acústiques en 2D via diferències finites, en canvi per al cas elàstic s'ha fet servir un codi propi, que també utilitza diferències finites i que està basat en els treballs de Sochacki et al., 1987; Sochacki et al., 1991 i Zahradnik et al., 1994.

1.2 Metodologia: tomografia sísmica

La tomografia sísmica es va començar a desenvolupar a meitat dels anys 70 quan es va plantejar la necessitat d'obtenir imatges en 3D que establissin la distribució de velocitats de l'interior de la terra, va ser llavors quan van aparèixer les primeres publicacions sobre el tema (Aki et al., 1974; Aki and Lee, 1976; Aki et al., 1976; Aki et al., 1977). Els bons resultats aconseguits amb la tomografia de raigs X (tomografia radiològica) en l'àmbit de la medicina van ser el precedent sobre el que es van basar les primeres experiències de tomografia sísmica. Malgrat els punts en comú amb la tomografia radiològica, hi han característiques pròpies de la sismologia (com ara la curvatura dels raigs) que fan que el problema esdevingui més complex matemàticament parlant. Tot i així des de principis dels anys 80 molts autors van dedicar els seus esforços en aquest sentit (Paige and Saunders, 1982; McMehan, 1983; Clayton and Comer, 1983; Nolet, 1983; Neumann-Denzau and Behrens, 1984), desenvolupant algoritmes que, amb més o menys modificacions, són

Material	Velocitat
Gres	2000 m/s
Calcària	3000 m/s
Lutita	2400 m/s
Sorra saturada	2500 m/s
Aigua	1500 m/s
Aire	360 m/s
Guix	5800 m/s
Marga	2700 m/s
Argila	2000 m/s
Dolomia	4000 m/s
Granit	5500 m/s
Basalt	5300 m/s

Table 1.1: *Velocitats típiques dels materials més comuns*

els que s'estan utilitzant actualment. En les inversions tomogràfiques s'acostuma a tractar amb una quantitat de dades respectable, per tant des d'un principi les necessitats computacionals van representar una restricció important sobre les possibilitats reals del processat. Malgrat tot, en els darrers anys l'electrònica ha posat a l'abast del públic màquines d'una capacitat considerable amb uns costos assequibles, raó per la qual la utilització d'aquesta tècnica s'està estenent cada cop més en l'àmbit de la prospecció geofísica.

La velocitat a que les ones mecàniques es propaguen a través d'un cos és una propietat intrínseca de cada material, per tant en base a aquest paràmetre podrem identificar diferents litologies. A la taula 1.1 mostrem alguns dels valors per als materials que trobem habitualment. La identificació velocitat-material no sempre és directa, hi ha materials que presenten velocitats molt similars i que no podrem discriminar amb els resultats obtinguts en la tomografia. A més a més, la velocitat típica d'un material pot variar substancialment segons l'estat en que es trobi, així la fracturació, la compactació o la saturació modifiquen notablement els valors que considerem estàndards. A mode d'exemple podem citar un treball de Martí et al., 2002 on en un experiment tomogràfic sobre granits s'han trobat per aquesta roca velocitats de 4500 m/s, lluny del valor típic per aquest material i que ha estat associat a l'estat de fracturació de la roca. Degut a aquest ventall de possibles interpretacions, en molts casos un coneixement geològic de la zona es fa imprescindible per tal de discriminar entre possibles solucions.

Com ja s'ha comentat previament, la tomografia sísmica té per objectiu trobar un

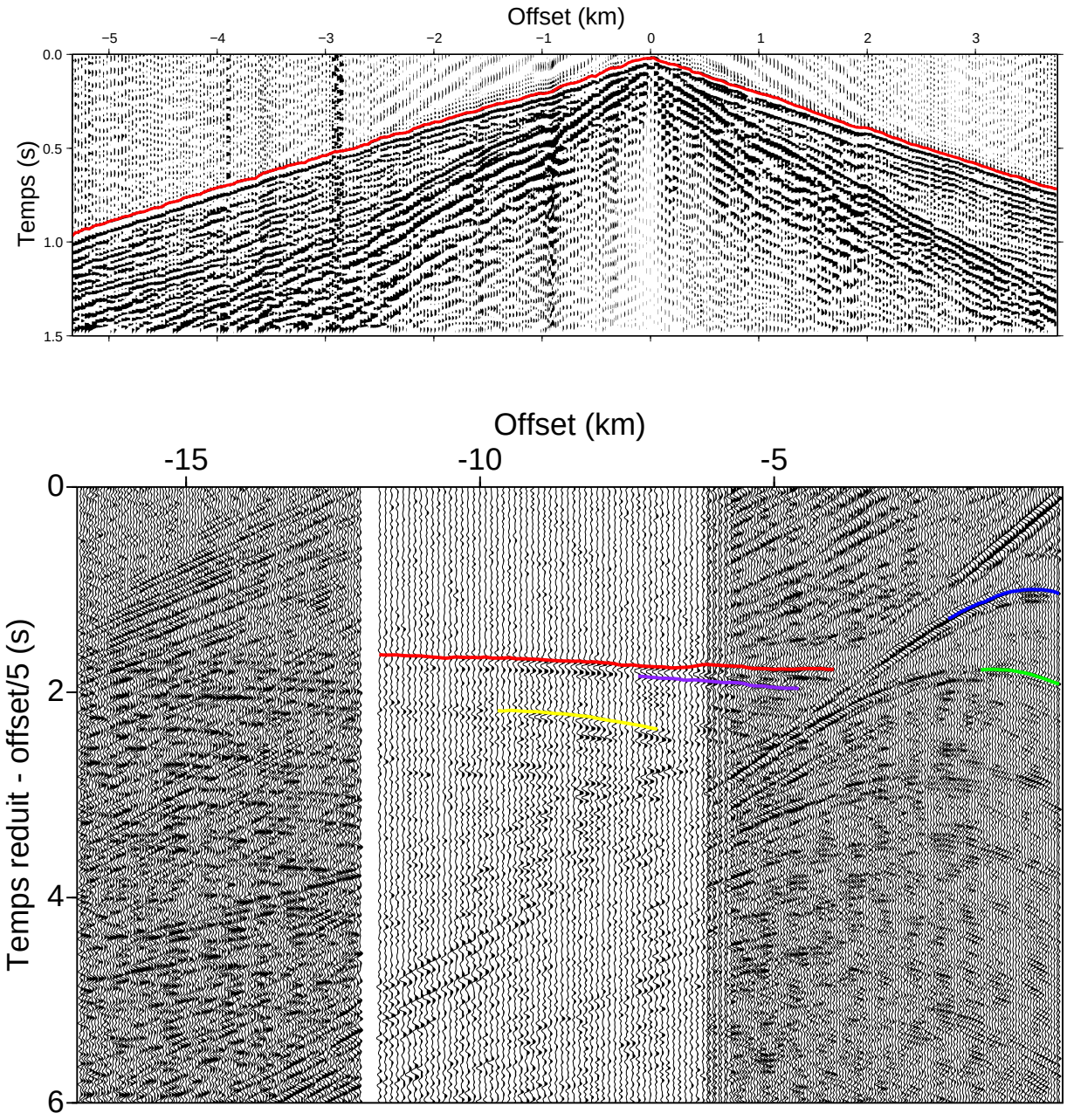

Fig. 1.1: *Exemple de dades sísmiques. A la part superior s'observen dades adquirides sobre el plutó granític de la Bazana i on es poden identificar clarament les primeres arribades (vermell). A la part inferior s'observen dades adquirides a la conca Faroe-Shetland i on es poden identificar diferents fases: reflexió del fons marí (blau), reflexió a la part superior del basalt (verd), refracció del basalt (vermell), reflexió de la base del basalt (lila) i reflexió de la part superior del basament (groc). Mentre que en les dades de la part superior la identificació de la primera arribada és clara i no es fa cap interpretació addicional, a les dades de la part inferior, el fet d'etiquetar i identificar cada fase amb una estructura geològica introdueix una interpretació subjectiva que en certs casos podria portar a resultats incorrectes.*

model de velocitats del subsòl, tenint com a dades les localitzacions de les fonts i dels receptors i els temps de viatge de les ones sísmiques entre unes i altres.

En sismologia, els terratrèmols representen una font d'energia gens menyspreable tant per la seva magnitud com per la seva abundància, de fet les primeres aplicacions de la tomografia sísmica es van fer utilitzant gran quantitat d'aquest tipus de dades. El problema que trobem en aquest cas és que no coneixem la localització exacta de les fonts, per tant això introdueix una font d'error important que es veu reflectida en una incertesa en el temps de viatge, en aquests casos els programes utilitzats acostumen a incorporar rutines de relocalització dels epicentres per tal de minimitzar aquest efecte.

En totes les aplicacions que aquí es presenten només tractarem amb dades de sísmica activa, per tant les fonts i els receptors estaran completament controlats pel que fa a la seva posició en l'espai i en el temps. Un altre aspecte important que cal considerar és l'escala d'estudi, en el sentit de que aquesta ens imposarà restriccions importants sobre el disseny de l'experiment i sobre el tipus de tomografia sísmica més adient per tractar el problema. Així, normalment, per estudis superficials (diguem entre 0 i 1500 m de fondària) només utilitzarem les primeres arribades de les ones P ja que, habitualment, les primeres capes del terreny exhibeixen una gran heterogeneitat cosa que dificulta la identificació d'altres fases. En canvi per estudis més profunds (nivell cortical) podrem utilitzar informació d'altres fases. Aquesta diferència és important i introdueix un grau de subjectivitat no menyspreable en el cas d'estudis profunds. En la major part de dades sísmiques d'una qualitat raonable és fàcil determinar unívocament la primera arribada per a un percentatge molt elevat de les traces de cada dispar. En aquest cas, la inversió de primeres arribades no comporta cap interpretació previa i per tant el resultat del càlcul matemàtic ens donarà un model simplement condicionat per les dades. En el cas de dades de sísmica profunda, a més de les primeres arribades, es poden identificar altres events coherents que reflecteixen discontinuïtats a l'escorça cosa que aporta informació addicional per a tractar el problema. El fet d'etiquetar diferents fases com corresponents a diferents events ens introdueix un element subjectiu previ al càlcul matemàtic: la nostra pròpia interpretació. En molts casos, el coneixement de la geologia de la zona i el fet de tractar amb estructures relativament simples fa que aquesta interpretació *a priori* sigui raonable i ens porti a resultats coherents. De totes maneres si la geologia implicada presenta dificultats (geometria complexa, inversió de velocitats...), la interpretació *a priori* pot portar-nos a identificacions errònies i en conseqüència a resultats incorrectes.

Resumint, la tomografia de primeres arribades és més limitada en quant a obtenir resultats ja que només aprofita una petita part de tota la informació continguda en una traça sísmica, però aquests són independents de cap interpretació previa. En canvi, en incloure d'altres fases en el processat, el model obtingut pot delimitar millor les estructures

i aportar una informació més completa, però els resultats obtinguts poden incorporar un cert grau de subjectivitat de l'interpretador. A la figura 1.1 es mostra un exemple dels dos tipus de dades.

La tomografia com a tal no deixa de ser un mot específic que s'ha adoptat per referir-se a la solució del problema invers en el món de la sísmica. La tomografia és la solució d'un problema invers no lineal. Així, la solució d'un problema tomogràfic es pot dividir en dues parts clarament diferenciades: el problema directe i el problema invers. Els quals tractarem de forma separada.

1.2.1 Problema directe

El problema directe consisteix en obtenir unes dades donats uns paràmetres coneguts. En el cas que ens ocupa, els paràmetres seran la localització de fonts $\vec{r}_f$ i de receptors $\vec{r}_r$ i un model de velocitats concret $v(\vec{r})$, i les dades a obtenir seran els temps de viatge t_{fr} entre fonts i receptors. La solució d'aquest problema passa per una discretització del model de velocitats conegut. Per aquest propòsit dividirem la zona d'estudi segons es tracti d'un problema 2D/3D en cel·les quadrades/cúbiques (cas de diferències finites) o elements triangulars/tetraèdrics (cas d'elements finits). A cada cel·la o element hi associarem una velocitat.

El tipus d'algoritme utilitzat per a resoldre aquest problema dependrà de si es treballarà només amb primeres arribades (problemes superficials) o bé s'inclouran altres fases obtingudes de les dades (problemes a més fondària). Per als casos profunds la discretització del model de velocitats es fa a base de capes de diferents velocitats, ja que les fases identificades correspondran a les refraccions en aquestes capes i a les reflexions en les seves interfícies. En aquest cas tradicionalment s'han utilitzat els anomenats *shooting methods* basats en la Llei d'Snell, ja que les reflexions i les refraccions a través de les diferents capes "forcen" als rajos a recórrer les parts del model que ens interessen. En el present estudi en concret s'ha utilitzat el software TTT (Trinks et al., 2005). Per als casos superficials com només s'utilitzen primeres arribades, els mètodes clàssics de traçat de rajos no obtenen bons resultats per models amb forts gradients de velocitat o amb inversions de velocitat, i per aquests casos en concret són relativament lents computacionalment parlant (Berryman, 1991). A més, les consideracions implícites de la llei d'Snell suggereixen que les anomalies de baixa velocitat no poden ser detectades només amb primeres arribades. Per tal d'evitar aquesta limitació tècnica s'han utilitzat dos paquets basats en dues variants de l'algoritme de Vidale per a la resolució de l'equació de l'eikonal en diferències finites (Vidale, 1988; Vidale, 1990). Aquests dos paquets són PSTOMO (Benz et al., 1996) basat en l'algoritme de Podvin and Lecomte, 1991 i FAST (Zelt and Barton, 1998) basat en l'algoritme de Hole and Zelt, 1995. Aquests algoritmes

estan basats en un esquema de diferències finites que calculen el temps de viatge per a qualsevol punt del model i no només aquells per on s'ha traçat un raig, per tant són més resolutius quan es treballa amb anomalies de baixa velocitat.

1.2.2 Problema invers

En el problema invers tenim una situació diferent, donats certs paràmetres (localització de fonts i receptors) i unes dades (temps de viatge) hem de trobar uns altres paràmetres (el model de velocitats).

En un problema genèric, el temps de viatge al llarg d'un raig serà funció de la geometria d'aquest raig i de la velocitat $v(\vec{r})$ del medi a través del qual viatja, el que hem de fer és deduir $v(\vec{r})$ a partir de les mesures de temps de viatge, així, per un parell font-receptor donat, el temps de viatge vindrà donat per:

$$T_i = \int_{S_i} \frac{ds}{v(\vec{r})} \tag{1.1}$$

on S_i és la trajectòria que segueix el raig. Aquest problema és complex ja que la incògnita $v(\vec{r})$ té una dependència amb la trajectòria del raig. Com es pot observar, aquest problema és clarament no lineal, per tant per poder tractar-lo haurem de linealitzar-lo. Per fer això considerem un model de velocitats conegut $v_0(\vec{r})$, per aquest cas podem calcular, via la resolució d'un problema directe, els temps de viatge i la trajectòria dels rajos:

$$T_i^0 = \int_{S_i^0} \frac{ds}{v_0(\vec{r})} \tag{1.2}$$

on S_i^0 és la trajectòria que segueix el raig per al model conegut. Definirem el temps de retard com:

$$\delta T_i = T_i - T_0 = \int_{S_i} \frac{ds}{v_0(\vec{r})} - \int_{S_i^0} \frac{ds}{v(\vec{r})} \approx \int_{S_i^0} \left(\frac{1}{v(\vec{r})} - \frac{1}{v_0(\vec{r})} \right) ds \tag{1.3}$$

d'on queda:

$$\delta T_i = - \int_{S_i^0} \frac{\delta v(\vec{r})}{v_0(\vec{r})^2} ds \tag{1.4}$$

on $\delta v(\vec{r}) = v(\vec{r}) - v_0(\vec{r})$. S'ha substituït la trajectòria real (desconeguda) per la trajectòria coneguda, cosa que en funció del principi de Fermat només introdueix errors de segon ordre en el càlcul de δT_i. D'aquesta manera s'aconsegueix linealitzar el problema, encara que aquesta aproximació estarà mancada de realisme si el model inicial $v_0(\vec{r})$ no es troba realment proper al model real, el qual desconeixem. El següent pas consisteix en parametritzar el model de manera que sigui tractable per a un ordinador. Definim:

$$h_i(\vec{r}) = \begin{cases} V_i^{-\frac{1}{2}} & \text{si } \vec{r} \text{ es troba a la cel.la i} \\ 0 & \text{en cas contrari} \end{cases}$$

Això s'escull així perquè exigirem que aquesta parametrització estigui normalitzada, és a dir:

$$\int_V h_i(\vec{r}) h_j(\vec{r}) d^3r = \delta_{ij} \tag{1.5}$$

Podem considerar aquestes funcions com una base en la que podem expressar $\delta v(\vec{r})$, així per un model amb M cel.les tindrem:

$$\delta v(\vec{r}) = \sum_{k=1}^{M} \gamma_k h_k(\vec{r}) \tag{1.6}$$

d'on deduïm que:

$$\gamma_k = \int_V \delta v(\vec{r}) h_k(\vec{r}) d^3r \tag{1.7}$$

que substituint a 1.4:

$$\delta T_i = \sum_{k=1}^{M} - \int_{S_i^0} \frac{1}{v_0(\vec{r})^2} \gamma_k h_k(\vec{r}) ds = \sum_{k=1}^{M} A_{ik} \gamma_k \tag{1.8}$$

on:

$$A_{ik} = - \int_{S_i^0} \frac{h_k(\vec{r})}{v_0(\vec{r})^2} ds$$

En resum, hem partit d'un problema clarament no lineal, i mitjançant diverses aproximacions s'arriba a l'expressió 1.8 que correspon a un sistema d'equacions lineals que en forma matricial es pot expressar com:

$$A\gamma = \delta T \tag{1.9}$$

En tomografia les dades que tractarem tindran els seus corresponents errors, a més normalment el nombre de dades supera al d'incògnites, per tant tindrem un sistema sobredeterminat i incompatible, la qual cosa significa que, en general, no existirà una solució exacta per al sistema 1.9. Arribats aquí, el que s'intenta no és ja resoldre el sistema, sino minimitzar la quantitat $\|A_{ik}\gamma_k - \delta T_i\|^2$. Cal dir que aquest no és un problema específic de la tomografia sísmica, en molts àmbits de les ciències experimentals s'han de resoldre problemes similars, cosa que ha portat al desenvolupament d'una gran quantitat d'algoritmes i variants d'aquests. Per una explicació detallada dels algoritmes que implementen

els paquets de software utilitzats en aquest treball es poden consultar les fonts originals de Paige and Saunders, 1982 i de Tarantola, 1987.

1.2.3 Procés iteratiu

Un cop sabem resoldre els problemes invers i directe podem plantejar una estratègia per obtenir la solució que busquem. Degut a la no linealitat intrínseca del problema haurem d'utilitzar un procés iteratiu. Partirem d'un model inicial $v_0(\vec{r})$ que convindrà que sigui el més acurat possible. Amb aquest model resoldrem el problema directe cosa que ens proporcionarà uns temps de viatge teòrics T_i^0 i amb això obtindrem el temps de retard δT_i^0. Llavors s'ha de resoldre el problema invers del qual obtindrem un model de velocitats $v_1(\vec{r})$. Amb aquest model resolem novament el problema directe i calculem el nou temps de retard δT_i^1, si aquesta quantitat és suficientment petita per als nostres propòsits podem aturar el procés, altrament es continuarà calculant un model $v_2(\vec{r})$, al que li correspondrà el seu δT_i^2 i així successivament fins que obtinguem la precisió desitjada o el procés convergeixi, és a dir, fins que, després de n iteracions la quantitat δT_i^n no es modifiqui apreciablement. Aquest procés iteratiu està esquematitzat a la figura 1.2.

1.3 Context geològic i geofísic

Com ja s'ha comentat, aquest treball no es limita a una zona d'estudi amb un geologia concreta. En els cinc capítols que conformen aquesta tesis, es consideren cinc situacions diferents amb la seva corresponent geologia en les quals s'ha aplicat d'una manera o una altra la tomografia sísmica. De totes maneres els casos tractats es poden classificar en tres contextos geològics: plutons granítics (capítols 2 i 3), colades basàltiques (capítols 4 i 5) i intrusions màfiques en l'escorça inferior (capítol 6). El denominador comú a tots aquests casos és el contrast de velocitats, fet determinant per tal de que aquests problemes puguin ser tractats amb la tomografia sísmica.

Pel que fa a la correlació entre la velocitat de propagació de les ones sísmiques i la geologia, podriem establir una classificació considerant dos grans blocs interdependents: anomalies d'alta velocitat i anomalies de baixa velocitat. Els granits, basalts i materials màfics presenten altes velocitats sempre que considerem la roca poc o gens alterada. Per tant, estariem parlant del cas òptim per a l'aplicació de la tomografia sísmica quan el que ens interessa és localitzar, delimitar i caracteritzar les estructures formades per aquestes litologies. En aquests casos les zones d'alta velocitat estaran àmpliament mostrejades i obtindrem resultats de gran fiabilitat. Per contra, les parts del model que presentin baixes velocitats estaran inframostrejades i el model de velocitats per aquestes zones serà menys fiable. Aquests dos supòsits (anomalies d'alta i baixa velocitat) poden coexistir de forma

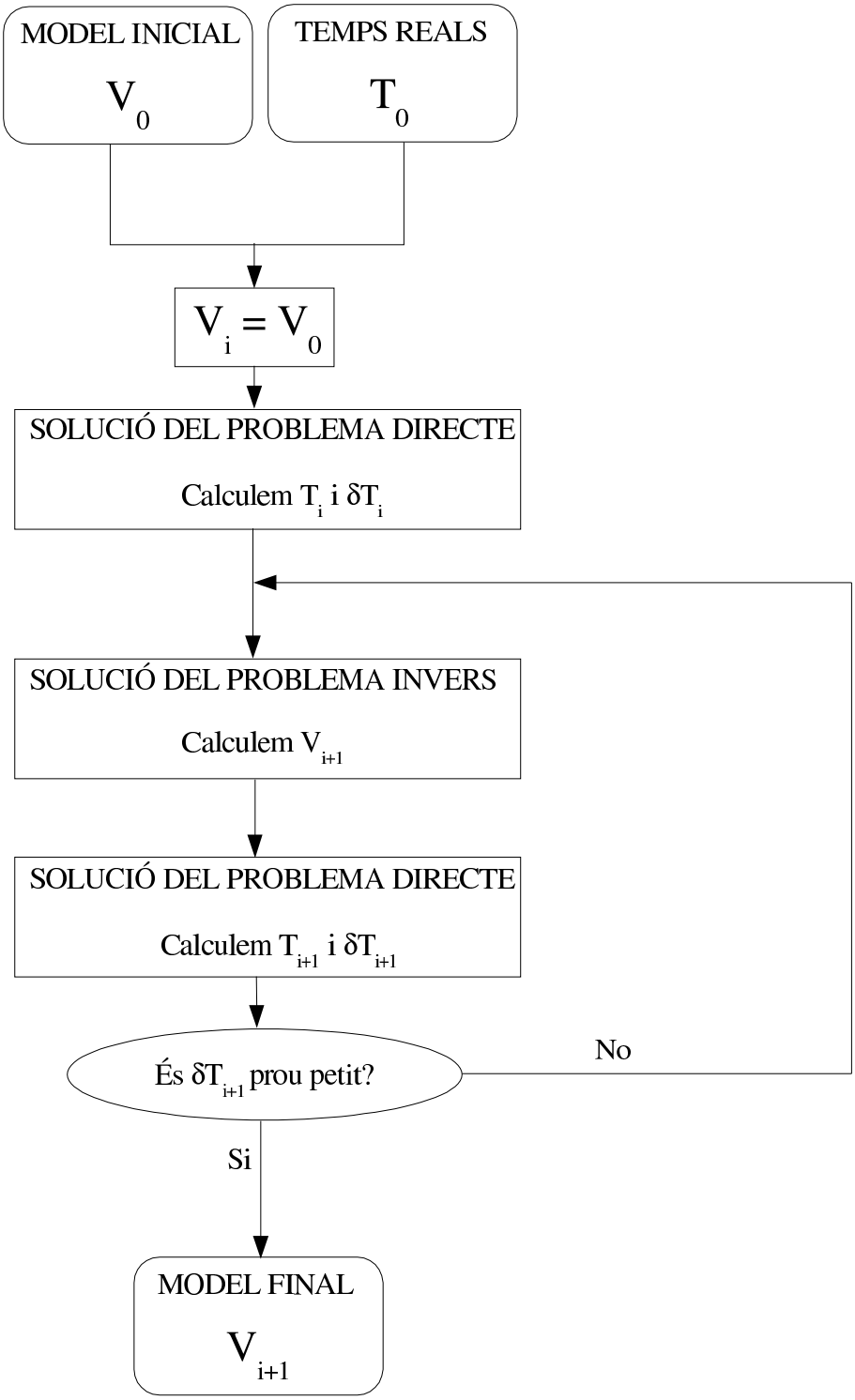

Fig. 1.2: *Esquema del procés iteratiu utilitzat per a la inversió tomogràfica*

conjunta en alguns casos, com ara una capa de sediments (baixes velocitats) coberta per una colada basàltica (alta velocitat) cosa que fa el problema particularment complex quan el que interessa és estudiar la zona de baixa velocitat.

1.3.1 Plutons granítics

En els capítols 2 i 3 s'han tractat dades adquirides sobre plutons granítics localitzats al SE de la Península Ibèrica. Encara que en els dos estudis es tracta d'estudiar el mateix tipus de roca, els dos treballs s'han fet a escales diferents, fet que afegeix altres diferències entre els dos casos com poden ser el tipus d'adquisició o bé el tipus de processat aplicat.

En el capítol 2 es caracteritzen els plutons granítics creuats pel perfil de sísmica de reflexió profunda IBERSEIS (Simancas et al., 2003; Carbonell et al., 2004) a la zona d'Ossa Morena. Aquests materials daten del Carbonífer o del Paleozoic Inferior i presenten un contrast de velocitats considerable davant dels materials encaixants consistents bàsicament en pissarres, esquistos i basalts. Tot i que algunes d'aquestes roques, com ara els basalts, presenten velocitats típiques similars a les dels granits (veure taula 1.1), hi han diversos factors que modifiquen aquest paràmetre físic. En un procés d'intrusió sempre tindrem que la roca que s'emplaça (en aquest cas granit) serà d'edat posterior a la roca encaixant i per tant en el moment de la intrusió encara no ha estat afectada per la meteorització (a nivell superficial) ni per la tectònica pròpia de la zona. Per una altra banda, el propi procés d'emplaçament comporta un augment de temperatura causant una alteració tèrmica de les propietats de la roca encaixant. Així, mentre la roca encaixant ha experimentat diverses modificacions, la roca emplaçada conserva les seves propietats físiques inalterades. Tots aquests factors fan que la velocitat típica de la roca encaixant estigui per sota del que esperariem basant-nos en mesures de laboratori sobre roques sense cap alteració, fet que possibilita que existeixi un contrast notable que ens permeti identificar clarament la intrusió granítica i determinar la seva morfologia fins a fondàries de més de 1000 m.

En el capítol 3 totes les dades utilitzades han estat adquirides íntegrament sobre el plutó granític d'Albalà. Per una descripció detallada de la geologia es pot consultar Escuder-Viruete et al., 2003. En aquest cas es tracta d'un estudi superficial d'alta resolució, per tant les fondàries assolides no van més enllà de 70 m. Al tractar-se de dades adquirides sobre un mateix massís rocós, els possibles contrastos de velocitats no són atribuïbles a diferents materials sino al diferent estat en que aquests es troben. Hi ha diversos factors que modificaran la velocitat típica que caldria esperar per a un material granític:

- Meteorització: Per tractar-se d'un estudi superficial, els agents atmosfèrics tenen

una gran influència en els primers metres de l'àrea prospectada alterant la roca i com a conseqüència la velocitat típica de les ones sísmiques en travessar-la.

- Estat de fracturació: La presència de falles o fractures deterioren la qualitat de la roca fent-la menys compacta fet que es veurà reflectit en una reducció de la velocitat.

- Saturació: La presència de fluïds també és un factor que modifica la velocitat típica d'un material ja que aquest paràmetre físic no és independent del grau de saturació de la roca.

- Alteracions químiques: Sovint, com a conseqüència de la circulació de fluïds dins del cos rocós, la roca es veu alterada químicament cosa que també tindrà un efecte no menyspreable en la velocitat.

Llevat de la meteorització, els efectes de la qual només són funció de la fondària i de la meteorologia de la zona d'estudi, la resta de factors que poden influir en la velocitat solen ser interdependents. La circulació de fluïds sovint es troba associada a la presència de falles i fractures, en ser aquestes zones preferents que possibiliten el trànsit de líquids en el subsòl. El mateix succeeix en considerar les alteracions químiques, ja que aquestes es donaran majoritàriament en les proximitats de zones amb presència de fluïds en moviment que puguin transportar els ions causants de les diferents reaccions.

La velocitat sísmica en un massís granític pot aportar molta informació sobre l'estat de la roca i si es complementa amb dades de sondejos, fa possible l'extensió d'una informació puntual a tota l'àrea d'estudi mitjançant la correlació entre velocitats i d'altres paràmetres, com ara l'índex de fracturació.

1.3.2 Colades basàltiques

Els capítols 4 i 5 tracten el problema de la visualització sota capes de basalt al Mar del Nord, més concretament a la conca Faroe-Shetland. Aquesta àrea ha estat sistemàticament estudiada per empreses petroleres ja que representa un reservori potencial d'hidrocarburs. La conca Faroe-Shetland està formada per una seqüència de sediments mesozoics i terciaris però en la proximitat de la plataforma de les Illes Faroes, aquests sediments estan coberts per laves basàltiques del Paleocè-Eocè que van ser les responsables de la formació de les Illes Faroe. La topografia de la conca prèvia als episodis volcànics es caracteritza per falles normals provocades per l'extensió i la subsidència durant el Cretàcic i el Paleocè. Les colades basàltiques generades per les erupcions van omplir els espais entre els blocs de falla i es van extendre en direcció al centre de la conca. Posteriorment una altra seqüència de sediments es va dipositar sobre la capa basàltica. Això ens porta a una configuració en la que una capa amb materials basàltics (alta velocitat) es troba

emplaçada entre dos seqüències sedimentàries (baixes velocitats). Aquesta inversió de velocitats representa, ja de per sí, una limitació per a la tomografia sísmica.

En els estudis realitzats fins al moment, no hi ha hagut cap limitació (llevat dels problemes típics de les dades marines: múltiples, marees, etc.) per obtenir l'estructura de la capa de sediments que es sobreposen al basalt, doncs per aquests casos les tècniques convencionals de sísmica de reflexió són suficientment resolutives. El problema es planteja quan es tracta d'estudiar la capa basàltica i els materials que aquesta cobreix. En funció de l'enfoc del problema, sovint s'han considerat les colades basàltiques com a cossos amb propietats homogènies, però des del punt de vista de la prospecció sísmica s'ha de considerar una capa basàltica com un cos extremadament heterogeni pel que fa a la propagació de les ones sísmiques en el seu interior. En particular, en la zona de les Illes Faroe hi han diversos indicis geològics i geofísics que així ho confirmen (Chalmers and Waagstein, 2006).

En el cas que ens ocupa, les erupcions es succeïren en diferents episodis i han estat classificades en tres sèries: Inferior, Mitja i Superior. La composició química i la potència varien substancialment d'una sèrie a una altra. En els períodes sense activitat volcànica es van dipositar en els mínims topogràfics lutites, carbons lacustres i sediments. Com a causa de les diferents erupcions també es dipositaren gran quantitat de cendres volcàniques, que degut a les seves caracterísitiques es van extendre fins i tot més enllà de l'abast de les laves. Les parts més externes de les colades basàltiques es van veure afectades per la meteorització, causant una disminució en la seva velocitat si es compara amb les parts més internes que es van refredar lentament, sense cap influència externa, i per tant conservant una alta velocitat característica. Malgrat que a gran escala les colades basàltiques tendeixin a ser subhoritzontals, a petita escala les irregularitats en les interfícies són molt marcades, fins i tot hi han autors que han atribuït a aquestes interfícies propietats fractals (Martini and Bean, 2002). Les interfícies corresponents a diferents fluxos de lava no són suficientment importants com per a aparèixer com events diferenciats en la sísmica de reflexió, però si que provoquen múltiples interns, conversió d'ones, reverberacions i dispersió i atenuació de l'energia sísmica eliminant en gran part la coherència del senyal i alterant-ne la continuitat lateral que permetria identificar diferents events dins del cos basàltic. Tots aquests factors que dificulten l'estudi d'un cos basàltic també s'han de considerar quan es volen estudiar les estructures per sota d'aquest cos. Una capa d'alta velocitat sempre causa un gran contrast d'impedància acústica amb el seu entorn, en aquest cas el principal problema que existeix per obtenir informació de les estructures sub-basàltiques és que la major part de l'energia sísmica o bé es reflecteix o bé viatja per l'interior de la capa de basalt, per tant el percentatge d'energia que arriba a estructures més profundes és molt reduït. Si a això hi afegim que la qualitat (en termes

de coherència) del senyal experimenta un deteriorament notable en travessar el basalt, les possibilitats d'obtenir una imatge sísmica raonable de les estructures sub-basàltiques es redueixen dràsticament.

Mitjançant la sísmica de reflexió convencional s'obtenen bons resultats en medis estratificats i amb certa continuïtat lateral, premises que no es verifiquen a la conca Faroe-Shetland en les proximitats de les Illes Faroe. Per tant, per tal de millorar els resultats obtinguts fins al moment s'ha optat per aplicar una migració pre-stack en fondària. En aquest apartat no es pretén fer una exposició detallada sobre els fonaments teòrics d′aquesta metodologia, el que sí cal comentar és que el fet clau per a una correcta aplicació d'aquesta metodologia passa per un control exhaustiu de les velocitats. En aquest sentit, el capítol 4 està dedicat a l'estudi de les limitacions intrínseques en l'obtenció d'un model de velocitats en presència d'una inversió de velocitats. Determinar les velocitats en les zones sub-basàltiques del model requereix de l'inversió de diferents fases (no només primeres arribades), ja que en certa manera s'ha de forçar a l'algoritme que resol el problema directe a "visitar" aquestes zones del model mitjançant les reflexions i refraccions en capes profundes. Per tant, implícitament ja es fa una interpretació prèvia de les dades. En aquest capítol s'estudia l'efecte d'aquesta interpretació *a priori* sobre el resultat final mitjançant diverses simulacions sintètiques i s'estableixen certes limitacions que s'haurien de considerar en el tractament d'aquest problema.

Al capítol 5 s'han reprocessat unes dades d'una línia de sísmica de reflexió adquirida a la conca Faroe-Shetland. S'han aplicat dos tipus de processat: un processat de sísmica de reflexió més o menys convencional i la migració pre-stack en fondària. Amb la primera metodologia s'obté una imatge detallada dels sediments que es troben per sobre del basalt, però per sota de la interfície superior del basalt la imatge esdevé poc clara fent impossible qualsevol interpretació realista. En aplicar la migració pre-stack en fondària es perd definició en les capes més superficials, però es recupera senyal coherent per sota del basalt, cosa que permet fer una interpretació tant de la base de la capa basàltica com de la part superior del basament.

1.3.3 Intrusions màfiques

En el capítol 6 la zona d'estudi es situa al Massís Ibèric, al SO de la Península Ibèrica. Aquesta zona forma part de l'orogen Varisc i s'hi poden identificar tres unitats tectòniques clarament diferenciades: Zona Sud-Portuguesa (ZSP), Zona d'Ossa-Morena (ZOM) i Zona Centre-Ibèrica (ZCI). Els límits respectius d'aquestes tres unitats han estat interpretats com a zones de sutura degut a la presència de roques d'alta pressió i roques amb signatura oceànica. Cadascuna d'aquestes unitats mostren diferents característiques tant a nivell superficial com en profunditat. Un estudi detallat de la geologia de la zona es pot trobar

a Simancas et al., 2001. Aquesta zona ha estat recentment estudiada mitjançant el perfil de sísmica de reflexió IBERSEIS (Simancas et al., 2003; Carbonell et al., 2004) i un experiment de gran angle coincident en part amb l'anterior (Palomeras et al., 2008), fets que han permès conèixer l'estructura de l'escorça i la seva composició.

En la imatge obtinguda del perfil de reflexió IBERSEIS, un dels fets més rellevants és la presència d'una banda molt reflectiva d'uns 175 km de longitud situada a l'escorça mitjana (12-18 km) en la zona d'Ossa-Morena/Centre-Ibèrica. Aquest cos ha estat etiquetat com a IRB (*Iberseis Reflective Body*). En l'experiment de gran angle dut a terme amb posterioritat (Palomeras et al., 2008), els models de velocitats obtinguts han determinat unes velocitats per al IRB, d'entre 6.8-7.1 km/s més pròpies de l'escorça inferior que no pas de l'escorça mitjana. Degut a aquesta alta velocitat i a la gran reflectivitat s'ha atribuit a aquest cos una composició màfica amb orígen en un intrusió magmàtica. Aquesta hipòtesi explicaria la presència d'intrusions màfiques a la zona d'Ossa-Morena durant el Carbonífer. A més, la inusual concentració de dipòsits minerals i l'existència de roques amb metamorfismes que requereixen altes temperatures i baixes pressions també afavoririen aquesta interpretació.

El treball desenvolupat al capítol 6 d'aquesta tesi es centra en un dels perfils de gran angle adquirits a la zona. Aquest perfil es caracteritza per la gran quantitat de receptors utilitzats per a la seva adquisició. Això es tradueix en un perfil de gran angle amb un espaiat entre estacions de l'ordre de 150 m, fet que ha permès d'aplicar tècniques de sísmica de reflexió per obtenir un *stack*. La imatge resultant es caracteritza per una gran reflectivitat a nivells d'escorça mitja i escorça inferior. El Moho s'identifica amb una franja molt reflectiva d'un gruix variable que oscil.la entre 1 i 2 segons. Aquest fet no és extrany ja que l'escorça inferior es caracteritza, en general, per exhibir una alta reflectivitat formada per reflectors discontinus de poca longitud, en contrast amb una relativa transparència de l'escorça superior. Aquesta variació en la reflectivitat s'ha atribuït a canvis en la composició de l'escorça inferior.

Utilitzant el model de velocitats obtingut per Palomeras et al., 2008 s'ha realitzat una simulació sintètica per intentar reproduir les principals característiques identificades en els tirs de camp. Els events més rellevants es poden recuperar, però en comparar les dades sintètiques amb les dades reals es demostra que amb el model de velocitats utilitzat no es pot reproduir tota la complexitat que exhibeixen les dades reals pel que fa a la seva reflectivitat.

La teoria de la sísmica estableix que el diàmetre de Fresnel ve donat per l'expressió:

$$d \approx \sqrt{2z\lambda + \frac{\lambda^2}{4}} \tag{1.10}$$

i aquesta és la dimensió del cos més petit que es pot detectar amb mètodes sísmics. Per

tant aquesta dimensió representa el límit inferior per a la resolució lateral, i els cossos menors que el diàmetre de Fresnel no es podran visualitzar com a events sísmics coherents. De totes maneres, les difraccions provocades per les ones sísmiques tindran un efecte en les dades enregistrades, ja que la seva interferència constructiva pot justificar els coeficients de reflectivitat observats, sovint més alts que els calculats en base a la composició química de l'escorça. Aquests coeficients depenenen dels contrastos d'impedància acústica, per tant per explicar tant la seva magnitud com la reverberació observada en les dades reals s'ha considerat una escorça laminada. En aquest cas, el material intrusiu s'hauria dipositat en làmines de dimensions menors al diàmetre de Fresnel, fent impossible diferenciar-les com a events sísmics independents, però si que exercirien una influència tant en la reflectivitat sísmica com en l'augment de la velocitat de les ones P.

Per tal d'avaluar aquesta hipòtesi, s'han realitzat unes simulacions amb un model de velocitats basat en el model de Palomeras et al., 2008 però amb modificacions a nivell d'escorça mitjana, escorça inferior i Moho. Les variacions han consistit en unes alteracions aleatòries del model per tal de simular els efectes de la possible intrusió màfica. Els sismogrames sintètics resultants reprodueixen els principals events que s'observen en les dades reals, ja que l'aleatorietat en la modificació del model de velocitats no altera les propietats promig en quant a velocitats. En aquest cas però, els resultats obtinguts també reprodueixen parcialment els patrons de reflectivitat observats en les dades reals.

2. IMAGING GRANITIC PLUTONS ALONG THE IBERSEIS PROFILE

I. Flecha, R. Carbonell, H. Zeyen, D. Martí, I. Palomeras, F. Simancas and A. Pérez-Estaún, *Tectonophysics*, 420, 37-47, 2006.

Available online at www.sciencedirect.com
SCIENCE DIRECT
Tectonophysics 420 (2006) 37–47
TECTONOPHYSICS
www.elsevier.com/locate/tecto

Imaging granitic plutons along the IBERSEIS profile

I. Flecha [a,*], R. Carbonell [a,1], H. Zeyen [b,2], D. Martí [a,1], I. Palomeras [a,1], F. Simancas [c,3], A. Pérez-Estaún [a,1]

[a] Departament de Geofísica, Institut de Ciéncies de la Terra "Jaume Almera"-CSIC, C/ Lluis Solé i Sabaris s/n, 08028 Barcelona, Spain
[b] UMR 8148 IDES, CNRS-Universite de Paris-Sud, Bat. 504, F-91405 Orsay, Cedex, France
[c] Departamento de Geodinámica, Universidad de Granada, Avenida Fuentenueva, s/n, 18071 Granada, Spain

Received 14 January 2005; received in revised form 30 September 2005; accepted 4 January 2006
Available online 19 April 2006

Abstract

The parameters used for the acquisition of the IBERSEIS deep seismic reflection profile in the SW Iberian Peninsula provide seismic images of the deep crust as well as a high resolution section of the shallow subsurface. A very dense array of sources and receivers allowed high resolution tomographic studies in zones of special interest (granitic plutons). The three dimensional tomographic inversion produced velocity models along a 500 m wide and 1000 m deep strip along the IBERSEIS transect in the areas of La Bazana, La Dehesilla, Feria and Villafranca. In these high resolution velocity models (sampled by $50 \times 50 \times 50$ m cells), high velocity anomalies indicate the geology and extension of the granitic plutons at depth. This directly correlates with the surface outcrops. Moreover, tomographic models provided valuable information for the geometry and characterization of fractured and fresh domains in a rock volume. Furthermore, a piggy back seismic acquisition experiment using additional seismic instrumentation from the University of Paris Sud (40-channel DMT) provided perpendicular, offline recordings of the Vibroseis sources. This additional recording system was deployed perpendicularly to the main IBERSEIS seismic reflection line and provided additional 3D control.

Keywords: Seismic tomography; Seismic velocities; Granite seismic properties

1. Introduction

Granitic intrusions in the upper crust have been widely studied by means of several geophysical techniques. The most common among them have been gravimetric modeling (Bott and Smithson, 1967) and mapping of the anisotropy of magnetic susceptibility (Guillet et al., 1983; Román-Berdiel et al., 1995), combined with detailed surface information (Román-Berdiel et al., 1995; Yenes et al., 1999; Simancas et al., 2000; Galadí-Enríquez et al., 2003), to achieve large-scale 3D images which constrain the shape and extent of granitic bodies. Usually, this information, together with detailed surface geological observations, places valuable constraints on inferences about the ascent mechanism of granitic intrusions. Lately, seismic reflection techniques

* Corresponding author. Tel.: +34 93 409 54 10; fax: +34 93 411 00 12.
E-mail addresses: iflecha@ija.csic.es (I. Flecha), rcarbo@ija.csic.es (R. Carbonell), zeyen@geol.u-psud.fr (H. Zeyen), dmarti@ija.csic.es (D. Martí), ipalomer@ija.csic.es (I. Palomeras), simancas@ugr.es (F. Simancas), andres@ija.csic.es (A. Pérez-Estaún).
[1] Tel.: +34 93 409 54 10; fax: +34 93 411 00 12.
[2] Tel.: +33 1 69 15 40 09; fax: +33 1 69 15 49 05.
[3] Tel.: +34 958 24 33 53; fax: +34 958 24 85 27.

0040-1951/$ - see front matter © 2006 Elsevier B.V. All rights reserved.
doi:10.1016/j.tecto.2006.01.019

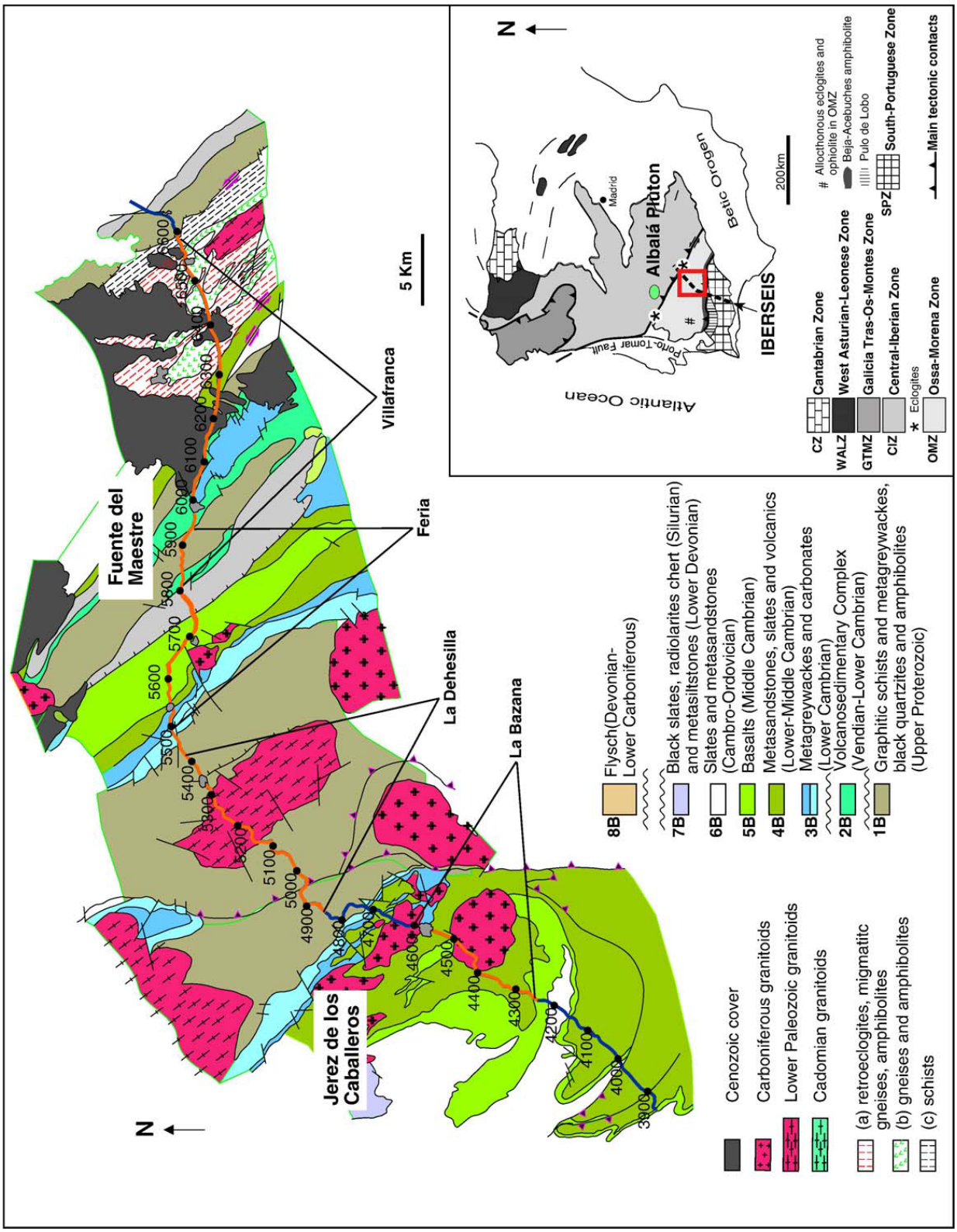

Fig. 1. Detailed geological map of the Ossa Morena Zone. Transect of the IBERSEIS profile (in blue). Studied areas (in orange) of: La Bazana, La Dehesilla, Feria and Villafranca include some granitic plutons. Note the crooked line acquisition geometry. In the tectonic map (on the lower right), the location and the trace of the IBERSEIS deep seismic reflection profile are indicated by a discontinuous line and the green area shows the Albalá granitic pluton. Numbers along profile represent stations. Modified from Simancas et al. (2003).

also have been used successfully in delineating the internal structure of granitic bodies (Mair and Green, 1981) and to obtain information about the emplacement mechanism (Brown and Tryggvason, 2001).

During the last decade, granitic plutons also have been studied in detail as a topic of interest for environmental applications (Juhlin, 1995; Juhlin and Palm, 1999). Among the crystalline rocks, granites show appropriate properties to become the host sites for hazardous waste (Astudillo, 2001). Therefore, knowing the internal structure and properties of the rock is mandatory. Application of geophysical techniques to image the shallow subsurface has shown that it is a difficult target (Steeples et al., 1997). This is mostly due to the high degree of heterogeneity and variability of physical properties that characterize the near surface zone. The first few meters are strongly influenced by weathering, for example the flow of water through fractured zones modifies the physical properties and induces chemical reactions, thus altering the rock properties around the fractures and changing the velocity structure within the shallow layer. In order to obtain a reliable model of this shallow layer, high resolution studies must be undertaken. Previous work (Morey and Schuster, 1999; Martí et al., 2002a,b; Flecha et al., 2004) has shown that 3D source-controlled seismic tomography techniques can provide a detailed velocity model of a rock volume. In massifs composed by single rock types, seismic velocity is a valuable parameter because it can be correlated with other physical properties of the rock such as porosity and/or degree of fracturing (Escuder-Viruete et al., 2001, 2003).

The IBERSEIS seismic profile was designed to provide a detailed high-resolution crustal image of the Variscan Belt in the Southwestern Iberian Peninsula (Simancas et al., 2003; Carbonell et al., 2004). The dense source and receiver spacing (70 and 35 m respectively) and the crooked-line acquisition geometry, provide the opportunity to perform specialized processing to assess the shallow subsurface (Fig. 1). The trace of this profile intersects several granitic plutons in the Ossa Morena Zone (Fig. 1). Some of these plutons have already been studied at a crustal scale which is the case for the La Bazana pluton (Simancas et al., 2000), but no previous studies have been carried out to obtain a detailed model of the internal structure of the shallower parts of these bodies.

In order to provide three dimensional constraints in the neighbourhood of the granitic plutons, a complementary piggy-back acquisition experiment was carried out by the high resolution research team of the University of Paris Sud at Orsay. This research team provided a 40-channel DMT system which was deployed perpendicular to the trace of the main profile in four areas: La Bazana, La Dehesilla, Feria and Villafranca (Fig. 1).

In the present work, three-dimensional high-resolution first arrival travel time tomographic inversions were performed using the first arrivals of the Vibroseis shots along the IBERSEIS profile that were recorded by both the main acquisition SERCEL and the DMT piggy-back recording systems. Crooked-line geometry along the IBERSEIS profile justifies the use of a 3D tomographic scheme by means of which a velocity model along 500 m wide and 500 to 1500 m deep strip is produced.

2. Geological and geophysical background

Exposed within the Iberian Massif are abundant plutonic rocks of Late Proterozoic and Paleozoic age. In this work four areas have been studied: La Bazana, La Dehesilla, Feria and Villafranca, all of which lie in the Ossa Morena Zone (SW Iberian Peninsula) (Fig. 1). Among the granites cropping out in those areas, geochronological data are available only for the Salvatierra de Barros granite, in La Dehesilla area (516 Ma, U–Pb monazites, Oschner, 1993). Deformation fabrics suggest a Carboniferous emplacement for the La Bazana and Feria granites (Simancas et al., 2003).

In the La Bazana area, the granitic pluton lies to the south of the town of Jerez de los Caballeros (Fig. 1) and consists of a 20 km^2 circular outcrop with a 250 m thick thermal aureole. Contacts with host rocks are shallowly dipping especially in the northern part of the area where contacts dip 15–20° to the north. The timing of the intrusion is not well defined but is certainly later than the first Hercynian deformation phase and probably is also later than the second deformation phase (Coullant et al., 1981).

In the La Dehesilla zone, the profile intersects the Salvatierra de Barros granite, a pre-Hercynian elongated

Table 1
Velocities for compressional waves from laboratory measurements (Carmichael, 1982)

Lithology	Velocity (km/s)
Amphibolite	6.06
Basalt	5.60
Eclogite	6.65
Gneiss	6.00
Greywacke	5.76
Schists	5.49
Slates	5.80

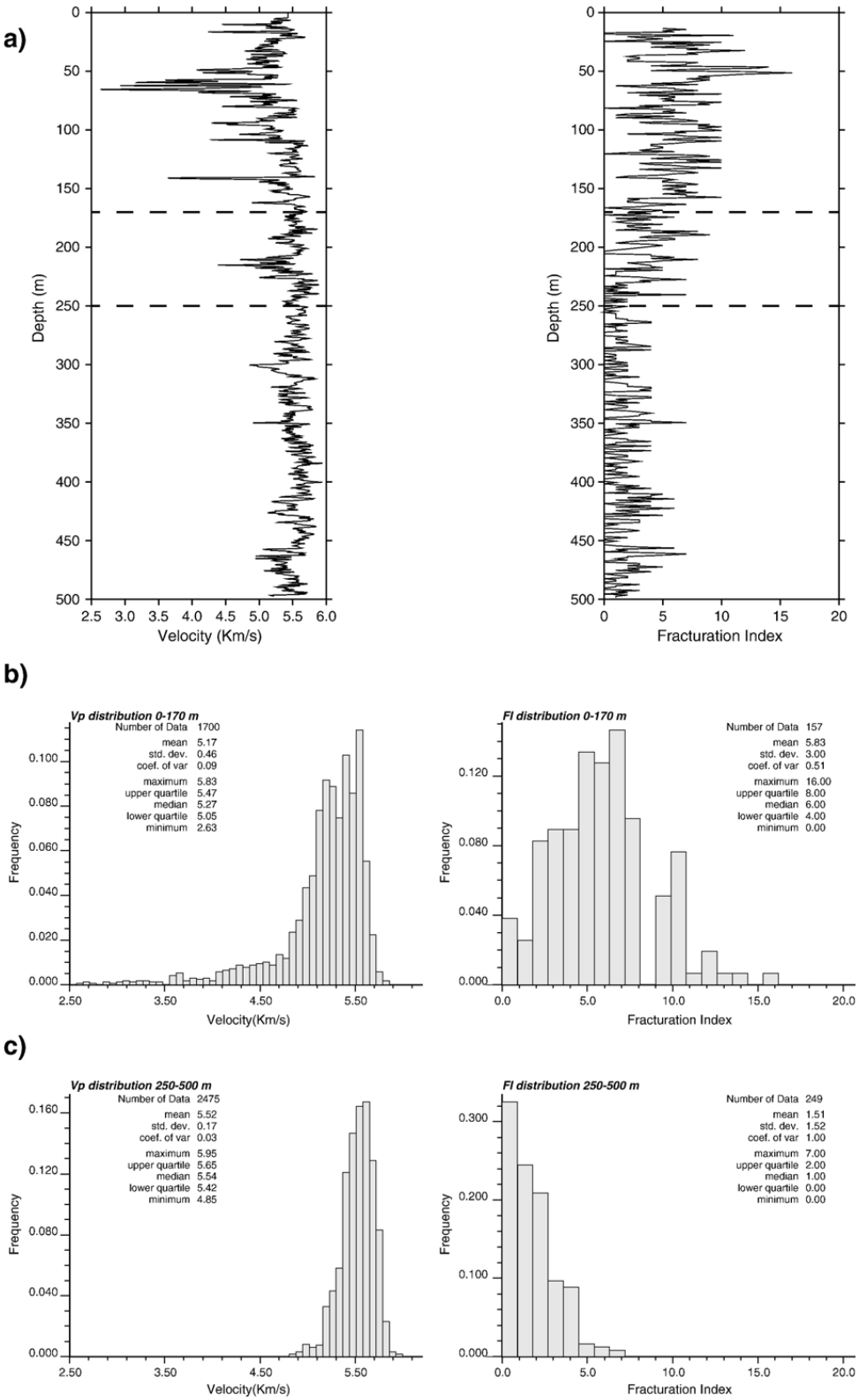

Fig. 2. a) P wave velocity log (left) and fracturation index (right) for the Albalá Pluton and statistical analysis for two regions: b) from 0 to 170 m, and c) from 250 to 500 m. The shallower region features a high variability with a mean value of 5.17 km/s for velocity and 5.83 for fracturation index while the deeper region shows a more regular distribution of the velocities and a higher mean value 5.52 km/s for velocity and 1.51 for fracturation index.

Table 2
Acquisition parameters used in the IBERSEIS profile (from Simancas et al., 2003)

Acquisition parameters	Description
Number of channels	(400 total) active minimum
Station spacing	35 m
Station configuration	12 geophones per string in line
Source type	4, 22 TM vibrators
Sweep frequencies	8–80 Hz
Sweeps per VP	6
Sweep length	20 s
Recording length	40 s listening time
Record length after correlation	20 s
Source spacing	70 m
Sample rate	0.002 ms

plutonic outcrop of 60 km^2, intruded in Upper Proterozoic rocks. The magmatic intrusion gave rise to a 1 km thick thermal aureole.

Little information is known about the Feria granitic body, which is located to the west of Feria. The identified granitic outcrop is not crossed by the profile but, as discussed in more detail below, a velocity anomaly can be identified at depth. Furthermore the surface geology suggests that the granite body extends towards the east, beneath the surface cover.

Villafranca area includes the Badajoz-Córdoba Shear Zone which represents the limit between two main tectonic units, the Ossa Morena Zone to the SW and the Central Iberian Zone to the NE. This area is highly heterogeneous; it includes some high-pressure metamorphic rocks, including retroeclogites and amphibolites with oceanic chemical signatures (Simancas et al., 2003), which contrast with slates and schists.

Compressional wave velocities for representative of those found along the profile have been obtained from laboratory measurements of rocks in several areas around the world (Table 1). Naturally, such measurements represent typical velocity values, which can change depending on water saturation, chemical composition and degree of metamorphism (Carmichael, 1982). In the area, greywackes, schists and slates are slightly metamorphized therefore the velocity expected for these rocks should be lower than values presented in Table 1. Furthermore, the rocks in the area were affected by Hercynian deformation that

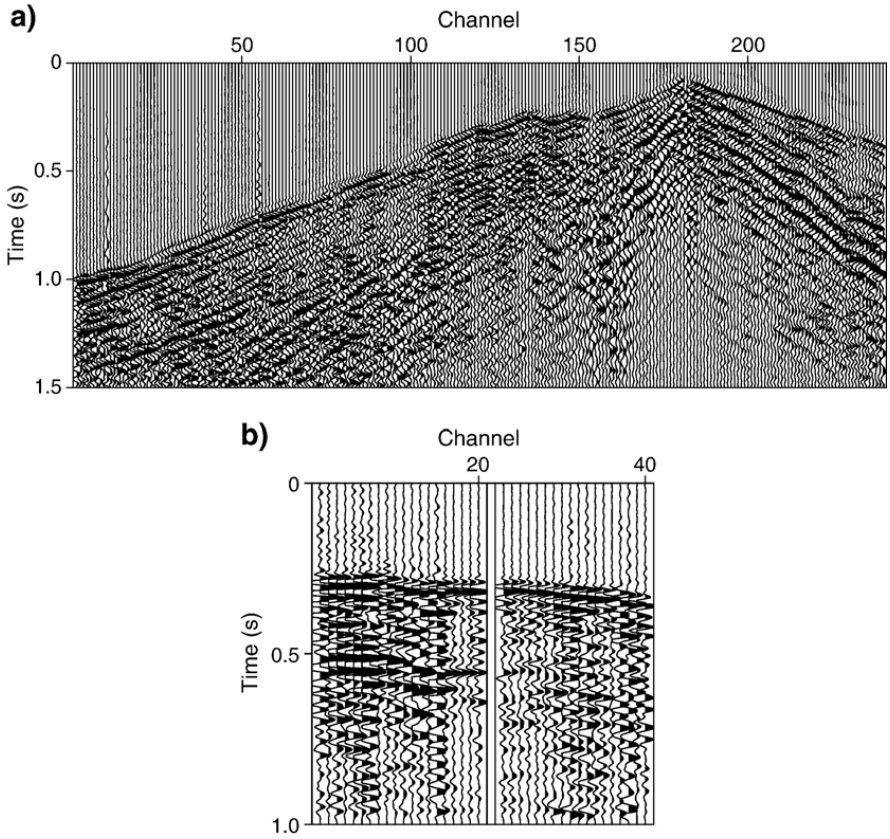

Fig. 3. Data recorded in the La Dehesilla area. a) Data from the main IBERSEIS profile and b) data from the additional DMT instrumentation. A Butterworth bandpass filter (5–10–50–60 Hz) has been applied in order to improve the signal to noise ratio. Divergence spreading correction and a gain have been used to enhance first breaks at long offsets. The distance between channels was 35 m for a) and 25 m for b).

may have resulted in an alteration of mechanical properties and a reduction in velocity. Log velocity data and fracturation index for granite (Fig. 2) were available to a depth of 500 m from a borehole in the Albalá Pluton (Escuder-Viruete et al., 2001; Martí et al., 2002a,b; Escuder-Viruete et al., 2003), which is located in a nearby area. Following this data, high velocity zones imaged in tomographic models can be correlated with granitic plutons in some cases. From the log measurements, two major domains can be differentiated as shown in the statistical analyses in Fig. 2: a shallower one from 0 to 170 m depth that features highly variable velocities due to fracturing and weathering, as shown in fracturation index graph, and a deeper one from 250 to 500 m depth with a more regular velocity distribution. Note that in the Villafranca zone some other high velocity materials outcrop along the trace of the profile as amphibolites, gneisses and eclogites (Fig. 1) that will be also mapped in the velocity models.

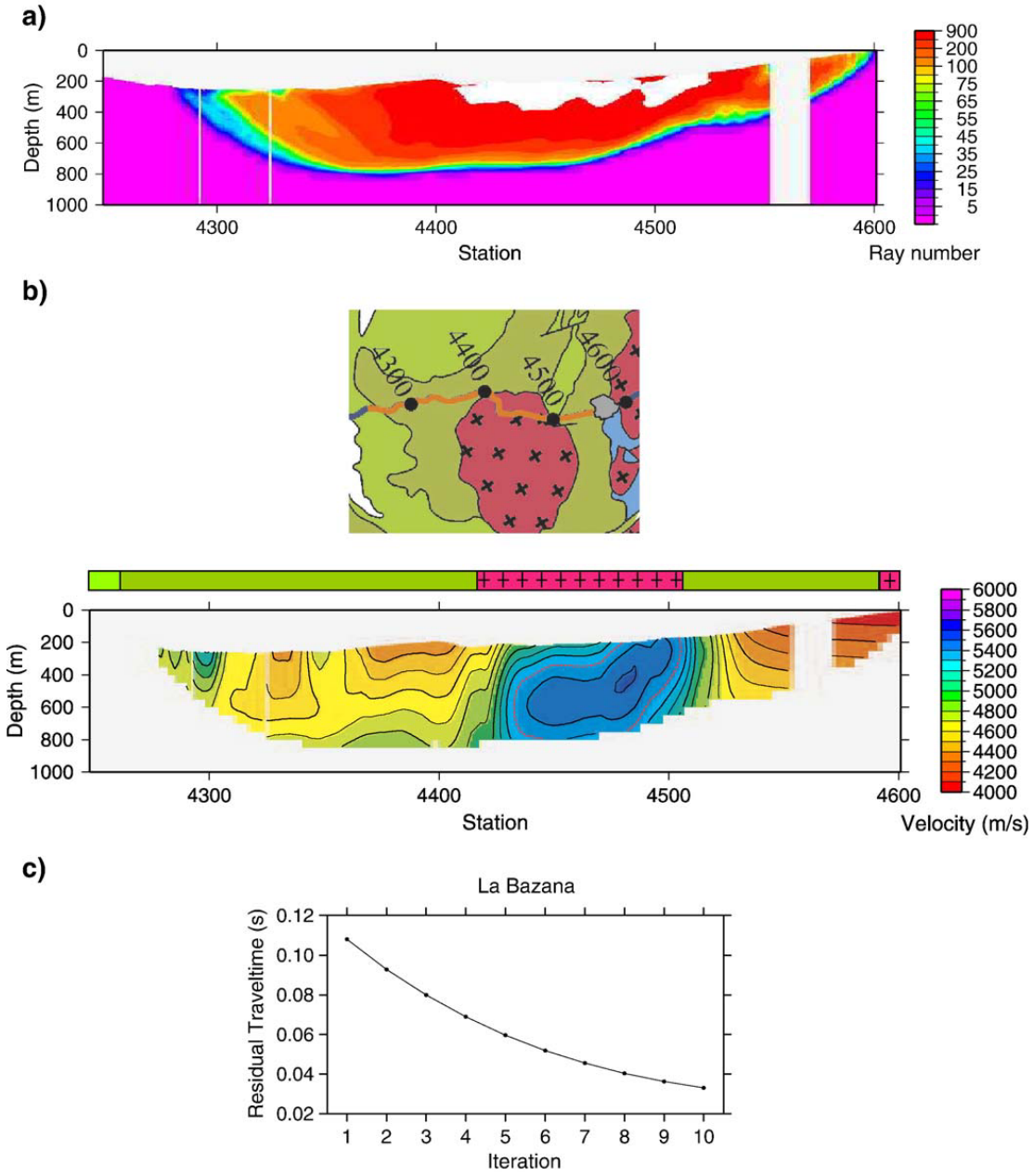

Fig. 4. Tomographic results of the La Bazana area. a) Ray coverage diagram, (white color below topography stands for coverage exceeding 900 rays), b) velocity model where ray coverage is not null and geology mapped at surface, and c) residual travel times for La Bazana area. Horizontal white band in the upper part of the images shows the topography. Vertical white bands are due to the lack of receivers because of the presence of towns. Red dashed lines delineate interpreted pluton boundaries.

3. Data processing

3.1. Data acquisition

The IBERSEIS deep seismic reflection profile was acquired in the southwestern part of the Iberian Massif during spring–summer 2001. Four 22-metric-ton Vibroseis trucks functioned as sources and a 20 s Vibroseis sweep with a frequency band from 8 to 80 Hz was used as input. The trace of the profile followed roads which resulted in a crooked-line geometry. Stations were deployed every 35 m, and sources were located with a spacing of 70 m between array centers. During the acquisition a minimum of 240 channels were active (Table 2). Details of the acquisition, processing, interpretation and application on the large scale profile can be found in Simancas et al. (2003) and Carbonell et al. (2004).

Additional instrumentation consisted of a 40-channel DMT system that provided perpendicular offline recordings of the Vibroseis shots. This instrumentation was deployed on the granitic bodies in the area of study, with a receiver-station spacing of 25 m.

3.2. Seismic tomography

First arrival seismic tomography, which was employed in this study, uses as inputs the travel times between sources and receivers and their locations. To achieve accurate first break picking, pre-processing is mandatory. In this case some first arrivals were not very clear and a bandpass Butterworth filter was applied (5–10–50–60 Hz) to improve the data quality and increase the signal-to-noise ratio (Fig. 3). Data from the IBERSEIS profile were amplitude corrected for spherical divergence to enhance signal at long offsets.

The tomographic inversion has been carried out using the "PStomo" software developed by Benz et al. (1996) and Tryggvason (1998). In this software package, a 3D finite-difference scheme is applied to

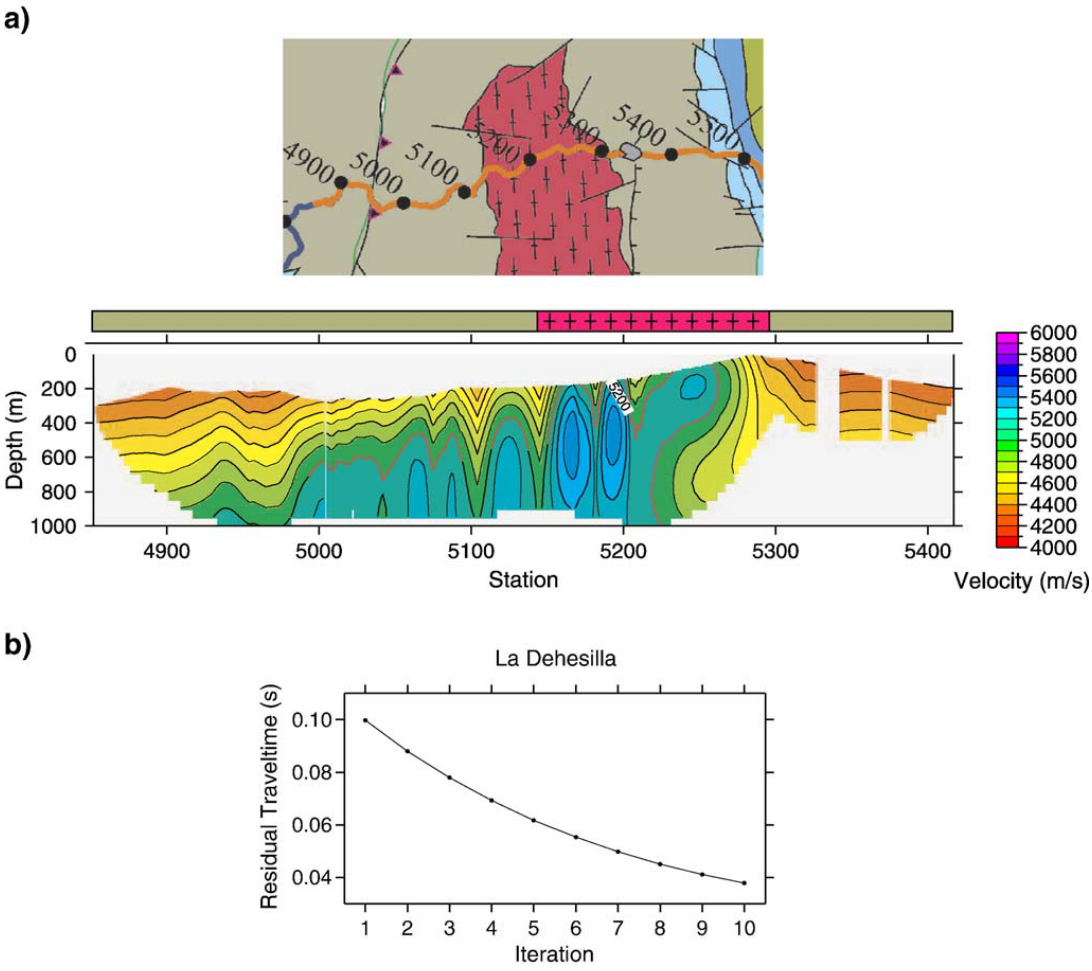

Fig. 5. Tomographic results of the La Dehesilla area. a) Velocity model for the La Dehesilla area and geology mapped at surface. Velocity model is only shown where cells are sampled by rays. b) Residual travel times. Horizontal white band in the upper part of the images shows the topography. Vertical white bands are due to the lack of receivers because of the presence of towns. Red dashed lines delineate interpreted pluton boundaries.

calculate forward travel times (Hole and Zelt, 1995) and the LSQR algorithm (Paige and Saunders, 1982) is used to solve the inverse problem. Since the inversion process is sensitive to the initial model parameters, a realistic (although highly simplified) initial velocity model was chosen to avoid local minima. The initial velocity model consisted of a vertical gradient increasing from 4000 m/s at the surface to 6000 m/s at 2000 m depth. These high velocities are supported by surface geology observed within the study area, which is characterized by a very thin sedimentary cover where slates, basalts and granites frequently outcrop (Fig. 1).

Since the computational effort in this iterative inversion scheme is proportional to the number of nodes in the velocity model, the target area was optimized looking for the minimum area of rectangular shape at the surface that enclosed sources and receivers obtaining a swath along the main transect. This resulted in a sensible decrease of the computing time. The final velocity models consisted of a grid of cubic cells with dimensions of $50 \times 50 \times 50$ m. Ten iterations were carried out in every case resulting in a regular decrease in the residual times, which assured the convergence of the iterative process. Final model results for each of the four studied are presented below.

4. Results

4.1. La Bazana

This area features a high velocity zone in the subsurface between stations 4400 and 4500 (Fig. 4a) which correlates with the exposed La Bazana granitic pluton (Fig. 1). Velocities up to 5800 m/s are observed in the inner part of the anomaly, inferred to correlate with the granitic body at depth, while near the interpreted margins of the granitic body, velocities decrease down to 5200 m/s. On the basis of its correlation with outcropping granite at the surface and the sharp velocity gradients toward the margins of the body, the contacts between granite and country rock can be inferred. Furthermore, the observed difference in velocities inside the granite probably correlates with rock properties. High velocities (inner core of the pluton) are likely related with fresh and unaltered rock and lower velocities could be indicative of alteration of

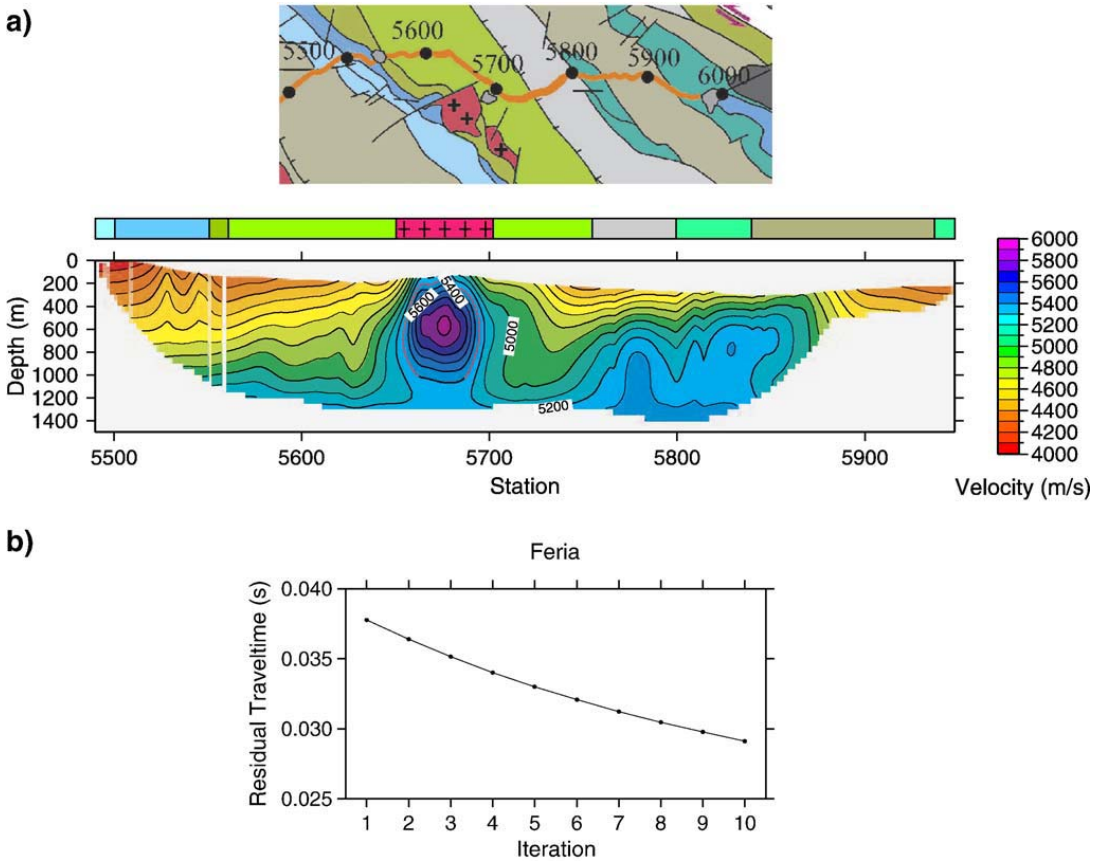

Fig. 6. Tomographic results of the Feria area. a) Velocity model for the Feria area and geology mapped at surface. Velocity model is only shown where cells are sampled by rays. b) Residual travel times. Horizontal white band in the upper part of the images shows the topography. Vertical white bands are due to the lack of receivers because of the presence of towns. Red dashed lines delineate interpreted pluton boundaries.

the rock due to the interaction between granite and host rock in the emplacement process as suggested by granitic log velocities in Fig. 2. The ray coverage diagram (Fig. 4b) shows that the velocity model is well constrained in the high velocity zone from the surface to a depth of 700 m.

4.2. La Dehesilla

In the La Dehesilla area, the velocity model from the tomographic inversion displays an extensive high-velocity region (5200–5300 m/s) between stations 5000 and 5300 (Fig. 5). The upper limit of this anomaly is at a depth of 700 m at station 5000 and becomes shallower towards the NE until it reaches the topographic surface at station 5150. From station 5150 to about station 5300, the anomaly can be followed along the surface and correlates with the location of the Salvatierra de Barros granitic unit (Fig. 1). The ray coverage diagram shows good coverage down to a depth of 900 m and, therefore the velocity model can be considered reliable to this depth. The horizontal irregularity of the high velocity anomaly between stations 5000 and 5300 can be caused by: (1) the crooked-line geometry of the acquisition and (2) the high deformation of the granitic body indicated in the geological mapping which results in narrow gradients which could be caused by narrow fractured areas within the granitic body. Probably, the image is a result of both contributions.

In order to separate both effects, a dense 3D experiment would be required. The inferred transition from the granitic body to the host rock is characterized by a smooth velocity gradient, which may be a consequence of the 1 km thick thermal aureole caused by the intrusion. These results also support an interpretation that the Salvatierra de Barros complex extends at depth to the SW.

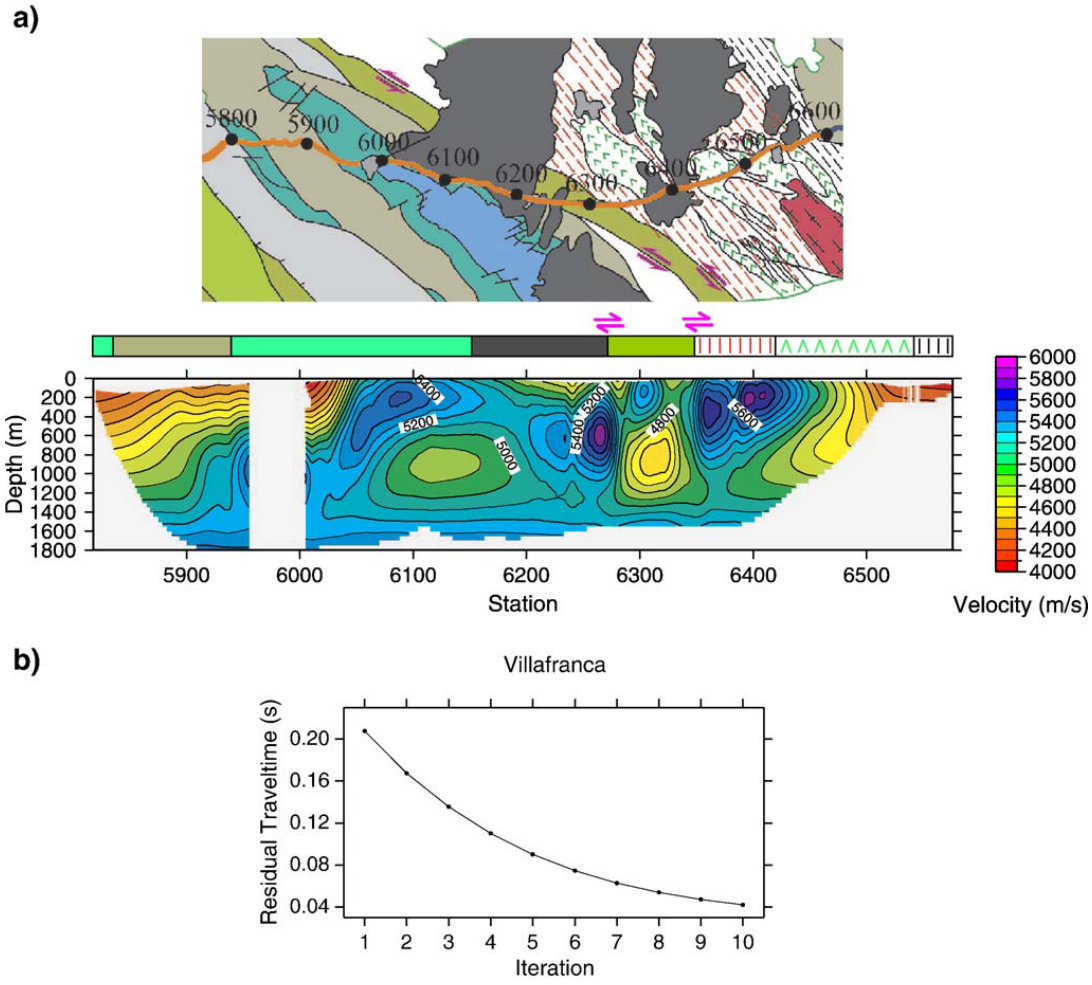

Fig. 7. Tomographic results of the Villafranca area. a) Velocity model for the Villafranca area and geology mapped at surface. Velocity model is only shown where cells are sampled by rays. b) Residual travel times. Horizontal white band in the upper part of the images shows the topography. Vertical white bands are due to the lack of receivers because of the presence of towns.

4.3. Feria

A prominent high-velocity anomaly is mapped in this area between stations 5650 and 5700 (Fig. 6). Although the IBERSEIS profile does not intersect the Feria granitic outcrop, this high velocity anomaly most probably can be correlated with the granitic body that outcrops 500 m to the S of the trace of the profile (Fig. 1). Therefore, as in the case of La Dehesilla, the tomograms indicate that this granitic body extends at depth from the outcrop to the north beneath the IBERSEIS profile. As in the La Bazana case, the inner part of this anomaly features higher velocities than the outer; therefore, different domains from fresh and unaltered (5800 m/s) to thermally metamorphosed rock (5200 m/s) can be inferred. Good ray coverage exists for this area to a depth of 1200 m, and thus the velocity increase towards the center of the velocity anomaly suggests an onion-like structural configuration for the granitic intrusion.

4.4. Villafranca

In this region, several high velocity zones are displayed in the final velocity model (Fig. 7). A 5800 m/s anomaly is located close to the surface between stations 6050 and 6120. Despite its shallow position no clear interpretation can be provided for this anomaly. A similar situation can be observed between stations 6250 and 6280 where a clear, localized, high velocity anomaly is displayed but its location in depth (from 400 to 800 m) makes an interpretation difficult because it cannot be correlated with any structure in the surface geology. However a sharp lateral discontinuity in velocity at station 6280 is imaged which correlates with a fault mapped at the surface and permits this structure to be traced in depth. In the area surrounding station 6400, a high-velocity anomaly can be correlated with outcropping high-pressure metamorphic rocks. A velocity of 6000 m/s agrees with values expected for amphibolites and retroeclogites (Table 1). In this case, good ray coverage is obtained down to 1500 m.

5. Conclusions

Along the IBERSEIS transect in the Ossa Morena Zone (OMZ) in southwestern Spain, 3D seismic tomography illustrates the correlation of high-velocity anomalies with granites mapped at the surface. Lower Paleozoic granitoids have been imaged as bodies with relatively uniform velocity distribution and average velocity of ~5300 m/s. In contrast, carboniferous granitoids show layered velocity distributions with high velocity cores (~5800 m/s) and lower velocity aureoles next to their margins (~5200 m/s). High velocities within the granites have been associated with fresh volumes of rock, while decreases in velocity are inferred to show altered/fractured zones within granites. Contacts with host rocks feature a negative velocity gradient caused by alteration that usually exists in the neighbourhood of thermal aureoles in granitic intrusions. The La Bazana and La Dehesilla granitic plutons seem to extend to 700 m in depth beneath the seismic profile, while the Feria pluton may reach a depth of as much as 1000 m. In the Villafranca area, some outcropping high-pressure metamorphic rocks are associated with high velocity anomalies (~6000 m/s). Furthermore, a sharp lateral discontinuity correlates with a fault mapped at the surface and enables mapping of this structure in depth. In the La Bazana case, results agree, at the experiment scale, with previous works, which used gravimetric and magnetic techniques to infer the geometry of the granitic pluton. The results obtained in this work demonstrate the success of a methodology rarely applied to the research of plutonic bodies.

Acknowledgements

Funding for the field acquisition of the IBERSEIS deep seismic reflection profile was provided by CICYT-FEDER (1FD1997-2179/RYEN1), Junta de Andalucía, ENRESA, Swedish Research Council and the Instituto Geológico y Minero de España. This research was supported also by the Spanish Ministry of Science and Technology (grants BTE2000-0583-C02-01, BTE2000-3035-E and BTE2000-1490-C02-01). We thank two anonymous reviewers for their valuable comments which have contributed to improve the manuscript.

References

Astudillo, J., 2001. El almacenamiento geológico profundo de los residuos radioactivos de alta actividad. Principios básicos y tecnología. ENRESA, Madrid.

Benz, H., Chouet, B., Dawson, P., Lahr, J., Page, R., Hole, J., 1996. Three dimensional P and S wave velocity structure of Redout Volcano, Alaska. J. Geophys. Res. 101, 8111–8128.

Bott, M.H.T., Smithson, S.B., 1967. Gravity investigations of subsurface shape and mass distribution of granite batholiths. Bull. Geol. Soc. Am. 78, 859–878.

Brown, D., Tryggvason, A., 2001. Ascent mechanism of the Dzhabyk batholith, southern Urals: constraints from URSEIS reflection seismic profiling. J. Geol. Soc. 158, 881–884.

Carbonell, R., Simancas, F., Juhlin, C., Pous, J., Pérez-Estaún, A., González-Lodeiro, F., Muñoz, G., Heise, W., Ayarza, P., 2004.

Geophysical evidence of a mantle derived intrusion in SW Iberia. Geophys. Res. Lett. 31, L11601.

Carmichael, R.S., 1982. Handbook of Physical Properties of Rocks, vol. II. CSC Press, Boston.

Coullant, J.L., Fernández-Carrasco, J., Aguilar, M.J., 1981. Mapa de la hoja no 875 (Jerez de los Caballeros). Escala 1:50.000. IGME, Madrid.

Escuder-Viruete, J., Carbonell, R., Jurado, M.J., Marti, D., Pérez-Estaún, A., 2001. Two-dimensional geostatistical modeling and prediction of the fracture system in the Albalá Granitic Pluton, SW Iberian Massif, Spain. J. Struct. Geol. 23, 2011–2023.

Escuder-Viruete, J., Carbonell, R., Martí, D., Jurado, M.J., Pérez-Estaún, A., 2003. Architecture of fault zones determined from outcrop, cores, 3-D seismic tomography and geostatistical modeling: example from the Albalá Granitic Pluton, SW Iberian Variscan Massif. Tectonophysics 361, 97–120.

Flecha, I., Martí, D., Carbonell, R., Viruete, J., Pérez-Estaún, E., 2004. Imaging low velocity anomalies with the aid of seismic tomography. Tectonophysics 388, 225–238.

Galadí-Enríquez, E., Galindo-Zaldívar, J., Simancas, F., Expósito, I., 2003. Diapiric emplacement in the upper crust of a granitic body: the La Bazana granite (SW Spain). Tectonophysics 361, 83–96.

Guillet, P., Bouchez, J.L., Wagner, J.J., 1983. Anisotropy of magnetic susceptibility and magmatic structures in the Gurande granite massif (France). Tectonics 2, 419–429.

Hole, J.A., Zelt, B.C., 1995. Three-dimensional finite-difference reflection travel times. Geophys. J. Int. 121, 427–434.

Juhlin, C., 1995. Imaging of fracture zones in the Finnsjön area, central Sweden, using the seismic reflection method. Geophysics 60, 66–75.

Juhlin, C., Palm, H., 1999. 3-D structure below Ävrö Island from high-resolution reflection seismic studies, southeastern Sweden. Geophysics 64, 662–667.

Mair, J., Green, A., 1981. High resolution seismic reflection profiles reveal fracture zones within a homogeneous granite batholith. Nature 294, 434–442.

Martí, D., Carbonell, R., Trygsvason, A., Escuder, J., Pérez-Estaún, A., 2002a. Calibrating 3D tomograms of a granitic pluton. Geophys. Res. Lett. 29, 15(1)–15(4).

Martí, D., Carbonell, R., Trygsvason, A., Escuder, J., Pérez-Estaún, A., 2002b. Mapping brittle fracture zones in 3 dimensions: high resolution travel time seismic tomography in a granitic pluton. Geophys. J. Int. 149, 134–148.

Morey, D., Schuster, G.T., 1999. Paleoseismicity of the Oquirrh fault, Utah from shallow seismic tomography. Geophys. J. Int. 138, 25–35.

Oschner, A., 1993. U–Pb Geochronology of the Upper Proterozoic–Lower Paleozoic geodynamic evolution in the Ossa-Morena Zone (SW Iberia): constraints on the timing of the Cadomian Orogeny, page 249. Diss. ETH No. 10392, Zurich.

Paige, C.C., Saunders, M.A., 1982. LSQR: an algorithm for sparse linear equations and sparse least squares. ACM Trans. Math. Softw. 8, 43–71.

Román-Berdiel, T., Pueyo-Morer, E.L., Casas-Sainz, A.M., 1995. Granite emplacement during contemporary shortening and normal faulting: structural and magnetic study of the Veiga Massif (NW Spain). J. Struct. Geol. 12, 1689–1706.

Simancas, J.F., Carbonell, R., González-Lodeiro, F., Pérez-Estaún, A., Juhlin, C., Ayarza, P., Kashubin, A., Azor, A., Martínez-Poyatos, D., Almodóvar, G.R., Pascual, E., Sáez, R., Expósito, I., 2003. Crustal structure of the transpressional Variscan orogen of SW Iberia: SW Iberia deep seismic reflection profile (IBERSEIS). Tectonics 22, 1-1–1-19.

Simancas, J.F., Galindo-Zaldívar, J., Azor, A., 2000. Three-dimensional shape and emplacement of the Cardenchosa deformed pluton (Variscan Orogen, southwestern Iberian Massif). J. Struct. Geol. 22, 489–503.

Steeples, D.W., Green, A.G., McEvilly, T.V., Miller, R.D., Doll, W.C., 1997. A workshop examination of shallow seismic reflection surveying. Lead. Edge 63, 1641–1648.

Tryggvason, A., 1998. Seismic Tomography.Inversion for P- and S-Wave Velocities. PhD thesis, Uppsala University.

Yenes, M., Álvarez, F., Gutiérrez-Alonso, G., 1999. Granite emplacement in orogenic compressional conditions: the La Alberca-Béjar granitic area (Spanish Central System, Variscan Iberian Belt). J. Struct. Geol. 21, 1419–1440.

3. IMAGING LOW VELOCITY ANOMALIES WITH THE AID OF SEISMIC TOMOGRAPHY

I. Flecha, D. Martí, R. Carbonell, J. Escuder-Viruete and A. Pérez-Estaún,
Tectonophysics, 388, 225-238, 2004.

Available online at www.sciencedirect.com

SCIENCE DIRECT®

Tectonophysics 388 (2004) 225–238

TECTONOPHYSICS

www.elsevier.com/locate/tecto

Imaging low-velocity anomalies with the aid of seismic tomography

I. Flecha[a,*], D. Martí[a,1], R. Carbonell[a,1], J. Escuder-Viruete[b,2], A. Pérez-Estaún[a,1]

[a]*Departamento de Geofisica, Institut de Ciencies de la Terra "Jaume Almera"-CSIC, C/Lluis Solé i Sabaris s/n, 08028 Barcelona, Spain*
[b]*Departamento de Petrología y Geoquímica, Facultad de Ciencias Geológicas, Universidad Complutense, 28040 Madrid, Spain*

Received 18 July 2003; received in revised form 13 April 2004; accepted 13 June 2004

Abstract

Theoretical considerations (Snell's law) suggest that low-velocity fanomalies are undersampled and therefore should be poorly resolved by inversion schemes based on ray-tracing methods. A synthetic study considering a 40×20 m low-velocity anomaly (300 m/s) placed at the center of a 400×50 m block with gradient background velocity model (from 3000 m/s at the surface to 4000 m/s at the base) indicates that the low ray density in ray-tracing coverage diagrams of tomographic inversion studies can be used as evidence for the existence of low-velocity anomalies. Combined normal incidence seismic reflection images and the velocity models obtained by tomographic inversions of first-arrival travel times form an efficient scheme to resolve low-velocity anomalies such as fracture zones. Furthermore, the velocity models derived from tomographic inversions are used in a wave equation datuming algorithm to account for statics caused by a strongly laterally variable shallow surface (weathering) layer and provide seismic reflection images of fracture zones (low-velocity anomaly) within a granitic pluton.

Keywords: Low-velocity anomalies; Wave equation datuming; Seismic tomography; Synthetic travel times

1. Introduction

A large amount of human activity involves an interaction with the shallow subsurface; therefore, knowing its internal structure is a topic of major interest among Earth scientists. For example, the shallow subsurface is the host of our waste (toxic, nontoxic, radioactive, etc.), and from the shallow subsurface, we also obtain valuable natural resources such as water and minerals. Therefore, this layer is the target of environmental assessment studies. For the last 20 years, geophysical imaging of the shallow subsurface has been a rapidly evolving topic. Among the geophysical methodologies that have been applied to high-resolution imaging of the shallow subsurface, seismic techniques have been one of the most

* Corresponding author. Tel.: +34 93 409 54 10; fax: +34 93 411 00 12.
E-mail addresses: iflecha@ija.csic.es (I. Flecha), dmarti@ija.csic.es (D. Martí), rcarbo@ija.csic.es (R. Carbonell), escuder@geo.ucm.es (J. Escuder-Viruete), aperez@ija.csic.es (A. Pérez-Estaún).
[1] Tel.: +34 93 409 54 10; fax: +34 93 411 00 12.
[2] Tel.: +34 91 394 50 14; fax: +34 91 544 25 35.

0040-1951/$ - see front matter © 2004 Elsevier B.V. All rights reserved.
doi:10.1016/j.tecto.2004.04.031

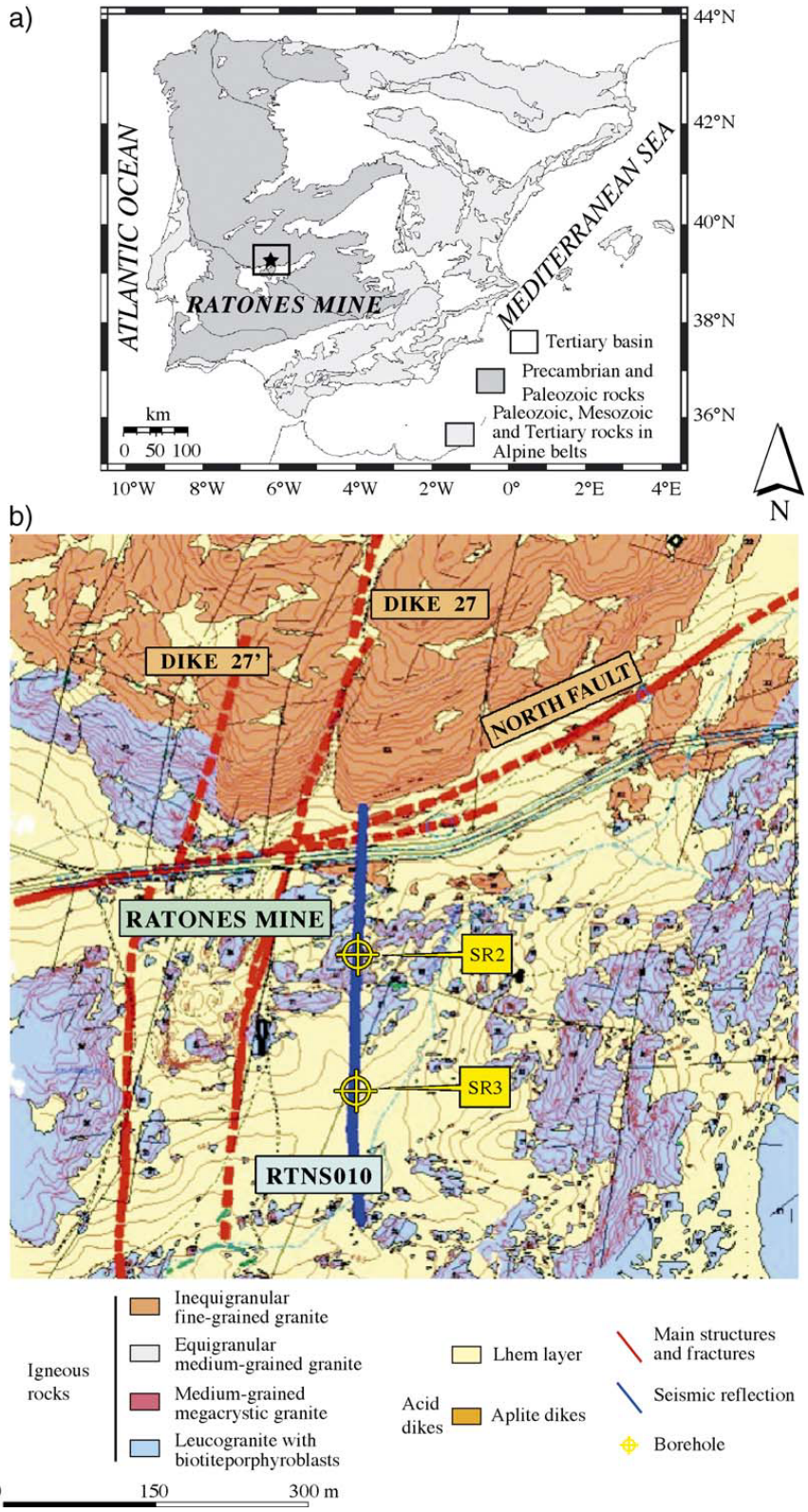

Fig. 1. (a) Simplified sketch map of the geology of the Iberian peninsula indicating the location of the Ratones mine. (b) Structural map of the study area, indicating the main structures (exploited dykes and NF). The location of the high resolution seismic reflection profile RTNS010 is indicated in blue. SR2 and SR3 indicate the location of the boreholes.

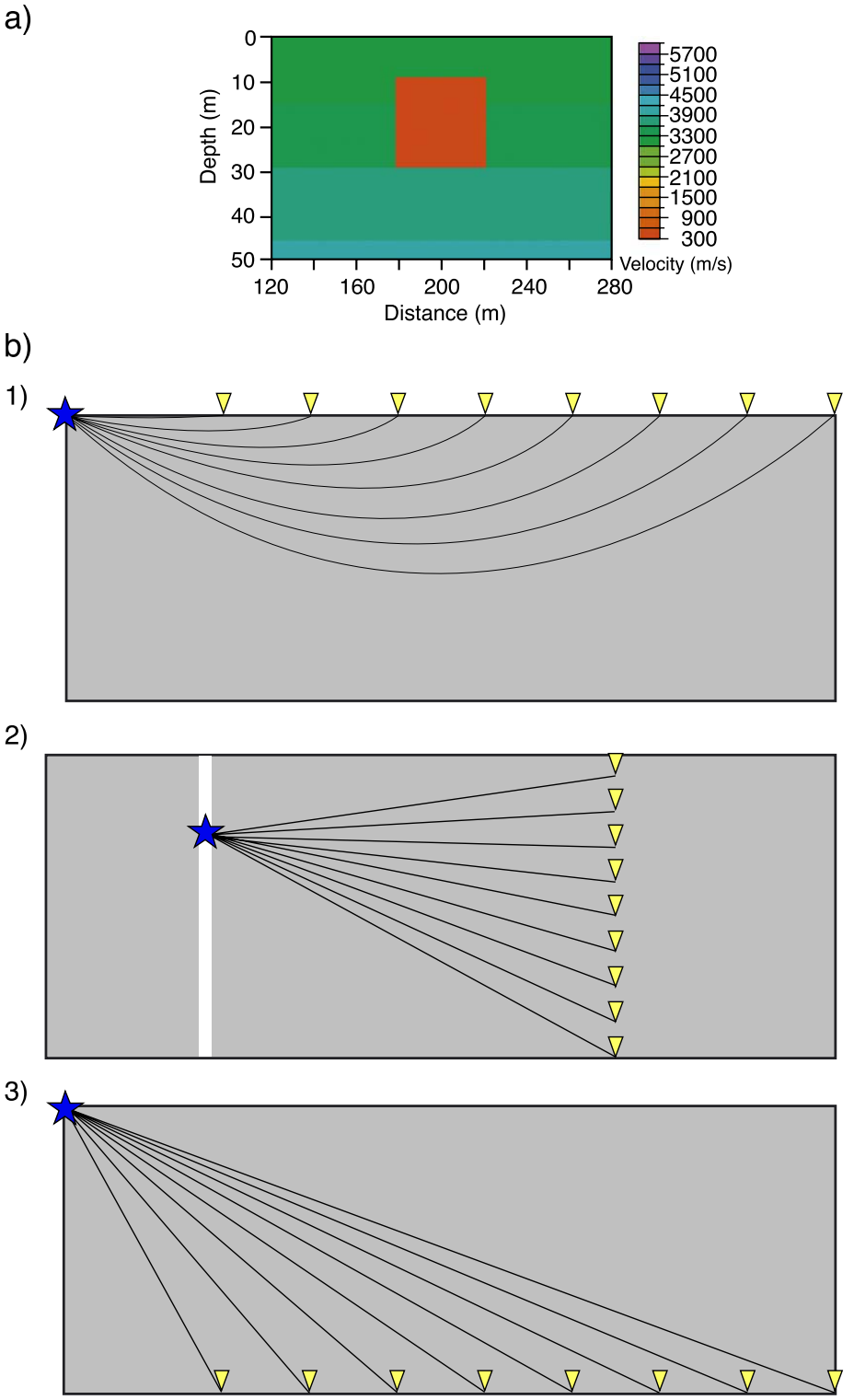

Fig. 2. (a) Theoretical velocity model used to generate synthetic data. This model has a cell of 2 m in length and 1 m in depth. (b) Geometries used to create synthetic data: (1) seismic reflection profile geometry, (2) crosshole geometry, sources and receivers inside wells. VSP geometry is like this case but with sources at the surface of the model and (3) geometry used to record data along the bottom of the model.

commonly employed and feature a large degree of success (Juhlin et al., 1991; Steeples, 1998; Morey and Schuster, 1999; Juhlin et al., 2000; Teixidó, 2000). The shallow subsurface is the zone that presents the largest variability in velocity constrasts. It is the most heterogeneous layer where most of the wave conversions and/or scattering phenomena take place (Kanasewich et al., 1983; Holliger and Robertsson, 1998). Low-velocity bodies are present within this layer (subterranean cavities, water flows or fractures).

Wave equation considerations imply that the heterogeneities and the velocity contrasts are responsible for the scattered energy, and ray bending breaks up the wavefront. All these disrupt the final image that can be produced by high-resolution shallow seismic techniques. In these cases, static corrections are a critical processing step. These static corrections need to be precise, and they require detailed knowledge of the velocity model and more than one trace to account for ray bending and scattered energy (Berryhill, 1979).

Within the research program of the Spanish radioactive waste managing company (ENRESA), we have tested, validated and studied the resolving power of several geophysical techniques to characterize heterogeneities in the shallow subsurface (Escuder-Viruete et al., 2001; Martí et al., 2002a,b; Escuder-Viruete et al., 2003a,b) in a granitic pluton located in the Variscan Iberian Massif (Julivert et al., 1966). The test site is an old abandoned uranium mine that exploited two subvertical dykes (27 and 27′) between 1955 and 1975 and has since been abandoned. The Albala granitic pluton can be described as a concentric zoned body elongated in the N–S direction. Surface geological mapping of the area of this pluton has revealed a complex network of subvertical faults and joints, which are indicative of a complex deformation pattern. The main surface geological feature is a 5 to 20 m variable width brittle, low-dipping (approximately 30°) fracture trending N072°E to N080°E known as the North Fault (NF) (Fig. 1). In order to image this low-velocity fracture zone, we use the NS oriented high-resolution seismic reflection profile "RTNS010" which intersects perpendicularly the trace of NF. Additional constraints were obtained from logs acquired in boreholes (SR2 and SR3) which intersect NF at depth (Fig. 1).

Imaging low-velocity anomalies using seismic techniques is the main objective of this paper. Therefore, we test the resolving power of high-resolution seismic tomography using synthetic data. The synthetic analysis indicates that low-velocity anomalies can be appropriately constrained by combining the stacked seismic image, the velocity model and the ray-tracing coverage diagrams. Furthermore, we use the seismic techniques to image the fracture network within a granitic pluton. The high-resolution seismic tomography provides a detailed velocity model of the shallow subsurface. This is used to perform wave equation consistent static corrections (wave equation datuming) which improve the seismic reflection images.

2. Synthetic study

2.1. Synthetic data set

In order to test the available travel time inversion schemes (Benz et al., 1996; Zelt and Barton, 1998), a series of synthetic data sets were obtained using a finite difference algorithm that simulates acoustic wave propagation in a two-dimensional velocity model. The model includes a 40×20 m low-velocity anomaly located within a 400×50 m background velocity field (Fig. 2a). This background velocity field consisted of a vertical gradient from 3000 m/s at surface to 4000 m/s at the base of the model, which was derived from results of previous studies in this area (Martí et al., 2002a,b). The cell size of

Fig. 3. (a) Wave propagation through the velocity model at different times for source located at x=0 and z=0. At 0.06 s, the wavefront reaches the anomalous zone undergoing a clear deformation (from 0.07 to 0.12 s). At 0.12 s, the perturbation has affected the whole model but for the inner anomaly zone. Note that diffractions caused by the low-velocity region, create a second wavefront, which will be detected in the shot gathers. (b) Some shot gathers from the surface synthetic data with the shot point placed at 0, 100 and 200 m. Everywhere, diffractions caused by the low-velocity anomaly are evident except for the case where the source is placed over the anomaly (x=200 m), which lacks the effects of the low-velocity zone. First arrivals delay are evident when sources are located far away from the anomalous zone, though this delay is not imaged when the source is over the low-velocity area (x=200 m).

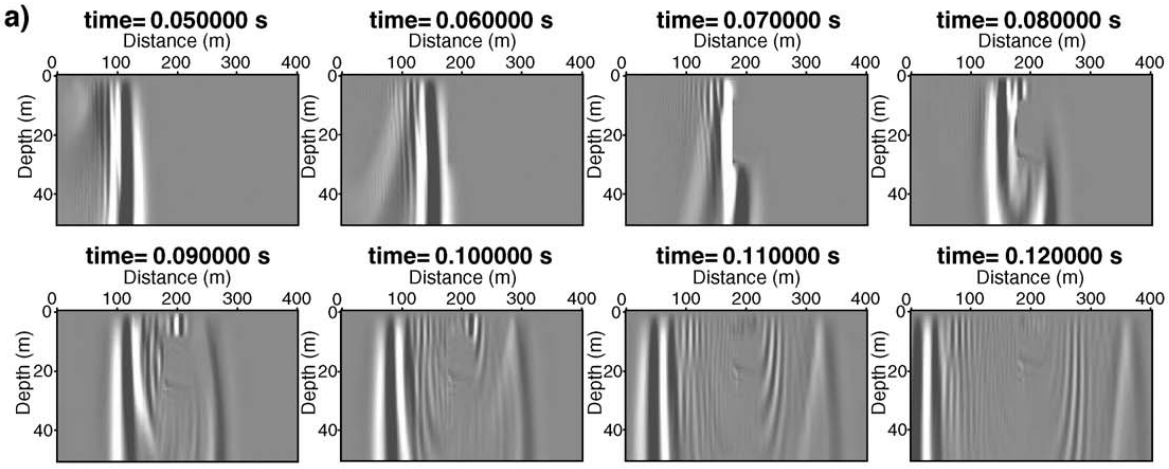
a)
time= 0.050000 s
time= 0.060000 s
time= 0.070000 s
time= 0.080000 s
time= 0.090000 s
time= 0.100000 s
time= 0.110000 s
time= 0.120000 s
Distance (m)
Depth (m)
0
100
200
300
400
20
40

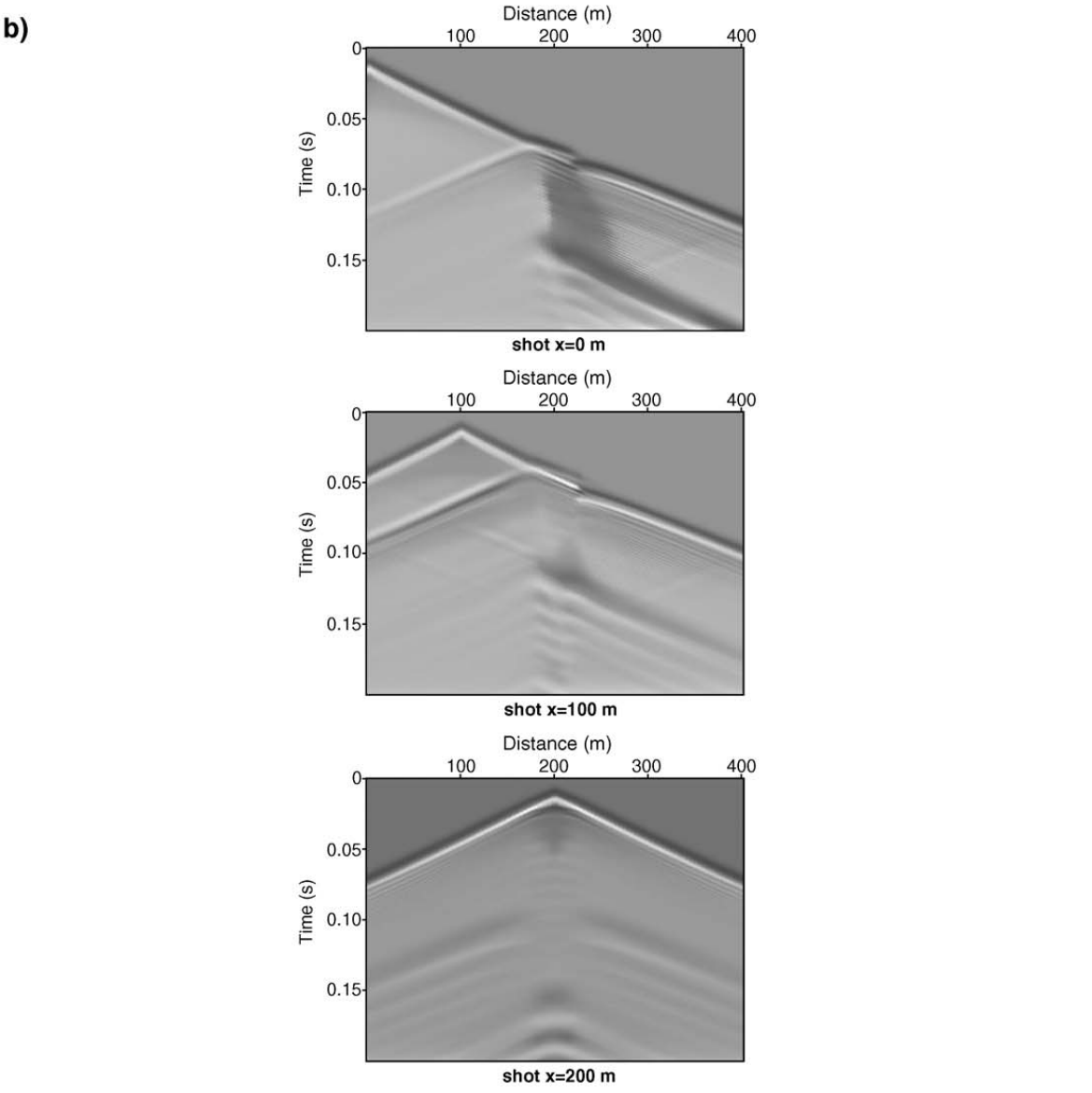
b)
Distance (m)
Time (s)
0
0.05
0.10
0.15
100
200
300
400
shot x=0 m
shot x=100 m
shot x=200 m

the model was 2×1 m. The source wavelet used, consisted of a maximum frequency at 150 Hz with a peak amplitude at 75 Hz. The data were recorded with a sampling rate of 0.125 m/s for 200 ms. The resulting first Fresnel zone radius is ≈15 m which assures that a 40-m anomaly must be imaged as an structure and not as an isolated diffraction point. To avoid the reflections from the limits of the model, absorbing boundary conditions were chosen. With these parameters different acquisition geometries were designed:

(a) A high-resolution seismic reflection profile acquired with sources located every 5 m and receivers every 2 m. Receivers cover the whole surface of the model; hence, 81 shot gathers with 200 traces were obtained (Fig. 2b, surface).
(b) Two vertical seismic profiles (VSPs) located at 100 and 300 m which cross vertically the whole model. Receivers were located every meter in depth and sources were placed at the surface as in data set 1 (Fig. 2b, VSP).
(c) Seismic data were also recorded along the base of the model. The sources were placed at the surface and the receivers located every 2 m at the base of the model (Fig. 2b, bottom). Although this acquisition geometry is not common, it has been used in some cases (Madrussani et al., 1999).

In order to follow the evolution of the wavefield through the model, several snapshots were stored. The snapshots (Fig. 3a) show the deformation undergone by the wavefront when it reaches the velocity anomaly, revealing the low-velocity anomaly as an area where there is weak propagation of the perturbation. This introduces a break in the first arrivals and a diffraction in the shot gathers (Fig. 3b). When the shot point is located immediately above the anomaly nothing is observed in the shot gathers. The first-arrival travel times from these data were inverted using seismic tomography.

2.2. High-resolution seismic tomography

The travel time picks of the first arrivals of the synthetic data were picked and inverted using two different 3D tomographic schemes: (A) Benz et al. (1996) and (B) Zelt and Barton (1998) (case of gradient based scheme). In the forward problem, these schemes use different modifications of the finite difference algorithm proposed by Vidale (1990) to solve the eikonal equation: Podvin and Lecomte (1991) for scheme A and Hole and Zelt (1995) for scheme B. Both of them use the LSQR method (Paige and Saunders, 1982) to solve the inverse problem. No noise was added to the synthetic data so that automatic picking of the first arrivals could be done. As a starting model in the inversion schemes a 400×40×80 m 3D volume (sampled by 2×2×2 m cubic cells) with a background vertical velocity gradient (from 3000 m/s at the surface to 4000 m/s at the base) was used.

In order to evaluate the resolution of the low-velocity anomaly, three data sets were used (Fig. 4): data set 1 which included all the available seismic data obtained using all the acquisition geometries; data set 2 which included the data obtained at the surface and the VSP data (geometries a and b); and data set 3 which consisted only of the surface seismic profile (geometry a).

2.3. Velocity models

The results obtained by both inversion schemes are qualitatively equivalent although it is possible to establish some differences. After inverting data set 1, accurate velocity models are obtained (Fig. 4). Both algorithms resolve a smooth geometry for the low-velocity anomaly at the correct location. Nevertheless, the velocity is higher (1500 m/s) than the model velocity (300 m/s). The ray-tracing diagram reveals a central area with low ray coverage.

The velocity models obtained by inverting data set 2 result in an area with a small decrease in the

Fig. 4. Velocity models obtained by the tomographic inversions (top) and the respective ray coverage diagram (bottom). (A) and (B) indicate that the results were obtained by the inversion schemes of Benz et al. (1996) and Zelt and Barton (1998), respectively; (C) indicates the ray coverage diagram. From top to bottom, three data sets are considered. Data set 1: An ideal data set which includes the seismic data acquired: at the surface and at the base of the models and it also includes the VSP data. Data set 2: Consists of the data acquired at the surface and the VSP data. Data set 3: Consists only of the seismic data acquired at the surface.

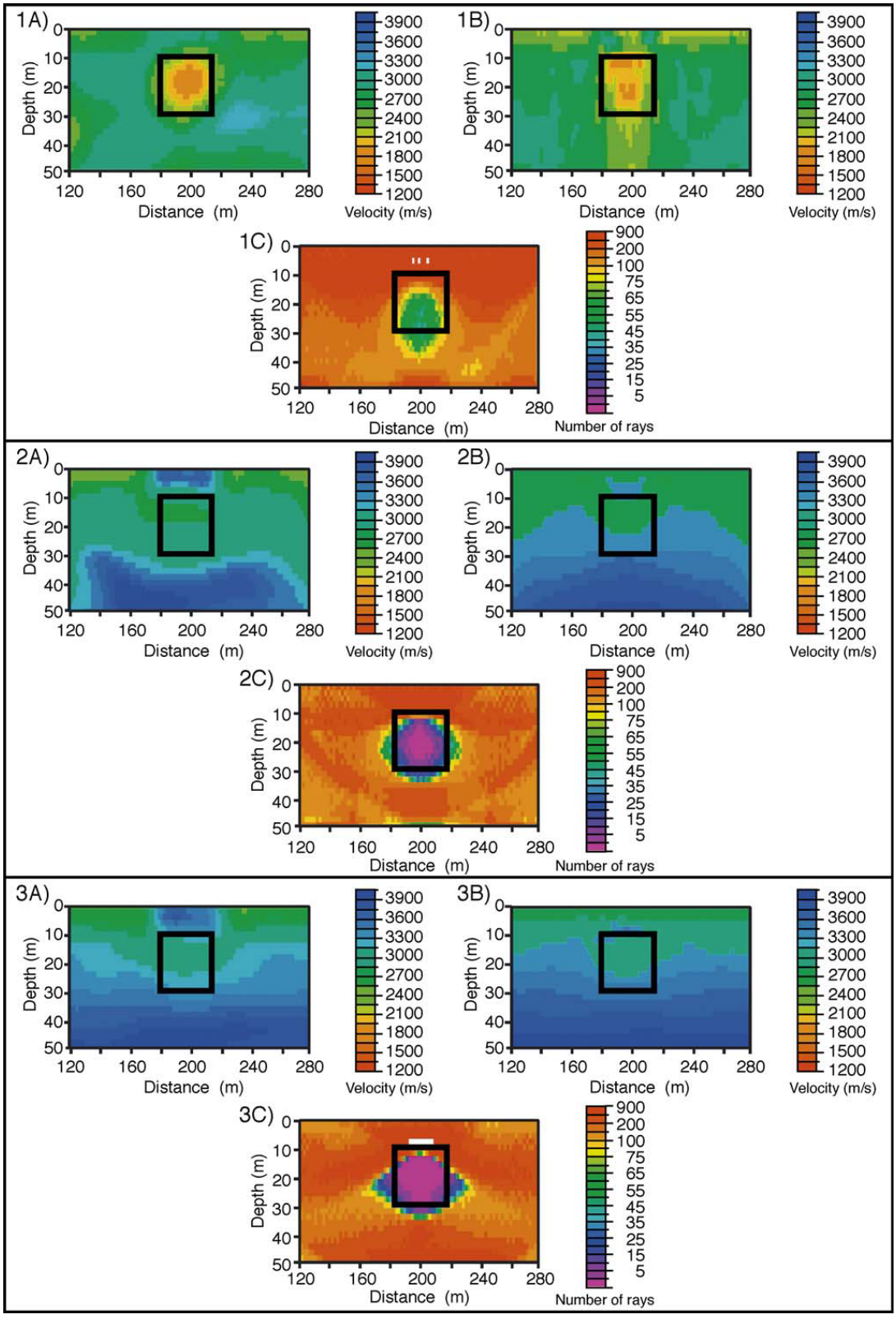
1A)
1B)
1C)
2A)
2B)
2C)
3A)
3B)
3C)
Depth (m)
Distance (m)
Velocity (m/s)
Number of rays
0
10
20
30
40
50
120
160
200
240
280
3900
3600
3300
3000
2700
2400
2100
1800
1500
1200
900
200
100
75
65
55
45
35
25
15
5

velocity. The geometry of the low-velocity anomaly is not well defined (Fig. 4). Again the ray-tracing coverage diagram reveals an area with low ray density which is characteristic of the low-velocity anomalies. Thus, the location and size of the low-velocity anomaly are resolved by the ray density diagrams.

The velocity models obtained by inverting data set 3 reveal an even less clearly defined low-velocity anomaly because this data set lacks the lateral constraints provided by the VSP data. The ray coverage diagram reveals an area of low ray density which is larger than the velocity anomaly.

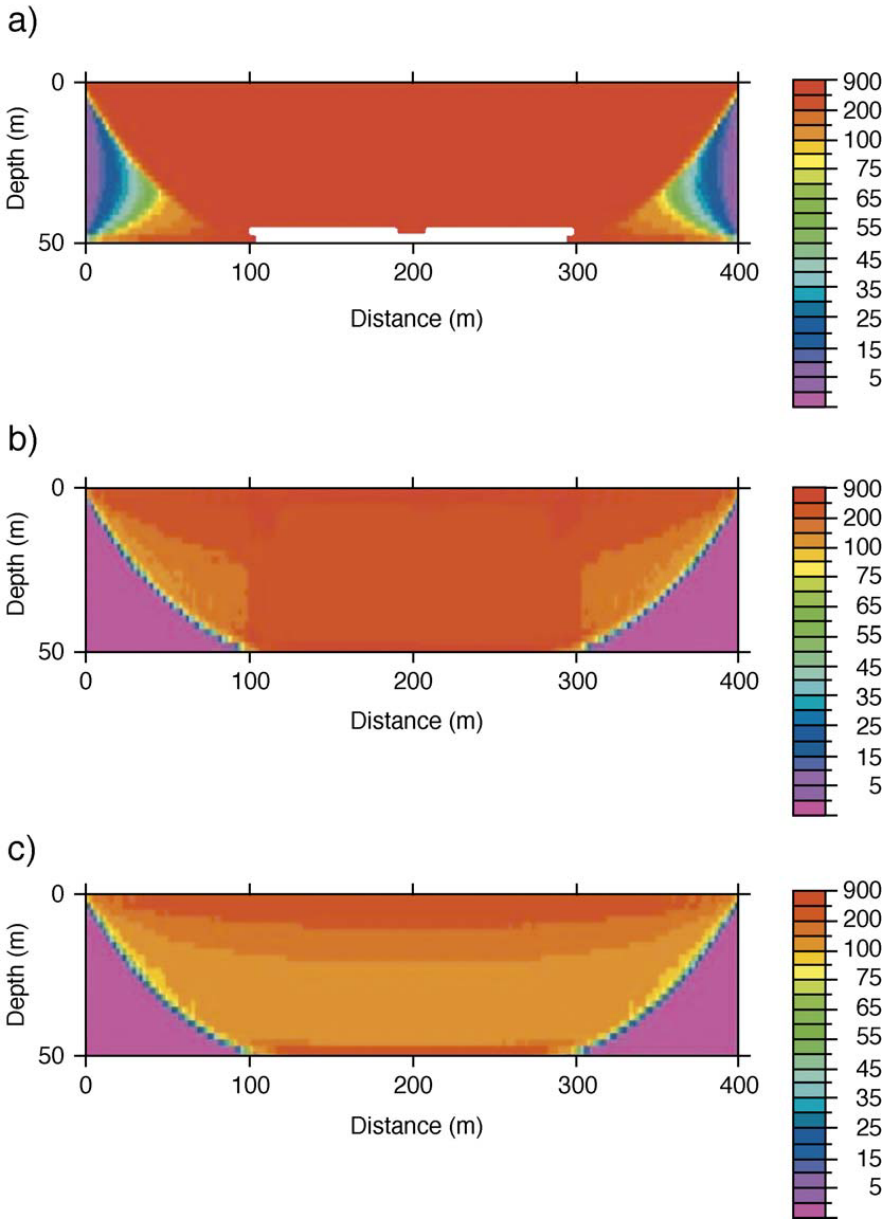

Fig. 5. Ray coverage calculated with the background velocity model (this model lacks the low-velocity anomaly) for the case of: (a) data set 1 which consists of the seismic data acquired at the surface, the seismic data acquired at the base of the model and the VSP data; (b) data set 2 which consists of the data acquired at the surface and the VSP; and (c) data set 3 which consists only of the data acquired at the surface. These three diagrams indicate that a model lacking a low-velocity anomaly is regularly sampled by rays of the three data sets. However, the best sampled case is (a) data set 1.

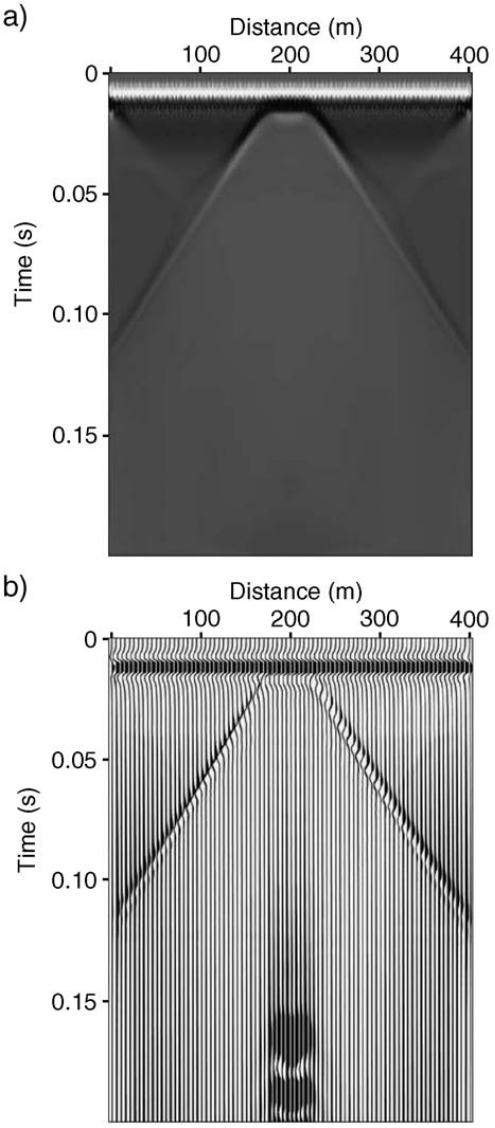

Fig. 6. Seismic images obtained using the 81 surface shot gathers: (a) stacked section and b) common offset section (zero offset) corrected for geometric spreading. In both sections, diffractions reveal the effect of the vertical structures and limit the horizontal range of the anomalous body. At about 0.02 s and between 180 and 220 m, the reflector caused by the top interface of the anomaly can be identified. The common offset section provides an additional event at 0.16 s that corresponds to bottom boundary of the anomaly.

The ray density diagrams for the starting velocity models which lack the low-velocity anomaly indicate that the central area of the model is properly imaged by the rays in all the data sets (1, 2 and 3; Fig. 5), suggesting that any anomaly located there would be detected. Nevertheless, the snapshots indicate that the wavefronts do not propagate through the anomaly; only the perturbations due to the large velocity contrast at the edges of the anomaly are recorded as first arrivals in the shot gathers. Therefore, the ray-tracing coverage diagrams can be appropriately used to determine the approximate geometry and location of the low-velocity anomalies.

2.4. Normal incidence seismic image

At normal incidence, high- over low-velocity interfaces are imaged by seismic reflection sections. Therefore, a normal incidence seismic image was obtained using the synthetic data (data set 3). A standard processing flow was used for the 2D acquisition geometry. The data were sorted into CDPs, and the background velocity model was used for the NMO corrections.

The normal incidence stacked section (Fig. 6) reveals diffractions at both sides of the anomaly, constraining the horizontal extent of the low-velocity anomaly. The top interface of the anomaly is defined by a reflection located at 30 ms and between 180 and 220 m. Nevertheless, the base of the anomaly is not imaged by the stacked section. Only for a single-fold stack consisting of the zero offset traces corrected for spherical spreading is the base of the model imaged (Fig. 6). Constant offset stacks, especially zero offset, need to be considered when constraining low-velocity anomalies.

3. Low-velocity zones in seismic reflection data: imaging fracture zones

The high-resolution seismic profile RTNS010 was used to image the NF located in the Albalá granitic pluton (Fig. 1). RTNS010 is a 480-m-long profile with a receiver and shot interval of 5 m. The instrumenta-

Table 1
Initial processing flow

(1) Geometry
(2) Trace editing and surface wave attenuation
(3) First break picking
(4) Static corrections
(5) Band-pass filter and F–K filter
(6) CDP sort
(7) Velocity analysis
(8) NMO
(9) Stack

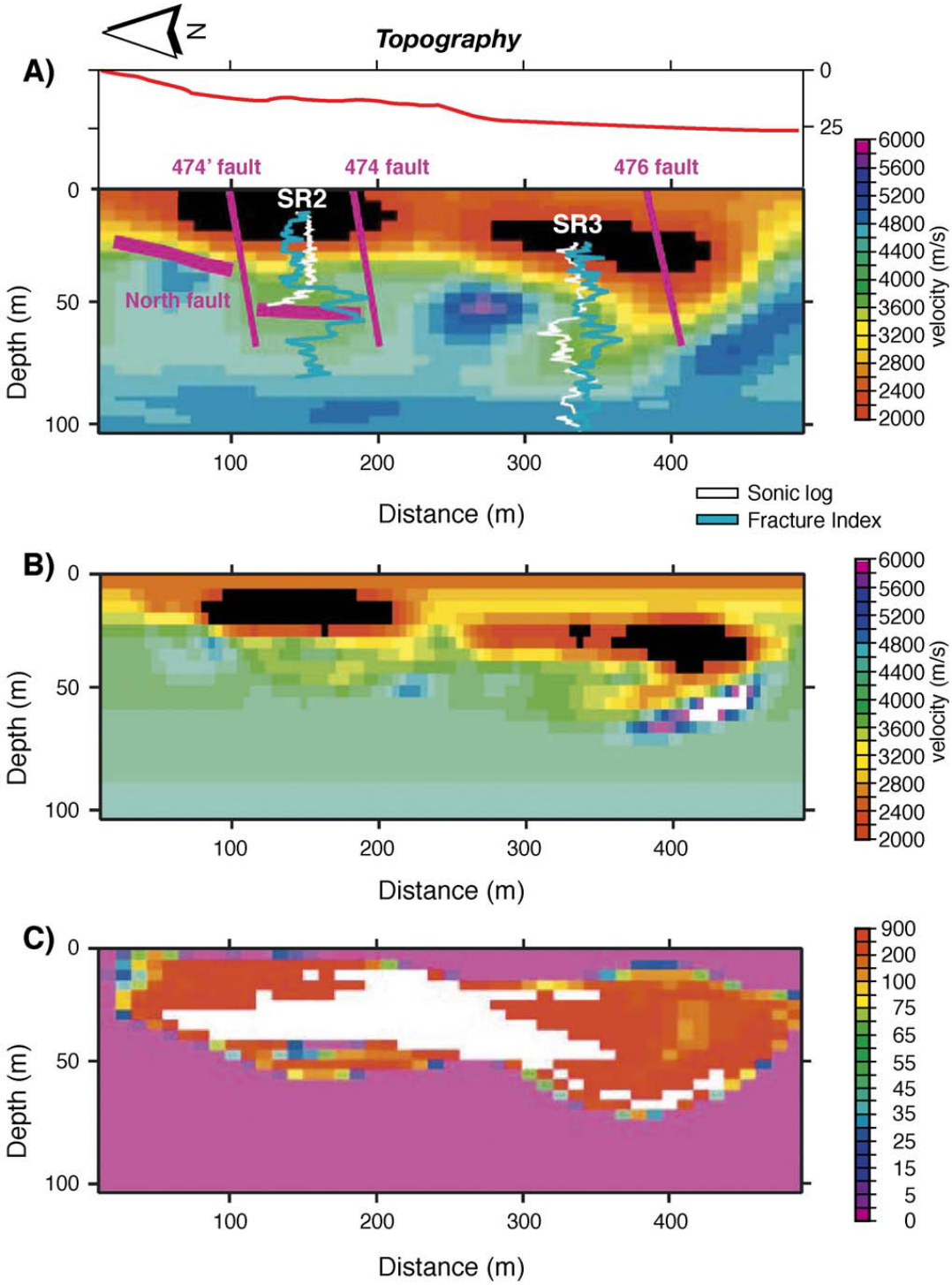

Fig. 7. Ray path diagrams and velocity models along the seismic profile RTNS010 obtained with two different tomographic inversion codes. The shallow low-velocity layer (red colors) is interpreted as the unconsolidated weathered layer. Black colors are out of scale and match velocities under 2000 m/s. On the other hand, white colors in the ray coverage diagram show values over 900 hits. The North Fault in pink is identified by relatively low velocities (green color) which correlate with high values of the fracture index logs (in white) at the base of the boreholes SR2 and SR3. Also, the NF is indicated by a decrease in the P-wave velocities determined from the sonic logs. (A) Velocity model that resulted from inversion scheme A (Benz et al., 1996). (B) Velocity model resulted of the inversion scheme B (Zelt and Barton, 1998). (C) Ray coverage diagram.

tion used was a 48-channel Bison seismograph, resulting in a total number of 96 stations and 94 shots, and an average of 13-fold CDP coverage. A sledge hammer was used as a source with frequencies between 30 and 120 Hz. In the initial processing of the RTNS010 seismic profile a conventional processing flow was used (Table 1). The data are characterized by low signal-to-noise (S/N) ratio, lateral velocity variations, scattered energy produced by the unconsolidated surface layer, and numerous diffractions due to subvertical joints and fractures. The NF is poorly defined in the initial stacked sections.

3.1. Velocity models derived by seismic tomography

Following the results of the synthetic tests a tomographic inversion of the first arrivals was attempted. Tomographic inversions proved to be successful in the area in previous studies (Martí et al., 2002a,b). The tomographic images obtained by the inversion schemes (A and B) of the RTNS010 seismic profile display small differences (Fig. 7). However, the velocity model resulting from scheme B displays better definition of the structures. This model reveals the presence of an unconsolidated weathered layer of laterally variable thickness and features low velocities within the range 2000 to 3500 m/s. This corresponds to the lehm cover characteristic of the mine site. The shallow low-velocity layer thickens towards the south and two relatively low-velocity anomalies are located around boreholes SR2 and SR3 at approximately 50- and 75-m depth, respectively (light green in Fig. 7). These relatively low velocities (of approximately 3500 m/s) correlate with prominent low P-wave velocities derived from the sonic logs, and picks of the fracture index logs (Fig. 7). The

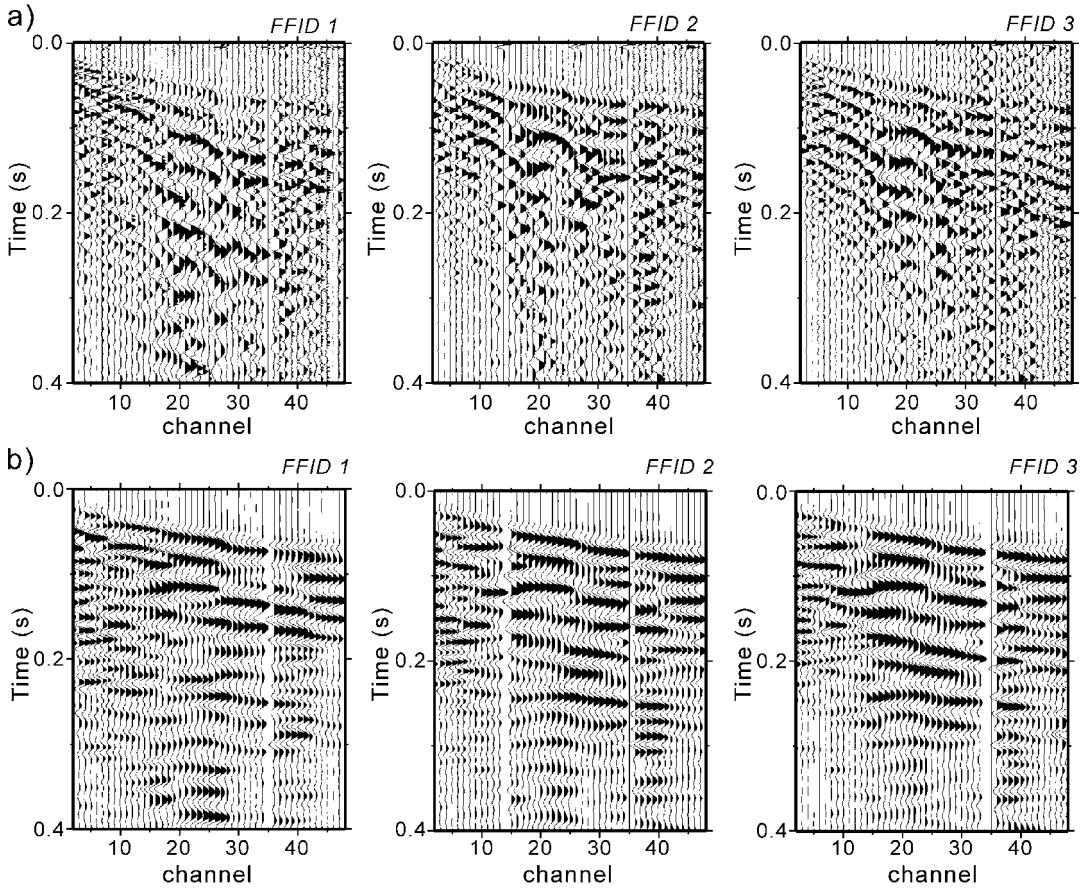

Fig. 8. Shot gathers recorded in RTNS010 seismic reflection profile: (a) conventional processing flow (with conventional statics), (b) after applying prestack wave equation datuming.

complementary standard logging data of two wells provide additional constraints for the interpretation of the tomographic images along RTNS010 seismic profile.

These correlations indicate that it probably corresponds to a major fracture zone (the NF). This anomaly is limited by two subvertical faults labeled 474 and 474′ (Fig. 7). The 476 fault can be also inferred as a vertical southern termination of the low-velocity anomaly located beneath the SR3.

3.2. Wave equation based static corrections

The strongly heterogeneous low-velocity layer generates a nonhyperbolic move-out of the seismic reflections, a product of the ray bending due to the nonvertical propagation of the waves through this layer. This causes delays in the arrivals of the different reflections, and the deeper interfaces lose their spatial continuity. Velocity replacement of this heterogeneous low-velocity layer applied before stack using wave

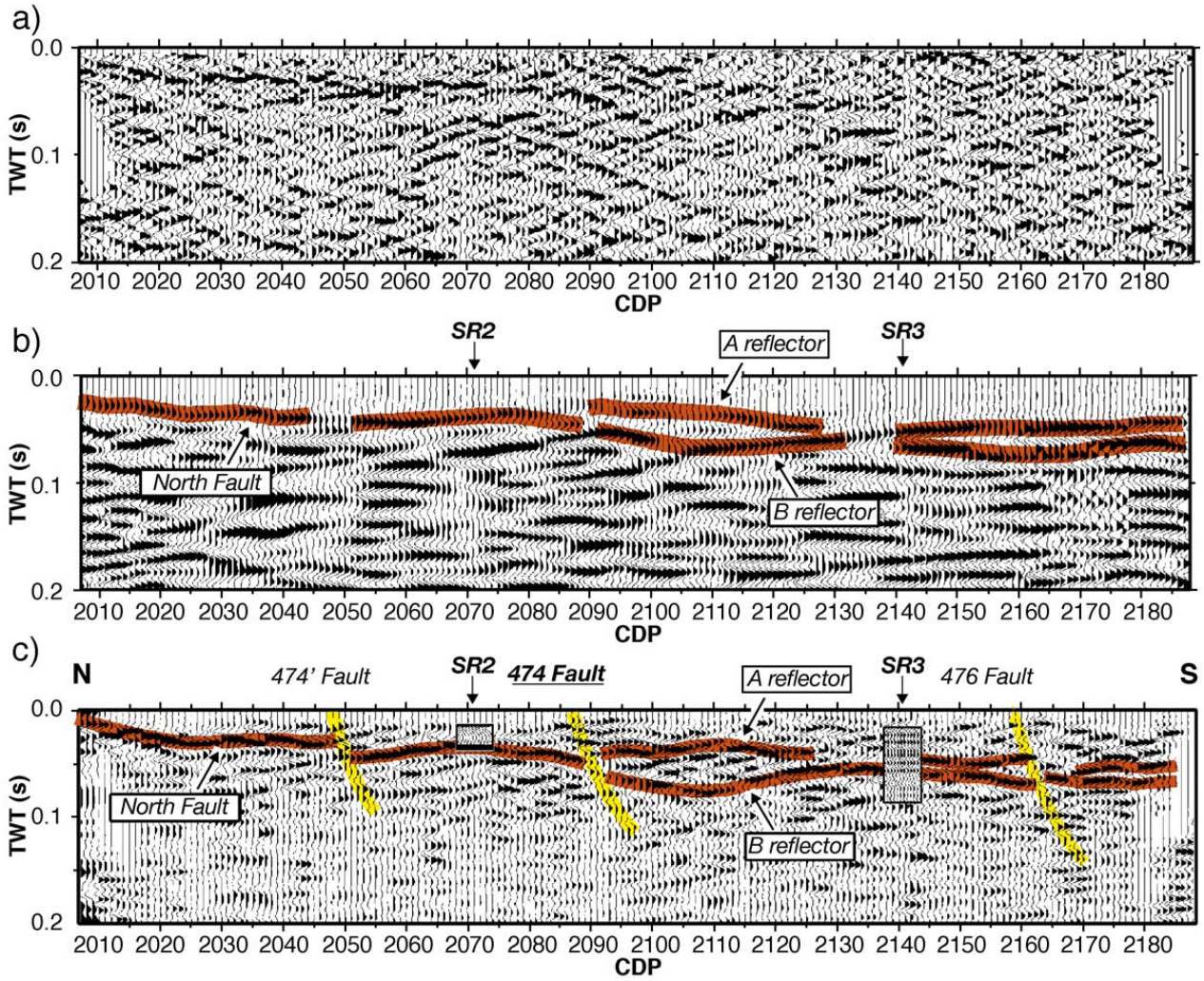

Fig. 9. RTNS010 seismic reflection profile under different processing flows: (a) conventional processing flow which included NMO and stack after refraction statics, (b) NMO and stack after wave equation datuming, (c) migrated seismic profile showing the location of SR-2 and SR-3 VSP records (small rectangles). The synthetic seismograms of SR2 and SR3 are superimposed on the time migrated section of RTNS010. The velocity model used in the migration was obtained from the sonic logs available along the seismic profile. The results show the prominent shallow reflection dipping to the South that can be correlated with the North Fault. The subvertical faults 474′ , 474, 476 identified from outcrops are also marked.

equation datuming can increase the lateral continuity of reflections (Yilmaz and Lucas, 1986).

Wave equation datuming is the upward/downward continuation of the seismic data to a new flat reference datum (Berryhill, 1979; Bevc, 1997). The advantage of using wave equation datuming over static corrections is that it properly propagates the recorded wavefield to the final datum, instead of applying time shifts to the data traces (Shtivelman and Canning, 1988). This procedure increases the signal-to-noise (S/N) ratio of the shot gathers and restores the reflections and diffractions, providing improved stacked seismic sections. Prestack wave equation datuming is particularly appropriate for data sets characterized by strongly variable near-surface velocities and rugged topography.

Following Berryhill (1979), the seismic data need to be downward continued to a specific horizontal datum located below the layer whose effect must be removed (Schneider et al., 1995; Zhu et al., 1998). Then the traces are upward, continued to a final datum (the datum used in the elevation statics) using a constant velocity which is the estimated velocity for the base of the low-velocity layer, 3500 m/s in this case. This procedure needs to be done twice, once for shot gathers and once for receiver gathers.

The velocity model obtained by the tomographic inversion provides a detailed representation of velocity model of the shallow surface which can be used in the wave equation datuming algorithm (Pratt and Goulty, 1991). Wave equation datuming accounts for the static corrections, removing the effects of the strongly laterally variable shallow surface layer. The shot gathers after wave equation datuming present stronger events with increased continuity (Fig. 8).

The corrected traces produced an improved stacked image where the main feature, the NF, can be identified as a prominent reflection dipping towards the south (Fig. 9). In the stacked section after wave equation datuming, the NF can be traced from the outcrop at surface to the base of SR2 and to the base of SR3. This is suggested by the synthetic seismograms estimated from the sonic logs (Fig. 9). The lateral continuity of the reflection has been improved particularly beyond the CMP 2110, where the low-velocity layer is thicker. The interpretation of the prominent reflector as NF is based on its intersection with the surface and the correlation between the reflection and the synthetic seismogram generated in SR2. Furthermore, geostatistical modeling also supports this interpretation (Escuder-Viruete et al., 2001; Escuder-Viruete et al., 2003a,b). The stacked section after wave equation datuming and the migrated section suggest that the internal structure of the NF varies laterally, producing a continuous reflector in some parts of the profile (CMP 2050–2090), while in other cases, the reflection splits into several events (CMP 2100–2130). The lateral change in the NF reflector is most probably a result of the subvertical faults (474 and 474′) mapped at the surface.

4. Conclusions

High-resolution tomographic inversion of first arrivals can be used to determine low-velocity anomalies. The velocity values of the low-velocity anomalies are theoretically not well resolved by this technique. However, the location and the size can be constrained by using the ray density diagrams. This can be done because the low-velocity anomalies are undersampled by the rays. Normal incidence seismic reflection sections image the top of low-velocity zones, while low-fold stacks produced by zero-offset traces can provide constraints on the base of low-velocity zones. The combination of high-resolution tomography of first arrivals and seismic reflection stacks has imaged successfully low-velocity zones corresponding to the NF, a low dipping laterally variable fracture zone within the Albalá granitic pluton (SW Iberia). This interpretation has been further constrained by geophysical logging in boreholes (P-wave velocity logs and fracture index logs available from the test site). Tomographic velocity models can be used to increase the S/N ratio and the lateral correlation of seismic reflection images by using the wave equation based static corrections (wave equation datuming).

References

Benz, H.M., Chouet, B.A., Dawson, P.B., Lahr, J.C., Page, R.A., Hole, J.A., 1996. Three dimensional P and S wave velocity structure of Redout Volcano, Alaska. J. Geophys. Res. 101, 8111–8128.

Berryhill, J.R., 1979. Wave equation datuming. Geophysics 44, 1329–1344.

Bevc, D., 1997. Flooding the topography: wave-equation datuming of land data with rugged acquisition topography. Geophysics 62-5, 1558–1569.

Escuder-Viruete, J., Carbonell, R., Jurado, M.J., Martí, D., Pérez-Estaún, A., 2001. Two dimensional geostatistical modelling and prediction of the fracture system in the Albalá Granitic Pluton SW Iberian Massif, Spain. J. Struct. Geol. 23, 2011–2023.

Escuder-Viruete, J., Carbonell, R., Martí, D., Jurado, M.J., Pérez-Estaún, A., 2003a. Architecture of fault zones determined from outcrop, cores, 3-D seismic tomography and geostatistical modeling: example from the Albalá Granitic Pluton, SW Iberian Variscan Massif. Tectonophysics 361, 97–120.

Escuder-Viruete, J., Carbonell, R., Martí, D., Pérez-Estaún, A., 2003b. 3-D stochastic modeling and simulation of fault zones in the Albalá Granitic Pluton, SW Iberian Variscan Massif. J. Struct. Geol. 25, 1487–1506.

Hole, J.A., Zelt, B.C., 1995. 3-D finite-difference reflection travel times. Geophys. J. Int. 121, 427–434.

Holliger, K., Robertsson, J.O.A., 1998. Effects of the shallow subsurface on upper crustal seismic reflection images. Tectonophysics 286, 161–169.

Juhlin, C., Lindgren, J., Collini, B., 1991. Interpretation of seismic reflection and borehole data from Precambrian rocks in the Dala Sandstone area, Central Sweden. First Break 9, 24–36.

Juhlin, C., Palm, H., Müllern, C., Wallberg, B., 2000. High resolution reflection seismics applied to detection of groundwater resources in glacial deposits, Sweden. Geophys. Res. Lett. 27, 1575–1578.

Julivert, M., Fontboté, J.M., Ribeiro, A., Nabais-Conde, L.E., 1966. Mapa tectónico de la Península Ibérica y Baleares. Inst. Geológico y Minero, Spain. 1:1000000.

Kanasewich, E.R., Kelamis, P.G., Abramovici, F., 1983. Exact seismograms for a point source using generalized ray theory. Geophysics 48, 1421–1427.

Madrussani, G., Böhm, G., Vesnaver, A., Schena, G., 1999. Tomographic detection of cavities in mines for acid drainage control. Eur. J. Environ. Eng. Geophys. 3, 115–130.

Martí, D., Carbonell, R., Trygsvason, A., Escuder, J., Pérez-Estaún, A., 2002a. Mapping brittle fractures zones in 3 dimensions: high resolution travel time seismic tomography in a granitic pluton. Geophys. J. Int. 149, 95–105.

Martí, D., Carbonell, R., Trygsvason, A., Escuder, J., Pérez-Estaún, A., 2002b. Calibrating 3D tomograms of a granitic pluton. Geophys. Res. Lett. 29 (17), 15-1–15-4.

Morey, D., Schuster, G.T., 1999. Paleoseismicity of the Oquirrh fault, Utah from shallow seismic tomography. Geophys. J. Int. 138, 25–35.

Paige, C.C., Saunders, M.A., 1982. LSQR: an algorithm for sparse linear equations and sparse least squares. ACM Trans. Math. Softw. 8, 43–71.

Podvin, P., Lecomte, I., 1991. Finite-difference computation of traveltimes in very contrasted velocity models: a massively parallel approach and its associated tools. Geophys. J. Int. 105, 271–284.

Pratt, R.G., Goulty, N.R., 1991. Combining wave-equation imaging with traveltime tomography to form high-resolution images from crosshole data. Geophysics 56, 208–224.

Schneider, W.A., Phillip, L.D., Paal, E.F., 1995. Wave-equation velocity replacement of the low-velocity layer for overthrust-belt data. Geophysics 60, 573–579.

Shtivelman, V., Canning, A., 1988. Datum correction by wave-equation extrapolation. Geophysics 53, 1311–1322.

Steeples, D.W., 1998. Shallow seismic reflection section-introduction. Geophysics 63, 1210–1212.

Teixidó, T., 2000. Caracterització del subsol mitjançant sísmica de reflexió d'alta resolució. PhD thesis, Universitat de Barcelona.

Vidale, J.E., 1990. Finite-difference calculation of traveltimes in three dimensions. Geophysics 55, 521–526.

Yilmaz, O., Lucas, D., 1986. Prestack layer replacement. Geophysics 51, 1355–1369.

Zelt, C.A., Barton, P.J., 1998. Three-dimensional seismic refraction tomography: a comparison of two methods applied to data from the Faeroe Basin. J. Geophys. Res. 103, 7187–7210.

Zhu, X., Angstman, B.G., Sixta, D.P., 1998. Overthrust imaging with tomo-datuming: a case study. Geophysics 63, 25–40.

4. STUDY ON THE LIMITATIONS OF TRAVELTIME INVERSION IN THE PRESENCE OF EXTREME VELOCITY ANOMALIES

I. Flecha, R. Carbonell, R. Hobbs and H. Zeyen.

Submitted to *Solid Earth*

Limitations of traveltime inversion in the presence of extreme velocity anomalies

I. Flecha[a], R. Carbonell[a] and R. W. Hobbs[b]

[a]Departament de Geofísica i Tectònica, Institut de Ciències de la Terra "Jaume Almera"-CSIC.

[b]Dept. of Earth Sciences, Univ. of Durham.

Abstract

The difficulties of seismic imaging beneath high velocity structures are widely recognised. In this setting, theoretical analysis of synthetic wide-angle seismic reflection data indicates that velocity models are not well constrained. A two-dimensional velocity model was built to simulate a simplified structural geometry given by a basaltic wedge placed within a sedimentary sequence. This model reproduces the geological setting in areas of special interest for the oil industry as the Faroe-Shetland Basin. A wide-angle synthetic dataset was calculated on this model using an elastic finite difference scheme. This dataset provided travel times for tomographic inversions. Results show that the original model can not be completely resolved without considering additional information. The resolution of nonlinear inversions lacks a functional mathematical relationship, therefore, statistical approaches are required. Stochastical tests based on Metropolis techniques support the need of additional information to properly resolve subbasalt structures.

1. Introduction

Subsalt and subbasalt imaging has been a key objective during the last 2 decades for the oil exploration (Rousseau et al., 2003; Williamson, 2003; Sava and Biondi, 2004). Oil exploration has revealed the imaging difficulties in the presence of high velocity features (such as salt and/or basalts). Low velocity structures under relatively high velocity features are poorly constrained by conventional processing and/or inversion schemes (Flecha et al., 2004). Velocity provides the link between seismic images and rock types. Ray tracing theory, based on Fermat's principle, states that regions surrounded by higher velocities are undersampled by rays. Seismic images of the subsurface strongly benefit from well resolved estimation of seismic velocities. These seismic velocities are currently determined by velocity analysis and, in the best case, by travel time tomography (or by the inversion of travel time of first arrivals) of wide-angle seismic reflection/refraction shotgathers (Zelt and Smith, 1992). The determination of the velocity models requires the interpretation/identification of the seismic arrivals within a shotgather. Furthermore, the

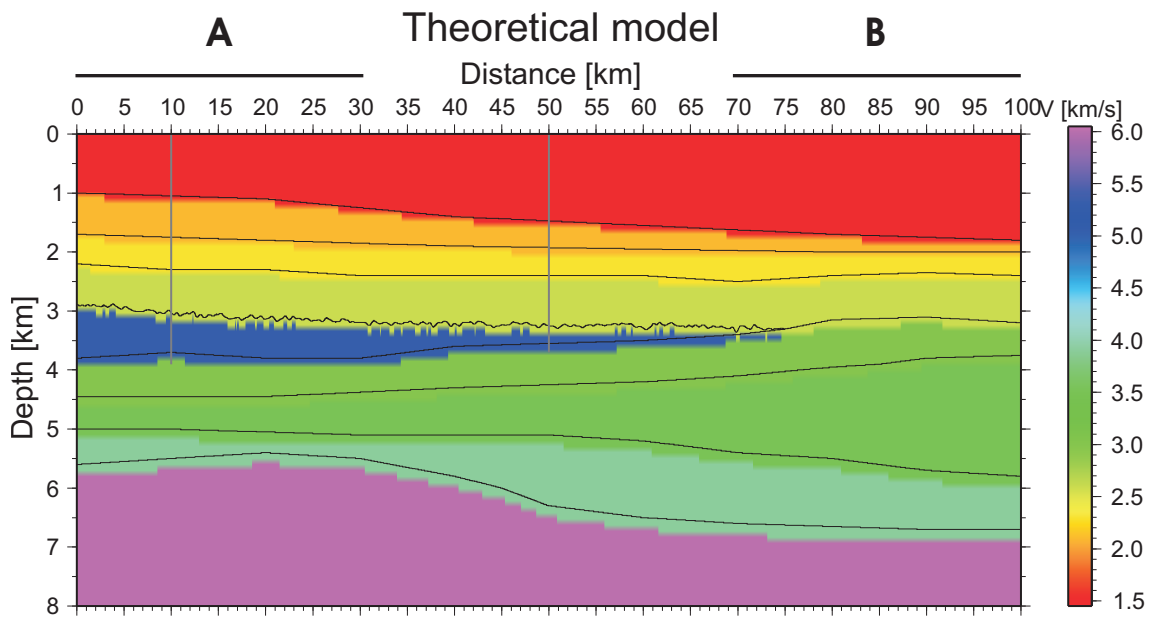

Fig. 4.1: *Synthetic velocity model resampled using 100 x 100 m squared cells. The original model used to run simulations was sampled by 10 x 10 squared cells. Vertical lines at 10 and 50 km show the location of hypothetical wells drilled through the basalt layer. Thus at this points, the thickness of the basaltic wedge was known. This information was used in the inversion (see text for more explanation)*

mathematical inversion schemes require digitized travel times, offset pairs, to calculate velocities. Usually, a standard crustal velocity model features an increasing velocity in depth, however in the presence of salt and/or basaltic intrusions this assumption fails. Intrusions often represent the emplacement of a high velocity body in the crust, therefore zones beneath these structures may feature low velocities. This is the case of basalt covered areas as erupted basalt buries previous structures that may feature low velocities such as in the Faroe Shelf. In the Faroe Shelf, covered areas represent potential hydrocarbon reservoirs, therefore this topic is of special interest for the industry.

This manuscript developes a theoretical study investigating the reliability and efectiveness of travel time inversion of wide-angle seismic reflection/refraction data. We investigated when and to what extent the low velocity structure beneath a high velocity basalt layer can be resolved.

2. Geological setting and imaging problems

In the Faroe-Shetland Basin, Mesozoic and Tertiary sedimentary sequences fill the basin but, close to the Faroe Shelf, these sedimentary sequences are covered by Paleocene-

Eocene basaltic lavas of which the Faroe Islands are composed. The previous topography of the basin was dominated by normal faults as a consequence of the extension and subsidence during Cretaceous and Paleocene (Richardson et al., 1999). As huge amounts of molten rock were extruded, after filling the lows between fault blocks, lava flows extended over long distances in the basin. Basalt flows were erupted in several episodes and three major units have been identified: Lower, Middle and Upper Series. The composition and thickness differs from one unit to another. Moreover, in periods without igneous activity, lacustrine shales and coals were accumulated and sediments were emplaced filling the basin floor deeps (White et al., 2003).

Velocities and densities in the synthetic model			
Layer	V_p	V_s	ρ
Water	1.5	0.86	1.0
Sediment1	2.1	1.21	2.20
Sediment2	2.3	1.33	2.24
Sediment3	2.6	1.50	2.29
Basalt	5.3	3.06	2.75
Sediment4	3.0	1.73	2.36
Sediment5	3.5	2.02	2.44
Sediment6	3.9	2.25	2.51
Basement	6.0	3.46	2.86

Table 4.1: *Velocities and densities used in the synthetic model. Physical properties were taken from (Carmichael, 1982). The Poisson ratio was 0.25 and the density was calculated using the Christensen relation (Christensen and Mooney, 1995):* $\rho = 1.85 + 0.169V_p$

In the Faroe Shelf, geologic and geophysical data suggest that a layer of basalt is placed within two low velocity sedimentary sequences (Hughes et al., 1998; Richardson et al., 1998; Richardson et al., 1999; Fliedner and White, 2003; Smallwood et al., 2001; Sørensen, 2003; White et al., 2003; Raum et al., 2005). The velocity structure for sediments above the basalt can be resolved by conventional techniques. The top of the basalt layer can be determined very effectively due to the high contrast in seismic physical properties between the basalt and the overlying sediments. However, the high velocity basalt layer represents a complex scenario for seismic imaging methodologies, acting as a barrier so that the underlying structures can not be imaged. The high velocity that characterizes the basalt constrasts with relatively low velocity of the surrounding materials. This causes that most of energy is reflected and/or travels along this layer.

Synthetic data parameters	
Model length	100 km
Model depth	8 km
Cell size	10 x 10 m
Number of shots	80
Number of channels	3294
Station spacing	30 m
Recording length	30 s
Source spacing	1 km
Sample rate	1 ms

Table 4.2: *Parameters used to generate synthetic data*

Although basalt flows tend to be subhorizontal on large scale, at small scale, rugged interfaces cause scattering and disperse the elastic energy destroying any lateral coherency of possible subbasalt events. In addition to the differences between the three major Series, within every unit, basaltic bodies are highly heterogeneous in composition and physical properties. These heterogeneities strongly disperse the seismic energy and destroy the signal coherence in the seismic wavefield. The outter parts of the basalt flows are affected by weathering causing a decrease in velocity, this constrasts with the internal parts which cooled slowly and without any external influence preserving a high velocity feature. Interfaces between individual flows in a basalt block produce internal multiples and wave conversions. Also some intrusive basalt flows were emplaced as sills within previous structures providing an additional cause for scattering at and beneath the base of the basalt.

In addition to these major imaging issues, the usual problems of marine seismic reflection data acquisition must be also considered (tidal noise, multiples, peg-leg, reverberation, converted-waves, etc.). In the Faroe Shelf, conventional seismic reflection techniques are insufficient to study subbasalt structures. Subbasalt imaging has undergone remarkable advances in last years, these improvements consist in designing new geometry acquisition patterns (White et al., 2003), designing new sources (Staples et al., 1999; White et al., 2002; Ziolkowski et al., 2003), understanding the scattering caused by the basalt (Martini et al., 2001; Martini and Bean, 2002) or combining several geophysical methodologies (Jegen-Kulcsar and Hobbs, 2005). Nevertheless, studying subbasalt structures requires a detailed velocity model to obtain valuable information and to apply more sophisticated approaches such as prestack depth migration.

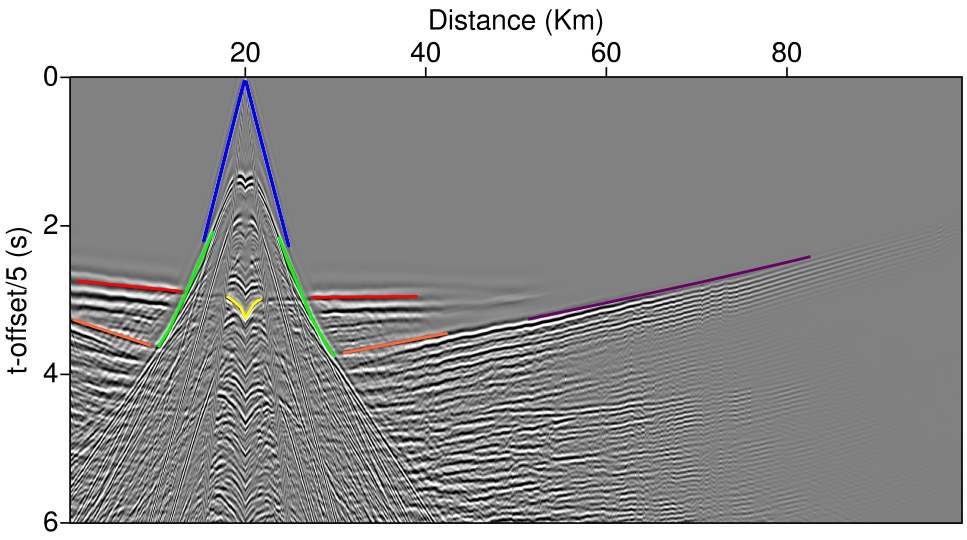

Fig. 4.2: *Synthetic shotgather. Different phases can be identified: water wave (blue), refraction from sediments over the basalt layer (green), refraction from basalt (red), reflection from the top of the basalt (yellow), refractions from basement (purple) and reflections from the top of the basement (orange).*

3. Theoretical geologic model and synthetic seismic data

A synthetic dataset was acquired using an idealized velocity model. The model consists of a wedge of basalt layer within a sedimentary column. The basalt layer features an irregular upper surface, and very high velocities and densities that contrast with the velocities and densities of the surrounding sediments. The choice of a thin wedge for the basalt is justified because it represents the best geological setting for exploration and explotation for the oil industry. In order to simulate a highly variable structure, we consider the small-scale top basalt topography to be a random field which was generated using Von Karman functions (Goff and Jordan, 1988). As there is a high velocity contrast between the sedimentary cover and the basalt, can this topography be recovered?. In addition, in the case of Shetland-Faroe Basin, the area where the basalt thins is close to the center of the basin where geology is well known and can be extrapolated to suggest the existence of subbasalt sedimentary structures. The P-wave velocities were taken from laboratory measurements (Carmichael, 1982). All the physical properties used in the simulation are summarized in table 4.1.

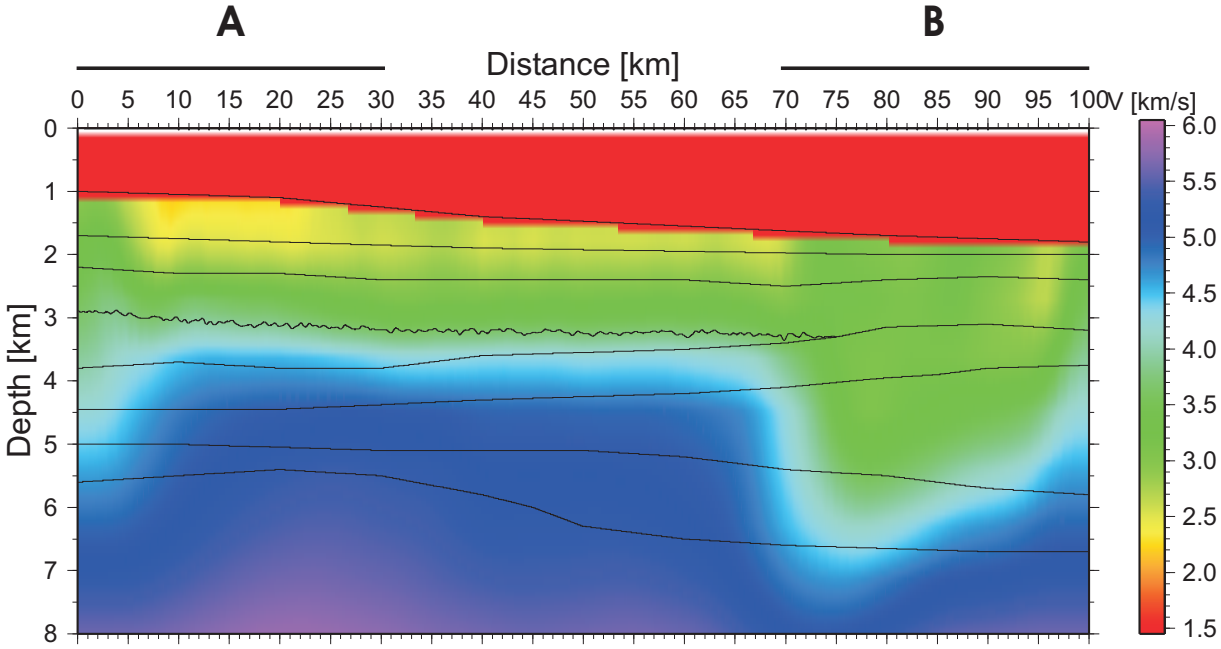

Fig. 4.3: *Velocity model obtained using TTT package (Trinks et al., 2005) considering only first arrivals. Interfaces between layers are the ones that were used in the theoretical model. Velocities over the basalt wedge are well constrained. A prominent velocity discontinuity can be observed for the first 70 km between 3 and 4 km in depth which provides the location for the top of basalt layer.*

A second order finite difference solver of the elastic wave equation using Sochacki's interface scheme (Sochacki et al., 1987; Sochacki et al., 1991) was used to generate a seismic dataset acquired over the velocity model. The 2-D model was of 100 km wide and 8 km deep and a 10×10 m grid was used (Fig. 4.1). After intense calculations, 80 shotgathers were simulated with more than 3000 traces per shot (one trace every 30 m) and 30 s of recording time. The sampling for this synthetic dataset was 1 ms. The parameters for these simulations are summarized in table 4.2. In this data several phases were identified (Fig. 4.2).

Water multiple and peg-leg signal were generated by the elastic finite difference algorithm, no additional noise was included in the data. Although in nature, basalts appear as highly heterogeneous layered structures, in order to simplify the problem, the basaltic wedge was considered as an homogeneus feature in its internal velocity distribution. Under these conditions we obtained a quite ideal dataset.

4. Tomographic inversions

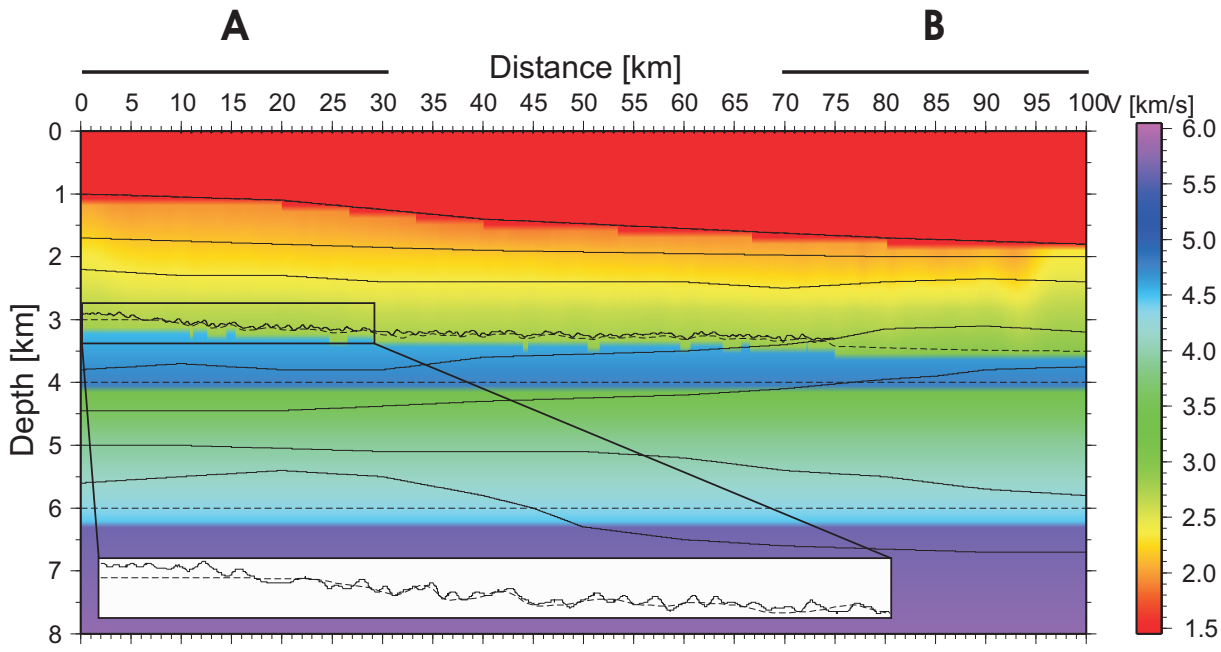

Fig. 4.4: *Velocity model obtained using TTT package (Trinks et al., 2005) after inverting refractions from the sediments over the basalt and reflections from the top of the basalt layer. Dashed lines represent layers from inversion and continous lines the theoretical layer interfaces. Note the coincidence between dashed line and continous line in the top of the basalt layer.*

The main aim of synthetic simulations was checking the possibility of recovering the original model using tomographic techniques. As a first attempt, first arrivals travel time seismic tomography was applied using the TTT software package (Trinks et al., 2005). This code is based on initial value ray tracing in velocity models constructed of Delaunay triangulated grids and interfaces. The tomography is implemented as a joint interface and velocity inversion using the bi-conjugated gradient method, for further details see Trinks, 2003. The result obtained for this inversion is shown in figure 4.3. The average velocity structure of the zone over the basalt layer was recovered as well as the top of the basalt layer where a sharp velocity contrast is displayed. However, no low velocity can be reproduced under the basalt, toward the right end of the model, where no basalt exists, some realistic information about velocities can be obtained for the deepest part of the model. These results suggest that there are physical limitations in constraining subbasalt structures by seismic travel time tomography.

TTT code can also invert additional phases. In order to include all the information from phases identified in synthetic shots, a layer by layer striping inversion was performed and develloped in detail in what follows. A five layer model was used as starting model:

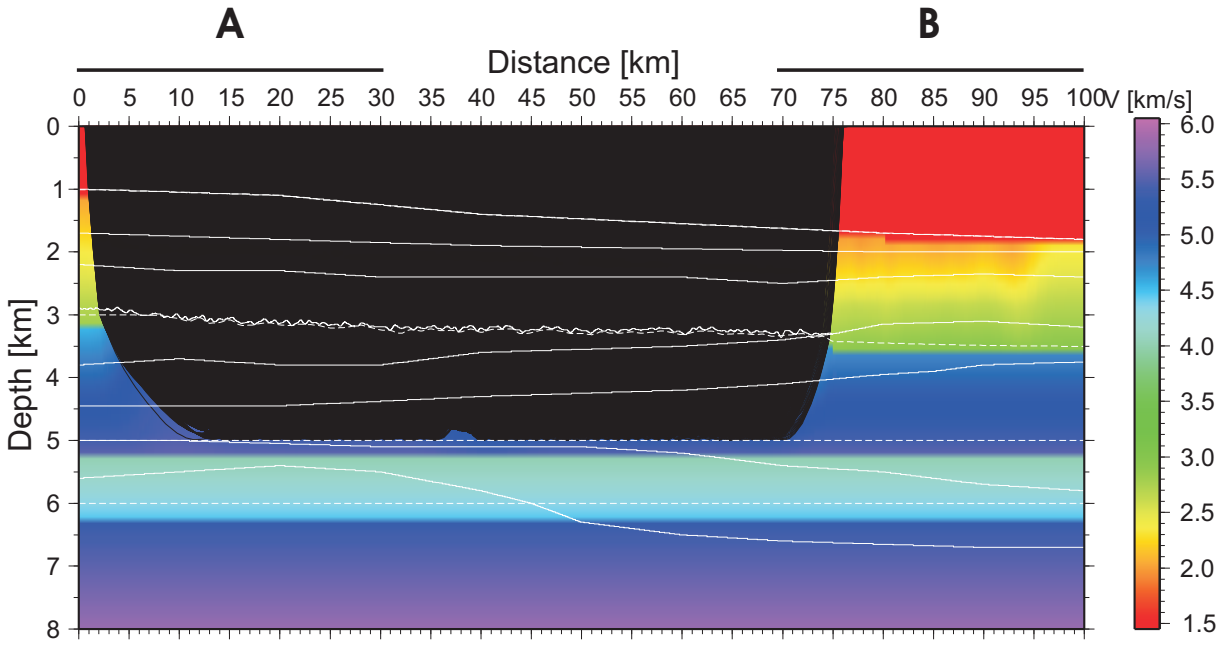

Fig. 4.5: *Results from the basalt refraction inversion. White dashed lines represent layers from inversion and continous lines the theoretical layer interfaces. The base of the basalt layer, which is overestimated, should be delineated by raypaths. The black area represents the part of the model sampled by rays.*

water, sediments (over basalt), basalt, sediments (under basalt) and basement. Top basalt interface was inferred from the model obtained using only first arrivals (Fig. 4.3). Even though in the theoretical model some sublayers were included in sedimentary sequences, the contrast in velocity between these sublayers is quite smooth which makes it difficult to identify events from these interfaces, therefore this minor discontinuities were not considered in the inverted model.

The additional information that TTT can use corresponds to the identification of traveltime branches related to the different features within the model. Therefore, a subjective interpretation of the travel time branch is required, and then the picks corresponding to the branch are associated to a particular structure.

4.1 Inverting phases over the basalt layer

Firstly, only the travel time branches interpreted to correspond to the sedimentary cover were included in the inversion. The results show a good recovery of the original model (Fig. 4.4). In the first part of the model (thin water layer, 0-30 km marked as A) this phase appears as first break and the results are similar to the first arrivals inversion (Fig.

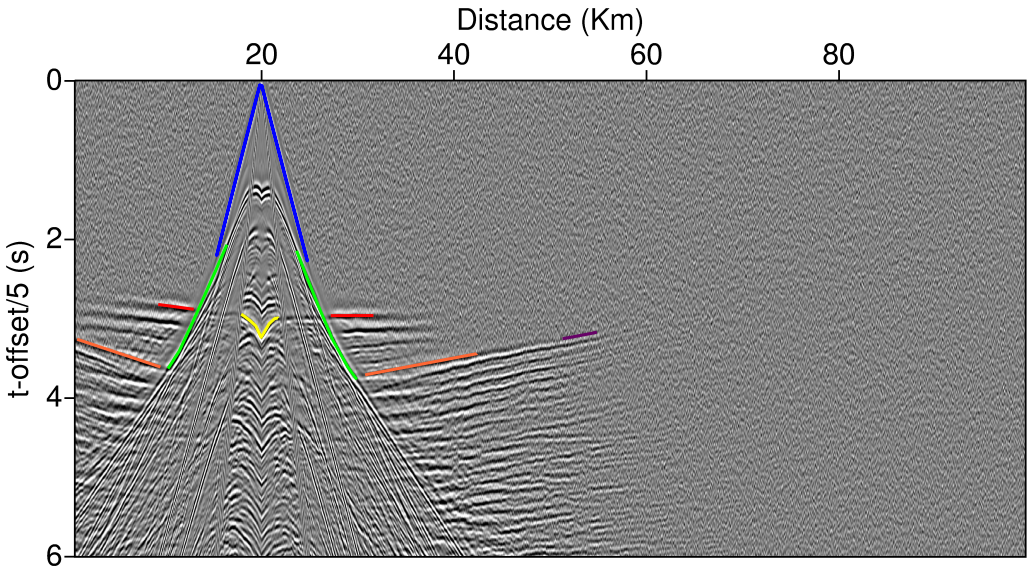

Fig. 4.6: *Synthetic shotgather with noise. Different phases can be identified: water wave (blue), refraction from sediments over the basalt layer (green), refraction from basalt (red), reflection from the top of the basalt (yellow), refractions from basement (purple) and reflections from the top of the basement (orange). Note the difference with figure 4.2 in the refractions from basalt (red).*

4.3) while in the last part of the model (thick water layer, 70-100 km marked as B) the picks used were not considered in first arrivals inversion, hence, the additional data provides further constraints on the sedimentary cover over the basalt layer.

The TTT code can include also reflected arrivals in the inversion scheme. As reflections from the top of the basalt are displayed as a very high amplitude events, the travel times of the reflected phases can be identified and picked at normal incidence.

Considering the final model of the previous case as starting model, and, without modifying the velocity values for this model, reflections from the top of the basalt layer were inverted in order to obtain the topography for this interface. A detailed structure was achieved which reproduces in some degree the rugged topography featured by the original model (Fig. 4.4).

4.2 Inverting refractions inside the basalt

In this case, the main aim is to constrain the base of the basalt using the refracted waves

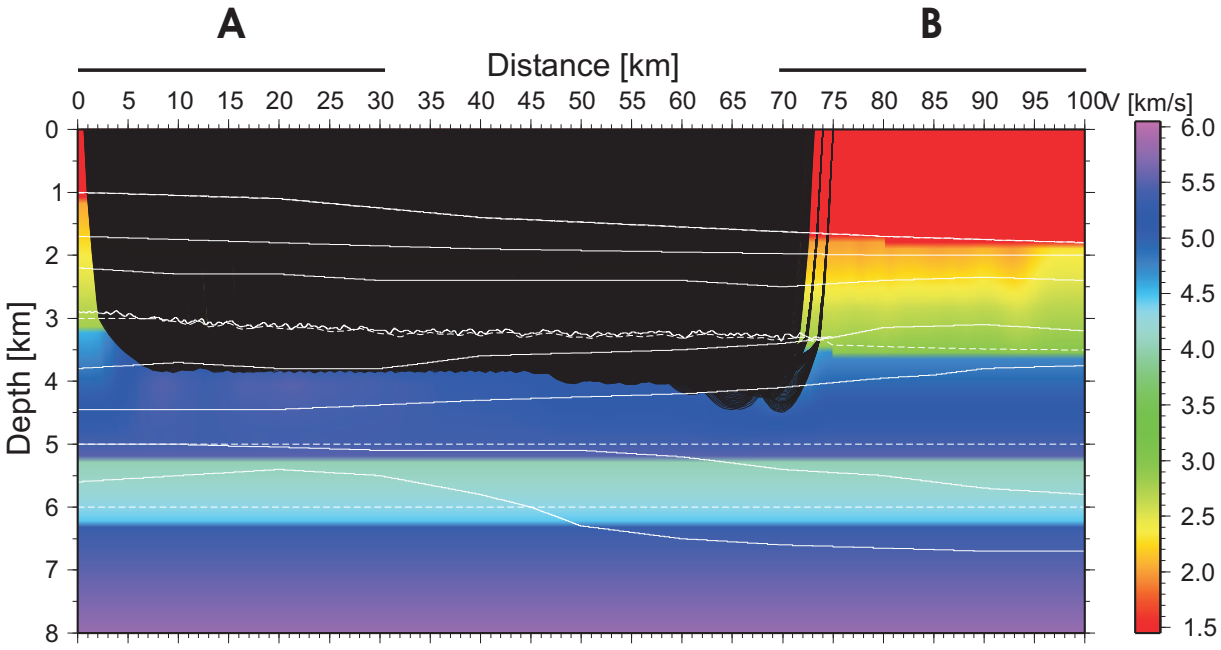

Fig. 4.7: *Results from the basalt refraction inversion using picks from data with noise. White dashed lines represent layers from inversion and continous lines the theoretical layer interfaces. The black area represents the part of the model sampled by rays. The base of the basalt layer should be delineated by raypaths. The constrain on the thickness of the basalt layer is failing where the layer is thinner, probably due to overpicking refractions.*

inside this layer. Raypaths are very sensitive to high velocity anomalies therefore some constraints on the base of the basalt should be gained by introducing these refractions. As no noise is present in this synthetic dataset, refraction from basalt can be followed up to far offsets (Fig. 4.2). The maximum offset to stop picking is arbitrary because there is no way to separate basalt refraction from base basalt reflection. In a first picking stage, refractions from the basalt were picked as far as possible and inverted. The results do not fit the theoretical model, overestimating the basalt thickness (Fig. 4.5).

To simulate a more realistic situation, some arbitrary noise was added to the data (Fig. 4.6). As a result, the noise limited the maximum offset for picking which was considerably reduced compared with the noise-free case. The inverted model correlates better with the synthetic model (Fig. 4.7) which is closer to the real model. However, the range between 30 and 75 km features again an overestimation of the basalt thickness. This effect is caused by the difficulty in differentiating basalt refractions from base basalt reflections which interfere at short offsets. In any case, in the travel time branch, the limit between the basalt refraction (head wave) and the subbasalt reflection is completely arbitrary (subjective, depends on the interpreter). The travel time picking of this arrival is complicated even farther by the existence of noise, and thus, the maximum picking offset depends critically on the quality of the data. The consequence of this subjectivity is that the thickness of the basalt layer is proportional to the offset picked, and this effect is stronger where the basalt layer thins.

This constrasts with the conventional idea of using large apertures for subbasalt imaging. This strategy may be useful in zones with thick basalt layers but, in the case of thin basalt layers, the basalt head wave and reflection from the base of the basalt interfere (see below) and there is no benefit by using large apertures to infere basalt seismic properties.

4.3 Inverting refractions and reflections from the basement

As shown above, the basalt layer cannot be resolved properly only considering refractions within this layer. In the case of a thicker basalt layer, reflection from the base of the basalt could be differentiated from the basalt refraction which may contribute to better constrain the base of this layer. However, for thin layers there are no possibilities of deducing the basaltic structure using refraction data. At this point, additional information is required to constrain the basalt layer thickness, in a real case, this additional information could be provided by drilling through the basalt layer, fixing in this way the velocity of the basalt, the thickness of the basalt layer and the velocity of the sediments beneath the basalt.

We introduced additional information in the inversion scheme, we assumed that two

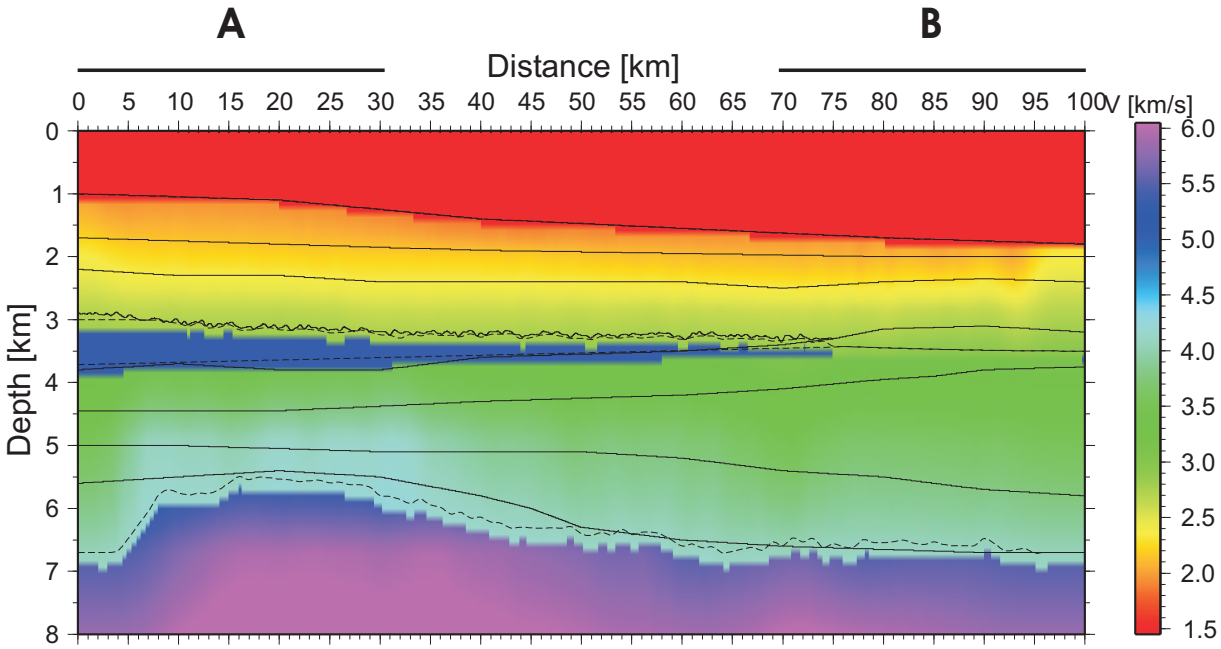

Fig. 4.8: *Final result obtained using all the phases after fixing the base of the basalt layer considering that two wells were drilled through this layer at 10 and 50 km. Dashed lines represent layers from inversion and continous lines the theoretical layer interfaces. Introducing additional information, the theoretical model is recovered quite accurately. Energy dispersion caused by the topography of the basalt wedge masks the reflected energy from the basement. Therefore the recovered basement has an irregular top which is not real but the influence of the overlying velocity heterogeneities.*

wells were drilled located at x=10 km and x=50 km (Fig. 4.1). In the last part of the model there is no basalt layer hence the signal coherence is preserved making it possible to identify and pick normal incidence reflections from the basement. Inverting this phase, a reliable estimation of the top of the basement was obtained for the last 25 km of the model which, jointly with the velocity obtained in first arrival inversions, constrained the model in this part. This results were extrapolated under the basalt layer and used as starting model to invert reflections and refractions from the basement which yielded to our final model where the theoretical model is reasonably well recovered (Fig. 4.8). Note that additional information is required by the travel time inversion methods to obtain reliable models.

5. Metropolis simulations

Statistical methods maybe used in order to assess the reliability of inverted velocity models. Among them, probably Monte-Carlo based simulations are the most used. These consist of generating a relatively large number of random velocity models from the same starting model and performing an inversion for each starting model. Finally, the results ara compared to asses which model fits the data the best. This method is also used to test the reliability of the starting model in a inversion scheme and the stability of the results (Korenaga et al., 2000; Sallarès et al., 2003; Martí et al., 2006). In this method every iteration is independent from the previous one and no information is inherited for every new case.

Metropolis algorithms (Metropolis et al., 1953) take advantage of the *a priori* knowledge of the previous model in the iterative scheme. In the first stages of the simulation the influence of the starting model is clear but, after some iterations, this influence decreases considerably, this is known as "burn-in". Using this technique the whole region of allowed paremeters is visited which yields a random walk within the region of possible parameters. A scheme of the algorithm is shown in figure 4.9 and a detailed description of the methodology can be found in Pearse, 2002. In this case, Rayinvr (Zelt and Smith, 1992) was used to solve the forward problem and to calculate χ^2 which provides the likelihood for every model. The iterative process starts using the starting model (in this case the real model used to build synthetic data) as the current model, then this was randomly modified to generate a new model. Then, the reliability of the model was tested based on the ratio obtained from dividing the likelihood of the current model versus the likelihood of the new model:

- If the ratio was equal or larger than one, the new model was accepted and the new model became the current model.

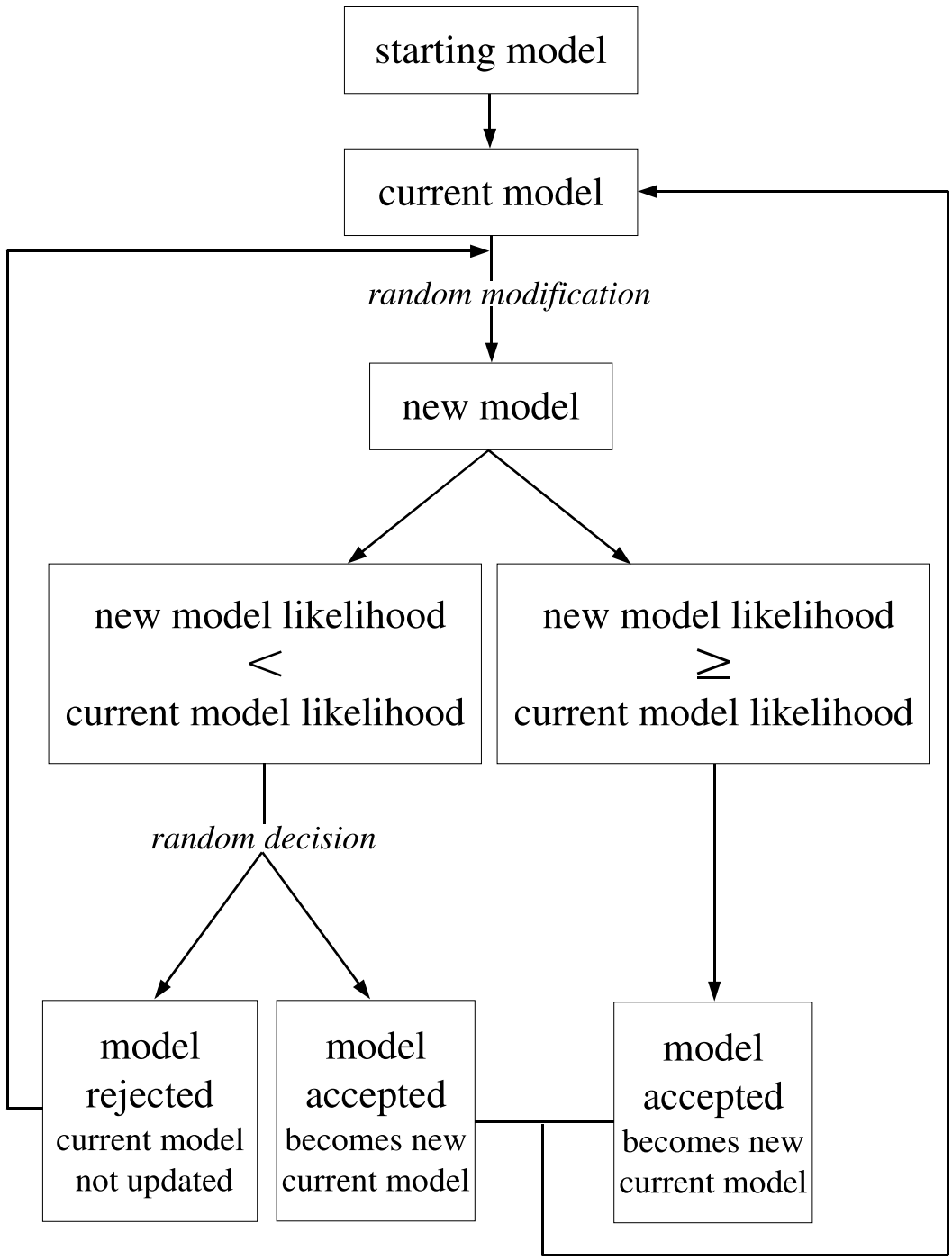

Fig. 4.9: *Scheme used in metropolis calculation as described in (Pearse, 2002). The random modification is subject to prior defined degrees of freedom. In the present case we divide the likelihood of the current versus likelihood of the new model, if ratio is greater than 1 then model is accepted, if ratio is between 0 and 1 then a random decision is taken based on a prior probability function (linear in this case) that will preferentially accept models that are close to the accepted boundary. The likelihood ratio is compared with a normalised random number, if ratio is larger than this number then model is accepted. In any other case, the model is rejected.*

- If ratio was smaller than one, a random number between 1 and 0 was calculated and another test was performed:
    - If the ratio was larger than the random number, the new model was accepted and the new model became the current model.
    - If the ratio was smaller than the random number, the new model was rejected and the current model remained unchanged.

The process is repeated for a large number of iterations giving as a result a set of different models that reasonably fit the picked travel times when a picking uncertainty is given. In this study, 40.000 iterations were performed for every case in order to obtain a set large enough to have a statistical value. The allowed variations in velocity, thickness and velocity gradient were: 0% for water, 2% for layer over basalt, 5% for basalt, 10% for subbasalt layer and 10% for basement (Table 4.3). Variations were chosen increasing in depth to account for the lost of accuracy in deeper layers.

Allowed variation for layers	
Layer	$\Delta(\%)$
Water	0
Sediments over basalt	2
Basalt	5
Sediments under basalt	10
Basement	10

Table 4.3: *Allowed variation to generate modified models for velocity, velocity gradient and thickness for every layer in models 1 and 2.*

Some synthetic shots have been generated using different 1-D models and two different frequencies 10 Hz and 20 Hz (Figs. 4.10 and 4.11):

- Model 1: model with subbasalt low velocity layer.
- Model 2: the same as model 1 but with a thicker basalt layer.

5.1 Model 1: results

The first analysis was done on the data from model 1 and 10 Hz. In this case, refraction from basalt layer seems to be very clear as shown in figure 4.10. However, this yields a phase identification which is not correct because the phase identified as a refraction from

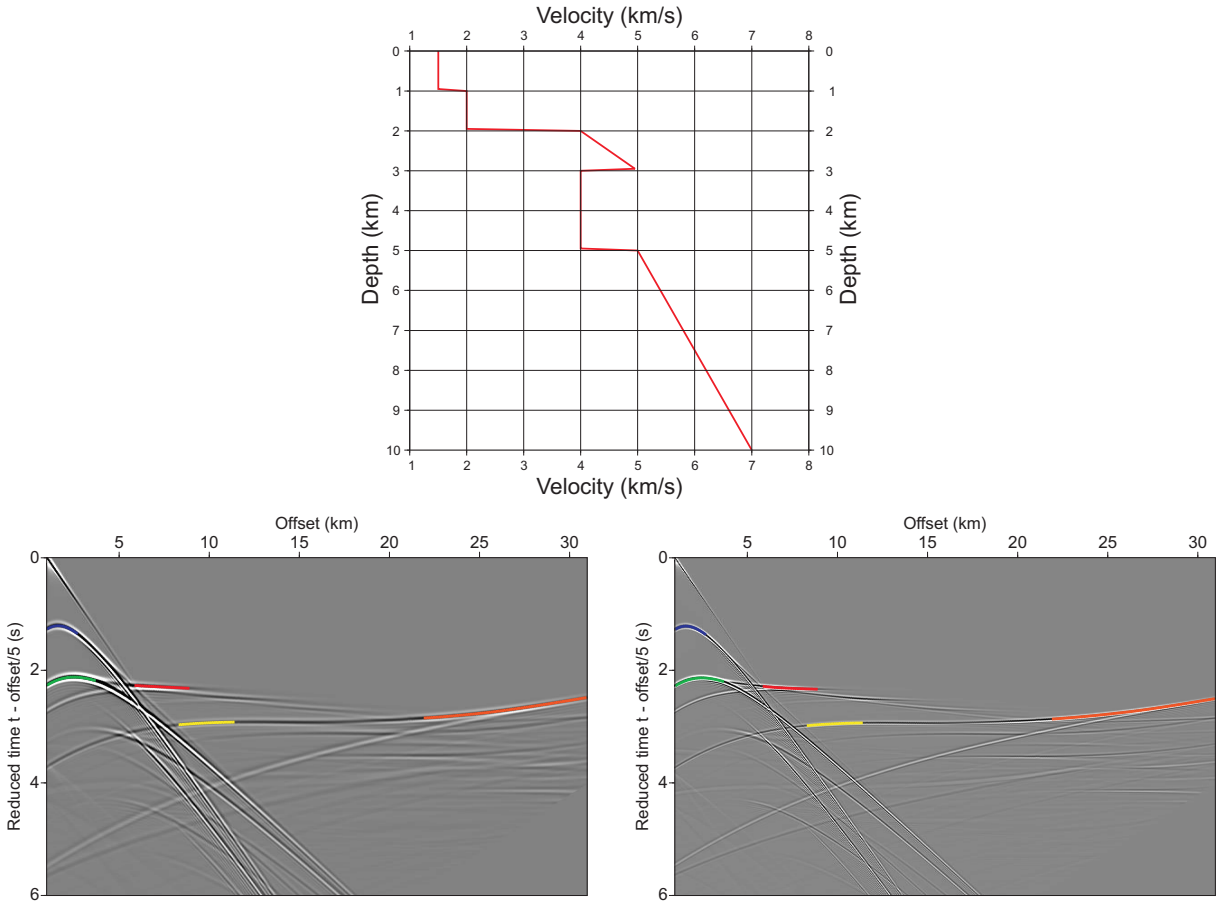

Fig. 4.10: *1-D model used to generate synthetic data (top). Shots generated using the model and different frequencies: 10 Hz (left) and 20 Hz (right). Main phases were identified: sea bottom reflection (blue), top basalt reflection (green), basalt refraction (red), top basement reflection (yellow) and basement refraction (orange). Under the top of the basalt no phases were picked within the water-wave cone because in real data this phases are difficult to identify.*

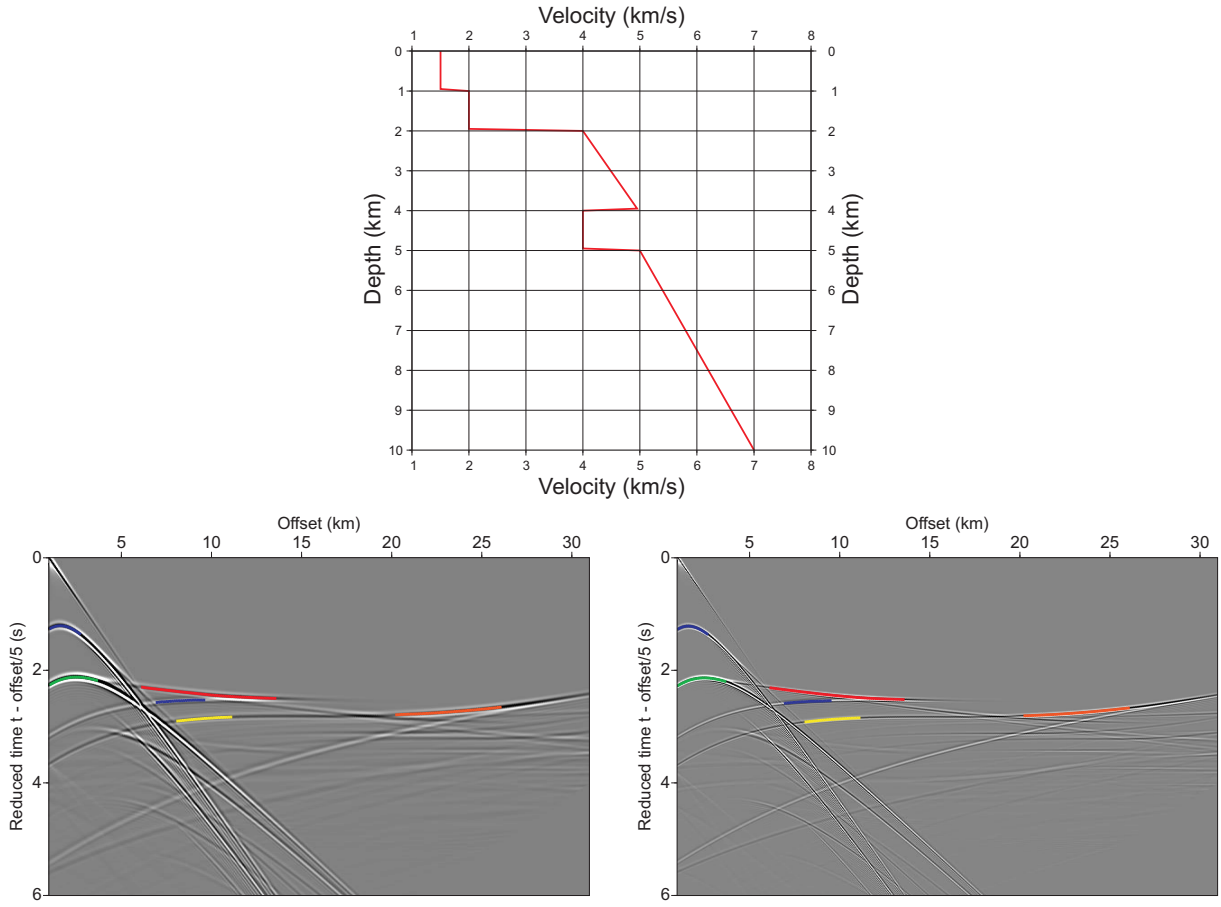

Fig. 4.11: *1-D model used to generate synthetic data (top). Shots generated using the model and different frequencies: 10 Hz (left) and 20 Hz (right). Main phases were identified: sea bottom reflection (blue), top basalt reflection (green), basalt refraction (red), base basalt reflection (purple),top basement reflection (yellow) and basement refraction (orange). Under the top of the basalt no phases were picked within the water-wave cone because in real data this phases are difficult to identify.*

basalt layer is the interference between two phases: refraction from basalt and reflection from the base of the basalt. To emphasize this effect, a shotgather was calculated using model 1 but replacing the subbasalt velocity by a layer of 5 km/s, in this way no reflection in the base of the basalt layer was generated obtaining a pure refraction in the basalt layer. This pure refraction was picked and compared with the identified in the previous case (Fig. 4.12). Thus, in the first case, we have identified an interference between basalt refraction and base basalt reflection as a pure refraction which is erroneous.

Picking uncertainties (ms)					
Phase	model1 10 Hz		model1 20 Hz	model2 10 Hz	model2 20 Hz
Seabed reflection	8	8	8	8	8
Top basalt reflection	24	16	16	24	16
Basalt refraction	50	24	24	50	24
Top basement reflection	100	50	50	100	50
Basement refraction	100	50	50	100	50
Figure	4.13	4.14	4.15	4.16,4.17	4.18

Table 4.4: *Picking uncertainty for every layer considered in metropolis algorithm*

Using the picks from the data obtained with model 1 in the Metropolis approach with a high picking error (see table 4.4) and considering 40.000 different cases, we obtained an overestimation in both, velocity and thickness of the subbasalt layer (Fig. 4.13). By reducing the picking error (case with low uncertainty) we would expect a better correlation between the more probable model and the theoretical one. In practice, under the same conditions but reducing the picking uncertaity, a worse result was obtained where there was no need of a subbasalt low velocity layer in order to fit the data (Fig. 4.14). This effect can be explained because considering a bigger error in the picks, the range of times can include both, refraction within the basalt and reflection from the base of the basalt. Therefore what was labelled as basalt refraction is within the allowed range of times for this phase. On the other hand, by reducing the picking error, the range of times do not include the real refraction and then our erroneous phase identification yields the unexpected result of fig. 4.14.

The same analysis was repeated using model 1 and data generated with 20 Hz. In this case results are better and fit the right model (Fig. 4.15).

5.2 Model 2: results

In model 2 the thickness of basalt layer was increased to test if it was possible to use a well identified base basalt reflection to constrain better the thickness and velocity of this layer. Two different simulations have been performed: one using a very conservative picking and avoiding picks in the "interference zone" (basalt refraction/base basalt reflection) displayed in figure 4.12 and another including more picks. For the first case (Fig. 4.16) the velocity gradient for basalt layer was well reproduced while for the second case (Fig. 4.17) this gradient did not fit the real model. For the basement velocity gradient the result was the opposite, obtaining a better result when considering a larger number of picks. In both cases, subbasalt velocity layer is not reliably recovered. As in model 1, better fit is obtained for 20 Hz data (Fig. 4.18), where the velocity gradient for basalt and basement are well reproduced. Again, in both cases, the subbasalt layer is not well recovered.

The Metropolis study reveals that the phase identification is a critical step. Despite objectivity provided by mathematics used in the inversion, phase identification turns travel time tomography in a subjective procedure. Additionally, uncertainty is also a critical parameter in the inversion which can influence the inversion algorithm. Moreover, considering data with different frequency content also has an effect on the selection of the most probable model. Not all models required a low velocity layer and there was an unresolvable trade-off between thickness and velocity, even for models where the base basalt reflection could be identified.

Synthetic shots were created using a full-waveform code while likelihood was calculated using a ray tracing code. Full-waveform techniques are more accurate than ray tracing methods because they take into account information about the amplitudes, which are ignored in ray tracing simulations. Due to the high computational cost of full-waveform methodologies, ray tracing methods are still conventionally used to obtain velocity models (Pratt et al., 1996). These results suggest that conventional travel time inversion (tomography) schemes without additional information are not sufficient to constrain the base of basalt or subbasalt geological structures.

In the synthetic tests performed in this study no noise has been considered. In this sense, some features that commonly are present in real data as tidal noise, electrical noise and some other effects affecting the quality of the data, have not been included. Results derived from these tests must be interpreted as results obtained in ideal conditions and in consequence, the best ones expected for a real case using this methodology.

5. Conclusions

This study, which involves synthetic data suggests that there are some physical limita-

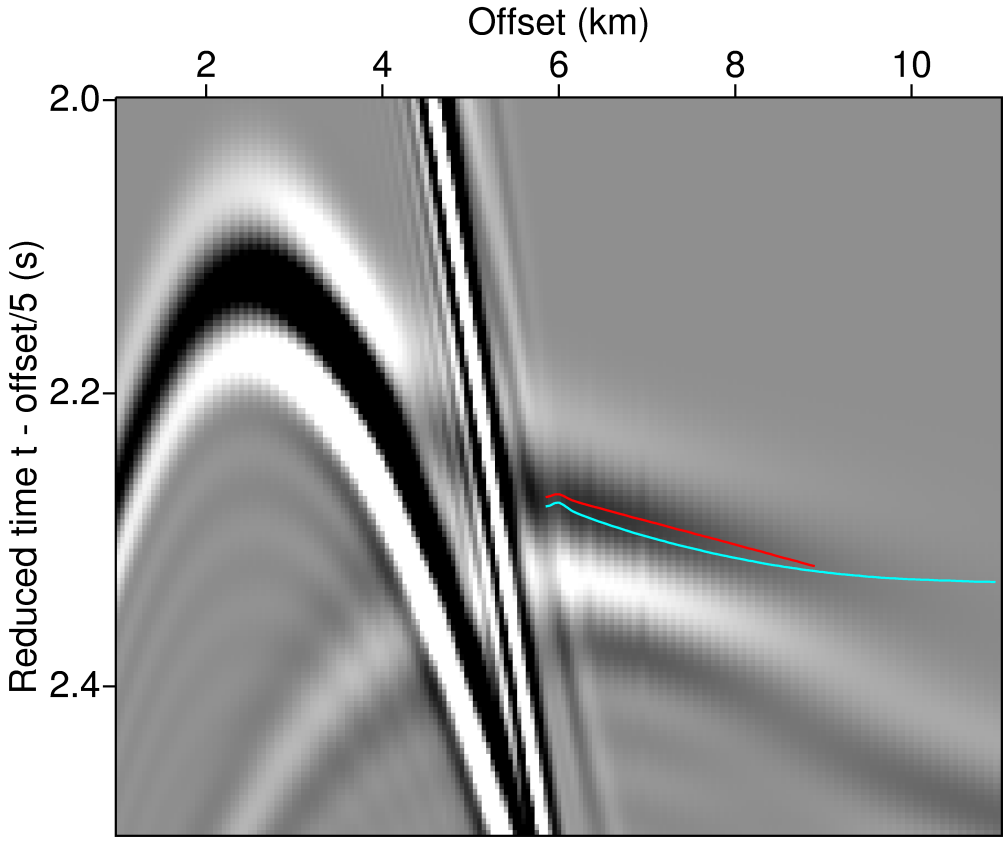

Fig. 4.12: *Basalt refraction picks for model with subbasalt low velocity layer (red) and for a model without subbasalt low velocity layer (cyan). In the case without subbasalt low velocity layer the picks represent a pure refraction while in the other case, the phase that is identified as a refraction is made by the basalt refraction interfering with the base basalt reflection.*

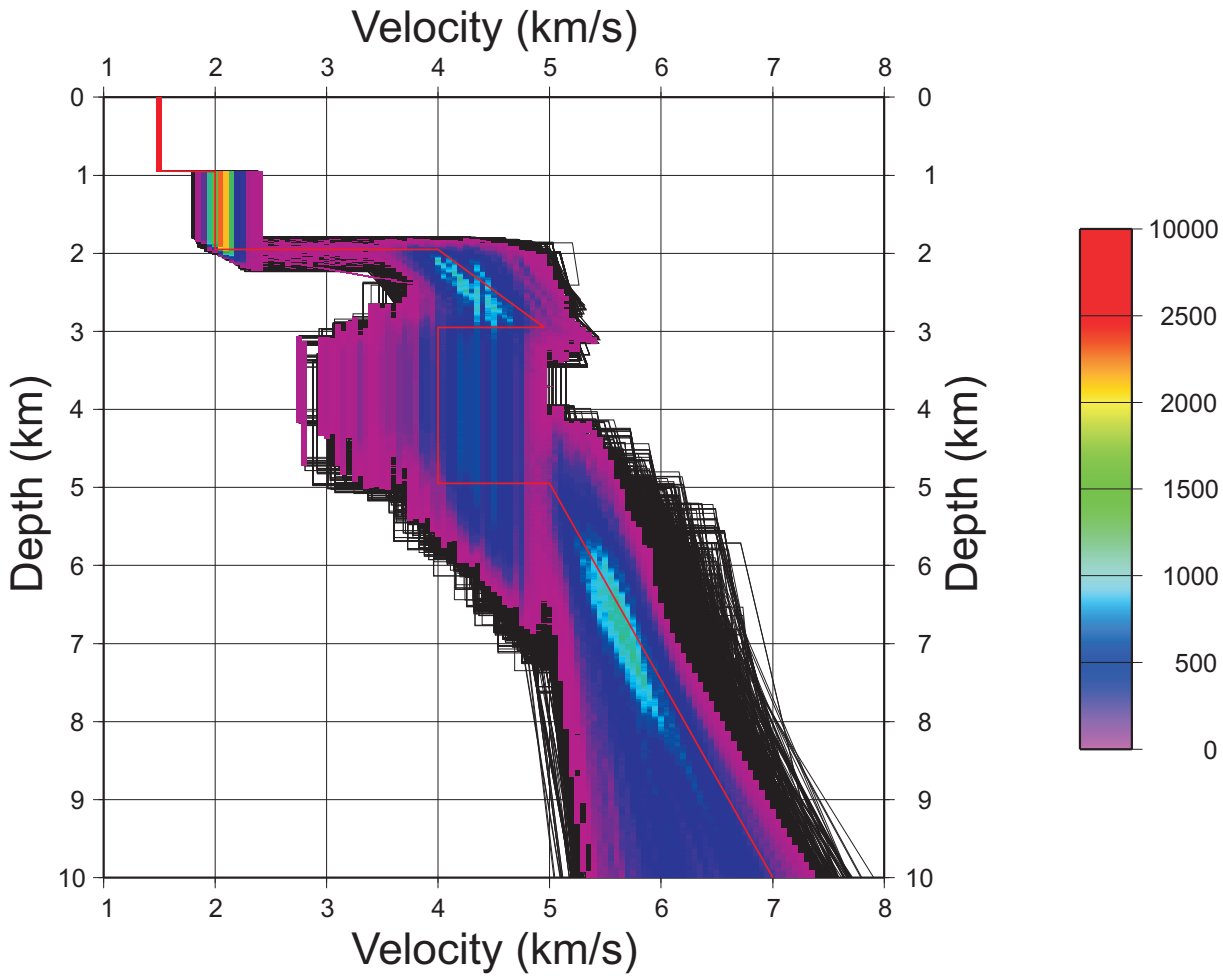

Fig. 4.13: *Results obtained after using the Metropolis algorithm on data from model 1 and 10 Hz for 40.000 cases. Red line represents the real model and every black line a modified model. The color scale stands for the number of times that a model (or part of it) is visited. The preferred model (blue colors) overestimates the subbasalt layer thickness as well as the velocity for this layer.*

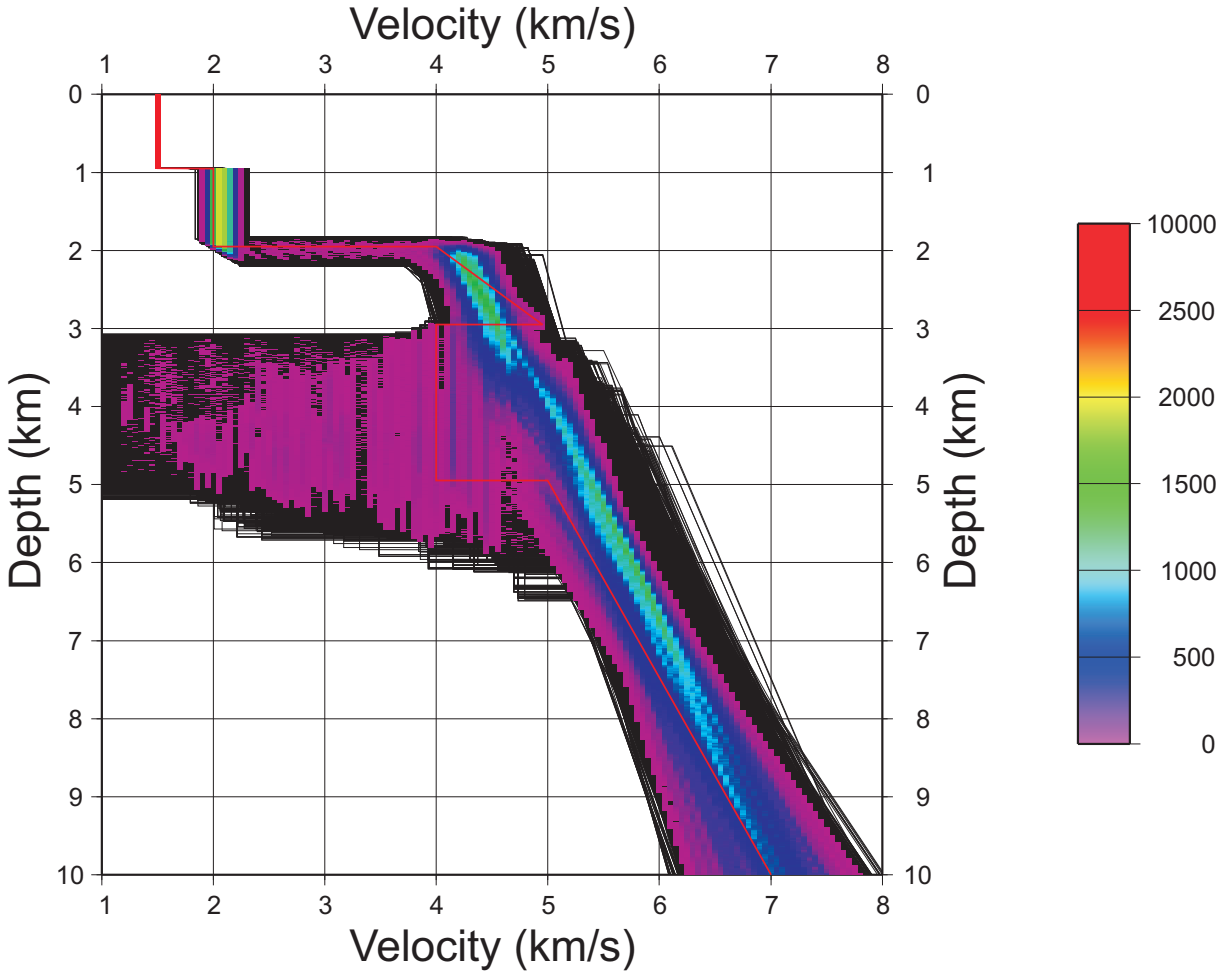

Fig. 4.14: *Results obtained after using the Metropolis algorithm on data from model 1 and 10 Hz for 40.000 cases. Uncertainties were reduced in comparison with the previous case (Fig. 4.13). Red line represents the real model and every black line a modified model. The color scale stands for the number of times that a model (or part of it) is visited. The preferred model consists in a velocity gradient which includes basalt, and basement layers, avoiding the need of a low velocity layer under the basalt.*

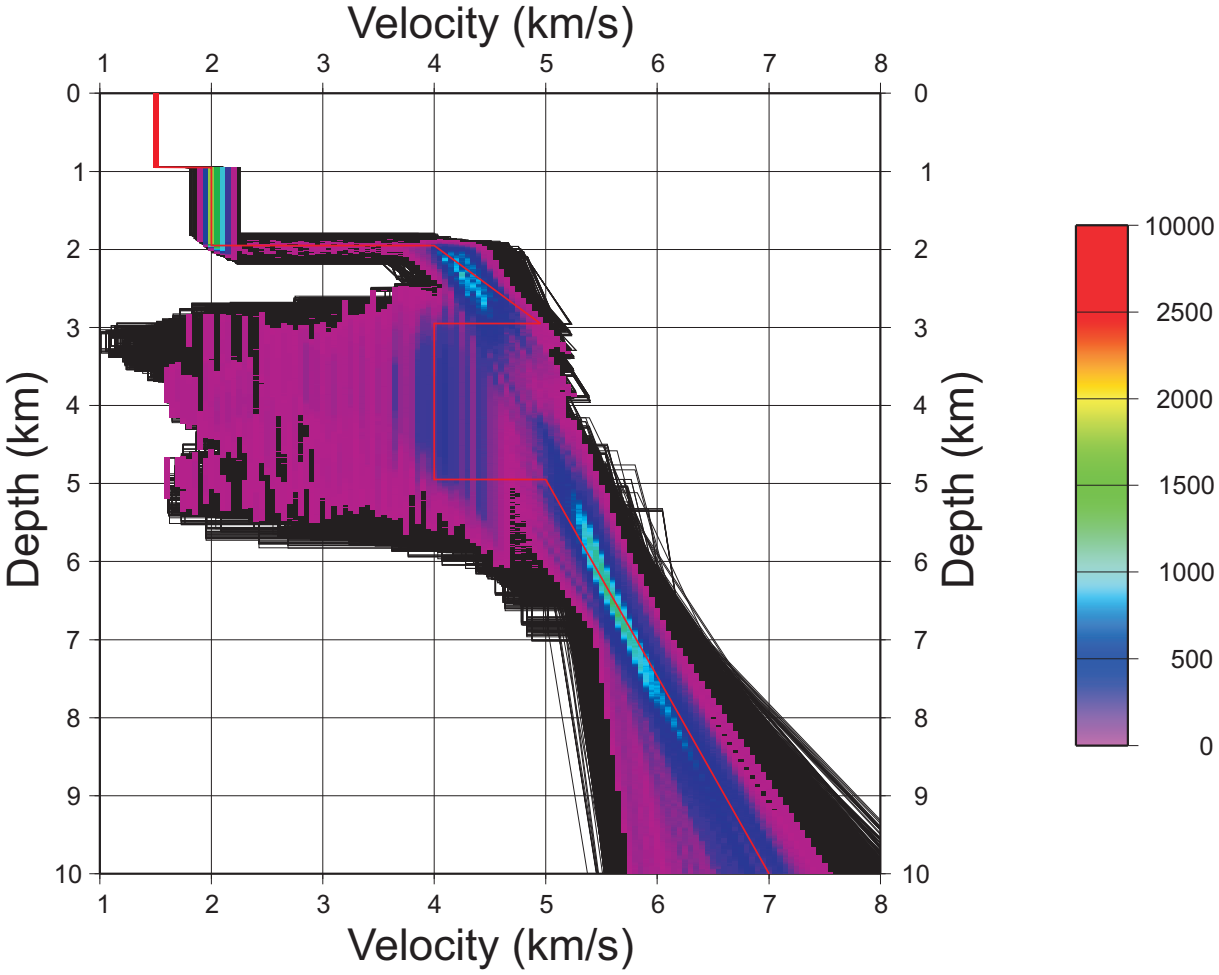

Fig. 4.15: *Results obtained after using the Metropolis algorithm on data from model 1 and 20 Hz for 40.000 cases. Red line represents the real model and every black line a modified model. The color scale stands for the number of times that a model (or part of it) is visited. The preferred model consists in a velocity gradient which includes basalt, subbasalt and basement layers. The subbasalt low velocity layer is reasonably well recovered in velocity and thickness.*

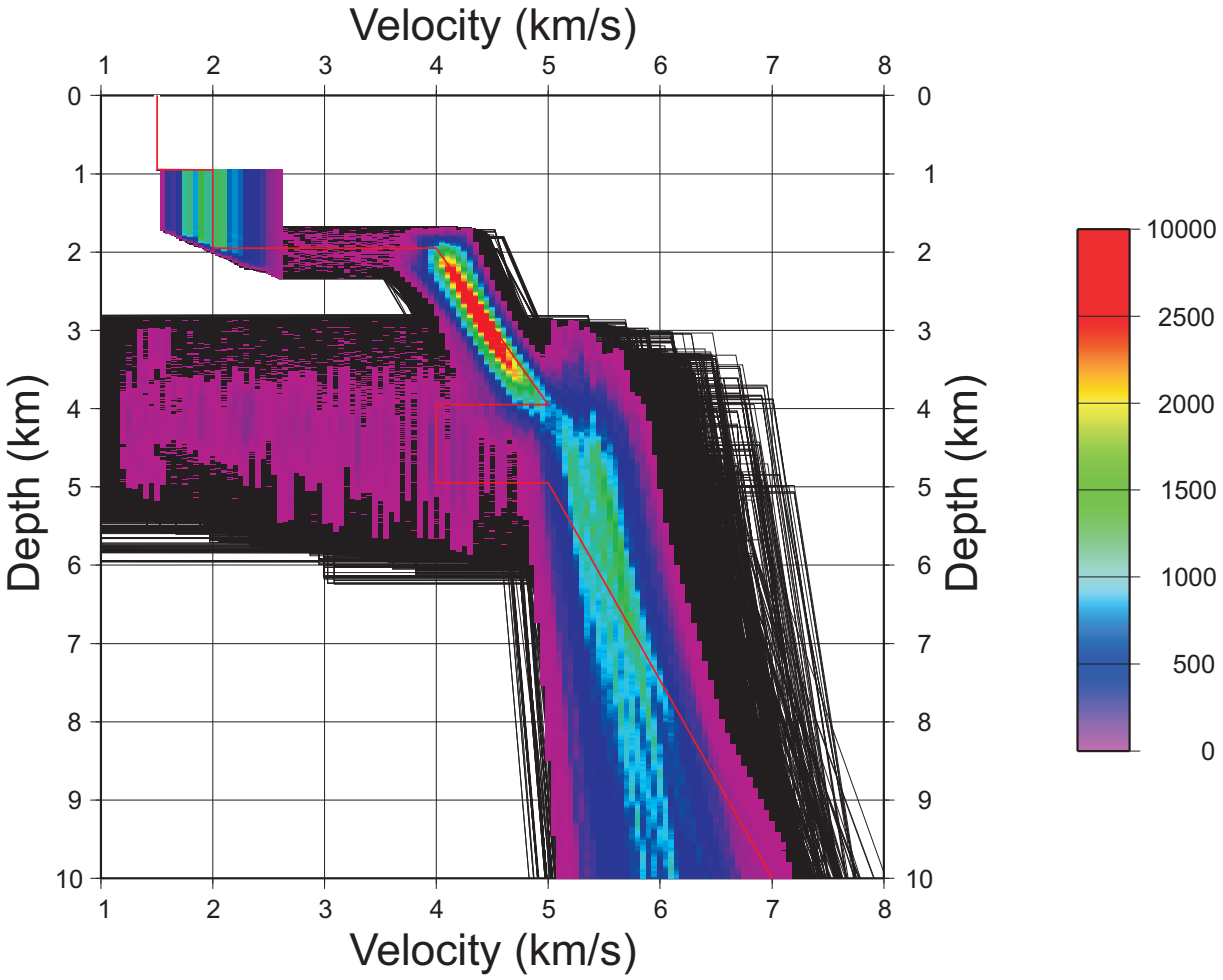

Fig. 4.16: *Results obtained after using the Metropolis algorithm on data from model 2 and 10 Hz for 40.000 cases considering a "conservative" picking avoiding picks in the "interference zone". Red line represents the real model and every black line a modified model. The color scale stands for the number of times that a model (or part of it) is visited.*

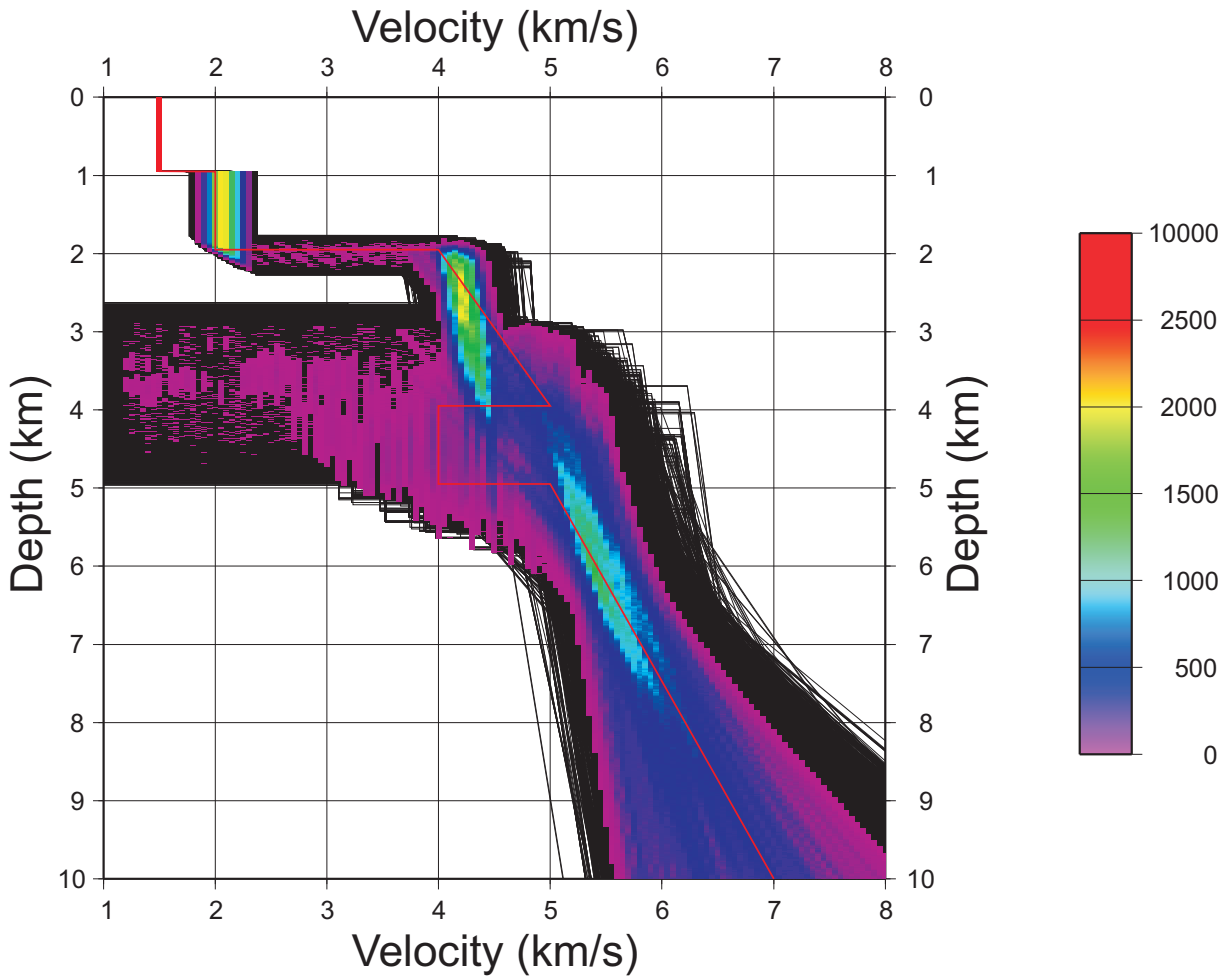

Fig. 4.17: *Results obtained after using the Metropolis algorithm on data from model 2 and 10 Hz for 40.000 cases considering more picks than in the previous case (Fig 4.16). Red line represents the real model and every black line a modified model. The color scale stands for the number of times that a model (or part of it) is visited.*

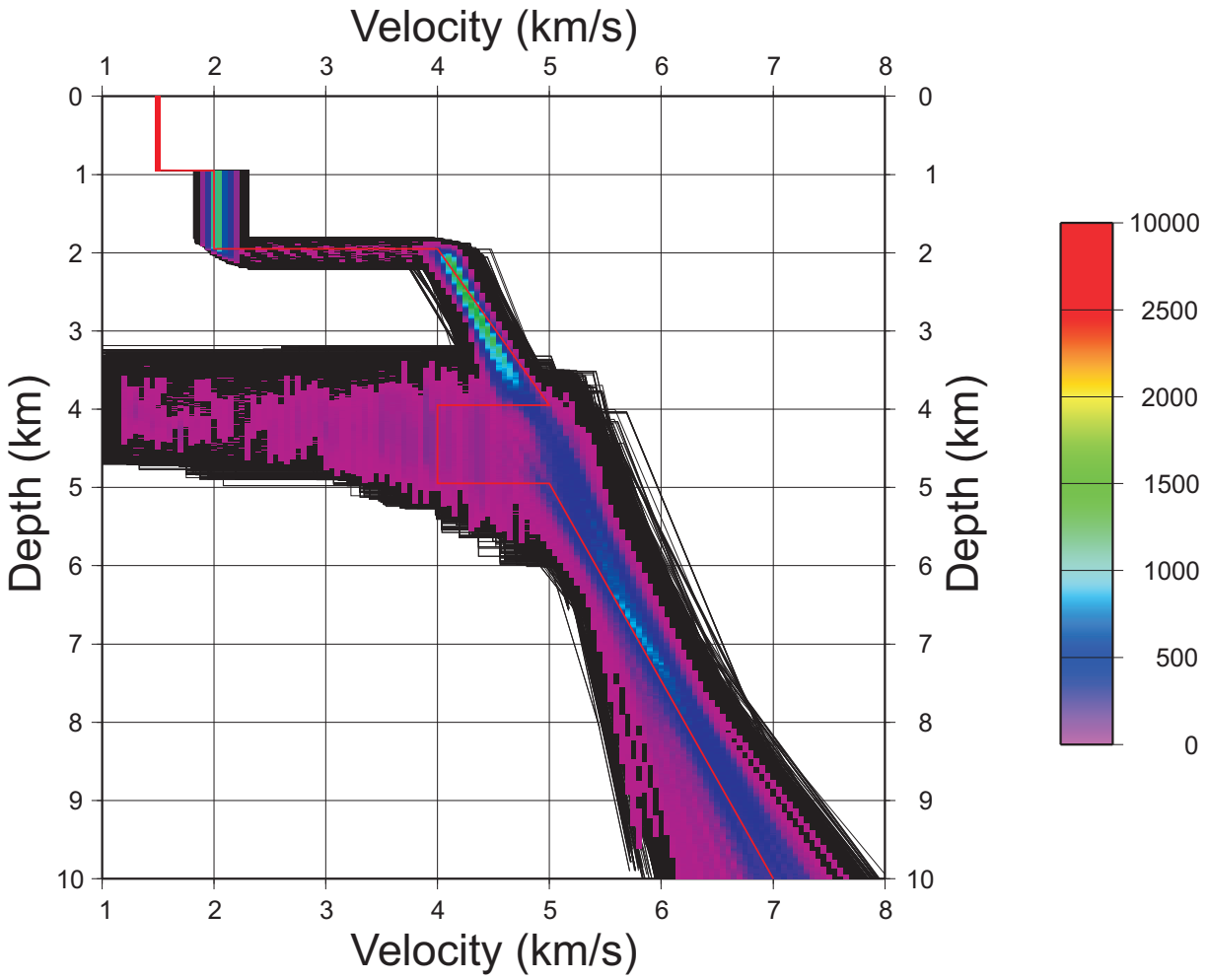

Fig. 4.18: *Results obtained after using the Metropolis algorithm on data from model 2 and 20 Hz for 40.000 cases. Red line represents the real model and every black line a modified model. The color scale stands for the number of times that a model (or part of it) is visited. The preferred model consists in a velocity gradient which includes basalt, subbasalt and basement layers, avoiding the need of a low velocity layer under the basalt.*

tions to obtain a reliable velocity model for subbasalt zones in areas covered by high velocity rocks (like basalts and salts). In the case of thin basalt layers, the base basalt reflection is totally masked within the water-wave cone and it cannot be separated from the basalt refraction. There are several subjective factors that can affect and condition the results from the inversion as maximum picking offset or picking uncertainty. Another important point is the frequency content of the signal, our Metropolis simulations suggest that the original model is best recovered using high frequencies and thicker basalt. This result is relevant because the actual tendency is using and designing airguns that produce low frequency data as single bubble source. The most critical point in the travel time inversion is the phase identification/interpretation in the shot record. Differentiating in the travel time branch, between the head wave travelling within the basalt (refraction) and, the base basalt reflection is a key element in determining the correct thickness of the basalt. The uncertainty associated to the travel time picks is also a relevant issue, as it can not distinguish between high and low velocity subbasalt structures. Moreover, a wrong determination of the basalt thickness and velocity has a direct influence on the resulting model for layers under the basalt. Reliable subbasalt imaging with wide-angle reflection/refraction datasets requires additional information as the knowledge on the thickness of the basalt at some point and its internal velocity distribution. This could be achieved by using other methodologies to infere basalt properties.

Acknowledgements. Funding for this research was provided by SINDRI (Quantitative evaluation of the existing technologies for imaging within basalt-covered areas from the Faroes region), the Spanish Ministry of Science and Technology (Ref: CGL2004-04623/BTE) and Generalitat de Catalunya (Ref: 2005SGR00874). We are grateful to Immo Trinks for training in the use of the TTT code.

Bibliografia

Carmichael, R. S. (1982). *Handbook of Physical Properties of rocks, vol II.* CSC Press, Boston.

Christensen, N. I. and Mooney, W. D. (1995). Seismic velocity structure and composition of the continental crust: A global view. *J. Geophys. Res.*, 100, 9761–9788.

Flecha, I., Martí, D., Carbonell, R., Escuder-Viruete, J., and Pérez-Estaún, A. (2004). Imaging low velocity anomalies with the aid of seismic tomography. *Tectonophysics*, 388, 225–238.

Fliedner, M. M. and White, R. S. (2003). Depth imaging of basalt flows in the Faeroe-Shetland Basin. *Geophys. J. Int.*, 152, 353–371.

Goff, J. A. and Jordan, T. H. (1988). Stochastic modeling of seafloor morphology: inversion of sea beam data for second-order statistics. *J. Geophys. Res.*, 96, 13589–13608.

Hughes, S., Barton, P. J., and Harrison, D. (1998). Exploration in the Shetland-Faeroe Basin using densely spaced arrays of ocean-bottom seismometers. *Geophysics*, 63, 490–501.

Jegen-Kulcsar, M. and Hobbs, R. (2005). Outline of a joint inversion of gravity, MT and seismic data. *Annales Societatis Scientiarum Færoensis*, 43, 163–167.

Korenaga, J., Holbrook, W. S., Kent, G. M., Kelemen, P. B., Detrick, R. S., Larsen, H. C., Hopper, J. R., and Dahl-Jensen, T. (2000). Crustal structure of the Southeast Greeenland margin from joint refraction and reflection seismic tomography. *J. Geophys. Res.*, 105, 21.591–21.614.

Martini, F. and Bean, C. J. (2002). Interface scattering versus body scattering in subbasalt imaging and application of prestack wave equation datuming. *Geophysics*, 67, 1593–1601.

Martini, F., Bean, C. J., Dolan, S., and Marsan, D. (2001). Seismic image quality beneath strongly scattering structures and implications for lower crustal imaging: numerical simulations. *Geophys. J. Int.*, 145, 423–435.

Martí, D., Carbonell, R., Escuder-Viruete, J., and Pérez-Estaún, A. (2006). Characterization of a fractured granitic pluton: P- and s-waves seismic tomography and uncertainty analysis. *Tectonophysics*, 422, 99–114.

Metropolis, N., Rosenbluth, A. W., Rosenbluth, M. N., and Teller, A. H. (1953). Equation of state calculations by fast computing machines. *Journal of Chemical Physics*, 21(6), 1087–1092.

Pearse, S. (2002). *Inversion and modelling of seismic data to assess the evolution of the Rockall Trough*. PhD thesis, Cambridge University.

Pratt, R. G., Song, Z. M., Williamson, P., and Warner, M. (1996). Two-dimensional velocity models from wide-angle seismic data by wavefield inversion. *Geophys. J. Int.*, 124, 323–340.

Raum, T., Mjelde, R., Berge, A. M., Paulsen, J. T., Digranes, P., Shimamura, H., Shiobara, H., Kodaira, S., Larsen, V. B., Fredsted, R., Harrison, D. J., and Johnson, M. (2005). Sub-basalt structures east of the Faroe Islands revealed from wide-angle seismic and gravity data. *Petroleum Geoscience*, 11, 291–308.

Richardson, K. R., Smallwood, J. R., White, R. S., Snyder, D. B., and Maguire, P. K. H. (1998). Crustal structure beneath the Faroe Islands and the Faroe-Iceland Ridge. *Tectonophysics*, 300, 159–180.

Richardson, K. R., White, R. S., England, R. W., and Fruehn, J. (1999). Crustal structure east of the Faroe Islands: mapping sub-basalt sediments using wide-angle seismic data. *Petroleum Geoscience*, 5, 161–172.

Rousseau, J. H. L., Calandra, H., and de Hoop, M. V. (2003). Three-dimensional depth imaging with generalized screens: A salt body case study. *Geophysics*, 68, 1132–1139.

Sallarès, V., Charvis, P., Flueh, E. R., and Bialas, J. (2003). Seismic structure of Cocos and Malpelo Ridges and implications for hot spot-ridge interaction. *J. Geophys. Res.*, 108, 5(1)–5(21).

Sava, P. and Biondi, B. (2004). Wave-equation migration velocity analysis. II. Subsalt imaging examples. *Geophys. Prosp.*, 52, 607–623.

Smallwood, J. R., Towns, M. J., and White, R. S. (2001). The structure of the Faeroe-Shetland Trough from integrated deep seismic and potential field modelling. *J. Geol. Soc.*, 158, 409–412.

Sochacki, J. S., George, J. H., Ewing, R. E., and Smithson, S. B. (1991). Interface conditions for acoustic and elastic wave propagation. *Geophysics*, 56, 168–181.

Sochacki, J. S., Kubichek, R., George, J. H., Fletcher, W. R., and Smithson, S. B. (1987). Absorbing boundary conditions and surface waves. *Geophysics*, 52, 60–71.

Sørensen, A. B. (2003). Cenozoic basin development and stratigraphy of the Faroes area. *Petroleum Geoscience*, 9, 189–207.

Staples, R. K., Hobbs, R. W., and White, R. S. (1999). A comparison between airguns and explosives as wide-angle seismic sources. *Geophys. Prosp.*, 47, 313–339.

Trinks, I. (2003). *Traveltime tomography of densely sampled seismic data.* PhD thesis, Cambridge University.

Trinks, I., Singh, S. C., Chapman, C. H., Barton, P. J., Bosch, M., and Cherrett, A. (2005). Adaptative traveltime tomography of densely sampled seismic data. *Geophys. J. Int.*, 160, 925–938.

White, R. S., Christie, P. A. F., Kusznir, N. J., Roberts, A., Davies, A., Hurst, N., Lunnon, Z., Parkin, C. J., Roberts, A. W., Smith, L. K., Spitzer, R., Surendra, A., and Tymms, V. (2002). iSIMM pushes frontiers of marine seismic acquisition. *First Break*, 20, 782–786.

White, R. S., Smallwood, J. R., Fliedner, M. M., Boslaugh, B., Maresh, J., and Fruehn, J. (2003). Imaging and regional distribution of basalt flows in the Faroe-Shetland Basin. *Geophys. Prosp.*, 51, 215–231.

Williamson, P. (2003). Introduction. *Geophys. Prosp.*, 53, 167–168.

Zelt, C. A. and Smith, R. B. (1992). Seismic traveltime inversion for 2-D crustal velocity structure. *Geophys. J. Int.*, 108, 16–34.

Ziolkowski, A., Hanssen, P., Gatliff, R., Jakubowicz, H., Dobson, A., Hampson, G., Li, X.-Y., and Liu, E. (2003). Use of low frequencies for sub-basalt imaging. *Geophys. Prosp.*, 51, 169–182.

5. SOME IMPROVEMENTS IN SUBBASALT IMAGING USING PRE-STACK DEPTH MIGRATION

I. Flecha, R. Carbonell, R. W. Hobbs and H. Zeyen, *Solid Earth*, 2, 1-7, 2011.

Solid Earth, 2, 1–7, 2011
www.solid-earth.net/2/1/2011/
doi:10.5194/se-2-1-2011

Solid Earth

Some improvements in subbasalt imaging using pre-stack depth migration

I. Flecha[1], **R. Carbonell**[1], **R. W. Hobbs**[2], **and H. Zeyen**[3]

[1]Departament de Geofísica i Tectònica, Institut de Ciències de la Terra "Jaume Almera"-CSIC, C/ Lluis Solé i Sabaris s/n, 08028 Barcelona, Spain
[2]Department of Earth Sciences, University of Durham, Durham DH1 3LE, UK
[3]Departement des Sciences de la Terre, Universite de Paris-Sud, Bat. 503, 91405 Orsay Cedex, France

Received: 29 December 2009 – Published in Solid Earth Discuss.: 8 February 2010
Revised: 8 November 2010 – Accepted: 22 November 2010 – Published: 3 January 2011

Abstract. Subbasalt imaging can be improved by carefully applying pre-stack depth migration. Pre-stack depth migration requires a detailed velocity model and an accurate traveltime calculation. Ray tracing methods are fast but, often fail in calculating traveltimes in complex models, specially, when they feature high velocity contrasts. Finitte difference solutions of the eikonal are more stable and can produce a traveltime field for the whole model avoiding shadow zones. A synthetic test was carried out to check the performance of a new pre-stack depth migration algorithm in a model that features a high velocity layer surrounded by lower velocities. The results reasonably reproduce the original model. The same scheme was used to process long-offset reflection data from the Faroe Shelf where conventional techniques (stack) were insufficient to assess the structure under a basalt layer. Pre-stack depth migration produced an improved image which recovered the main features in the stacked section and allowed to identify some subbasalt coherent events.

1 Introduction

Seismic imaging comprises a wide range of methodologies. Among these techniques, the most common in geophysical prospecting is seismic reflection, which has provided valuable data to infer the subsurface structure. Seismic reflection principles are based on approximations that simplify the imaging problem, two of the most restrictive are: the Earth is considered as a sequence of homogeneous subhorizontal layers and interfaces between layers consist in a vertically sharp and laterally smooth discontinuity (Yilmaz, 1987). Processing flows deduced from these premises generate detailed images in layered and laterally homogeneous media. However, in nature, there are often geological settings where these assumptions fail dramatically, and the methodology based on them is going to be insufficient. This is the case in basalt covered areas and beneath salt instrusions. The presence of a high-velocity and highly heterogeneous layer (basalt) embedded in low-velocity sediments, has a detrimental effect on imaging beneath this structure (Martini and Bean, 2002). The basalt acts as a barrier for seismic signal. Most of the energy reflects or travels along this layer, therefore little energy goes through the basalt layer. In addition, the backscattered energy that returns to the surface from basalt and subbasalt structures features a lack of coherence caused by the irregular interfaces of the basaltic body and the heterogeneities within the basalt itself. Hence, in this cases a more sophisticated approach, such as pre-stack depth migration, is needed.

The North Atlantic province has been widely studied by the oil industry. Standard seismic imaging techniques have been succesfully applied for many years in the sedimentary basins located in this area. The Faroe-Shetland Basin represents a potential hydrocarbon reservoir ready for exploration. To the center of the basin, geology is well known but, in the NW region, sequences of basalt cover underlying structures and make exploration both challenging and risky (Sørensen, 2003). In the present study, a new pre-stack depth migration scheme was implemented to address the subbasalt imaging problem. This manuscript shows the improvements obtained by this pre-stack depth migration approach applied to data acquired over the Faroe Shelf.

Correspondence to: I. Flecha
(iflecha@ija.csic.es)

Published by Copernicus Publications on behalf of the European Geosciences Union.

2 Geological and geophysical setting

In the Faroe-Shetland Basin, huge amounts of basaltic rock were erupted during the Paleocene-Eocene. Previous studies suggest this basalt is covering relatively low velocity materials which may be sediments (Hughes et al., 1998; Richardson et al., 1999; Fliedner and White, 2003; Raum et al., 2005). Topography before the emplacement of the basalt was dominated by normal faults as a consequence of extension and subsidence during the Cretaceous and Paleocene (Richardson et al., 1999). Basaltic flows extended over long distances in the basin after filling the lows between fault blocks. This causes an irregular bottom basalt interface. Basalt was erupted in different episodes. Three major basalt units have been identified: Lower, Middle and Upper Series. Their thicknesses and compositions differ from one unit to another (Noe-Nygaard and Rasmussen, 1968). Although, the basalt flow stratigraphy in this area is mainly layered, it includes tuffs and breccias increasing the inner velocity contrasts (Maresh and White, 2005). Moreover, in periods without igneous activity, lacustrine shales and coals were accumulated and sediments were emplaced filling the basin floor deeps (White et al., 2003). Those facts result in a highly heterogeneous distribution of physical properties within the basaltic body.

In the Faroe Shelf, the structure above the basalt and the top basalt interface can be succesfully resolved using conventional techniques because of the high contrast in physical properties between basalt and overlying sediments. However, attenuation and scattering of the seismic wavefield as it passes through the basaltic pile make seismic imaging difficult below the top basalt surface (Smallwood et al., 2001). The top basalt interface shows an irregular topography featuring fractal properties (Martini and Bean, 2002). This irregular topography is often at a scale similar to the seismic wavelength which causes the dispersion of elastic energy (scattering) degrading the signal coherence in the wavefield. In addition, heterogeneities within the basalt flows yield a high impedance contrast generating internal reverberations, mode conversions and internal multiples (Martini and Bean, 2002). Therefore, seismic energy reflected or refracted by these structures is incoherently scattered and dispersed resulting in a poor subbasalt image.

3 Pre-stack depth migration

An extensive revision of the algorithms and evolution of Pre-Stack migration can be found in the dedicated volume of Jones et al. (2008). Pre-stack depth migration aims to place the reflected amplitude at the precise location within the model from which the energy was reflected. Conventional migration algorithms requiere travel time tables to distribute the energy recorded (the amplitude of the seismograms) among the grid points in the model. The amplitudes of a trace in a shot gather, $a(t_i)$, are distributed (sprayed) among the points of a gridded model according to the t_i time at which it arrived at the sensor. Therefore, an algorithm to compute the travel times is imperative in order to be able to migrate. There are different ways to compute this travel times. A large majority of algorithms use conventional ray tracing approximations in one of each varieties, ray shooting, two point ray tracing, gausian beam etc. Once the travel time has been estimated we need to estimate how the amplitude is distributed among all the grid points in the model. The amplitude in the trace can be considered to be:

$$a(t_i) = \sum_j r_j \cdot a(t_i)_j$$

where j covers all the points of the model characterized by a time t_i. t_i is the time it took the seismic energy to travel from the source to that point in the model and then to the receiver.

The calculation of traveltime tables for a given velocity model is an essential stage in Kirchhoff prestack depth migration. Classical ray tracing techniques have been widely used to solve the forward problem (Zelt and Smith, 1992) and to calculate traveltime tables. Snell's law based algorithms are fast and provide an estimation of the traveltime for areas in the model sampled by rays traced. However, in some implementations, sampling all the model requires a large amount of rays and depending on the velocity model (e.g. high velocity gradients) some areas can be undersampled resulting in shadow zones where no traveltimes are calculated. Ray-tracing methods in the presence of high velocity contrasts, and/or structures with sharp edges have difficulties in calculating the travel times. The result is that a few grid points lack travel times. This can be solved in different ways, for example by performing interpolating schemes (see Jones et al., 2008 for a review) or by using a finite difference approach.

In the present work, we used a finite difference algorithm to solve the eikonal equation (Hole and Zelt, 1995). Using this algorithm, traveltimes are calculated for every node in the model, which slightly increases the computational cost compared with shooting ray methods, but, on the other hand, shadow zones are avoided. Moreover, using complete traveltime tables allows the handling of diffractions, correctly restoring the diffracted energy to its original position in the model. The finite difference solution of the eikonal equation is not unique to the algorithm used in this manuscript. This approach is used in other commercial packages. The advantages of using the eikonal to compute the travel times is that it is more robust than ray tracing methods as it is able to estimate travel times for all the points in a model grid being more stable when high velocity contrasts exist.

As migration consist of summation of the contributions from the wavefield for every source-receiver pair, once the traveltime field has been calculated, a half-derivative is performed on every trace and amplitudes are spread among the grid points of the model. The amplitudes have been

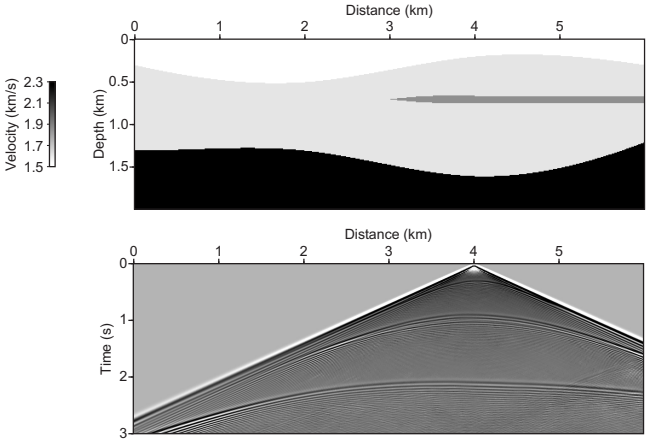

Fig. 1. Velocity model used to calculate synthetic data (top) and a shotgather generated at $x = 4$ km (bottom).

previously scaled by the apropriate obliquity factor (Yilmaz, 1987) that correspond to each grid point.

The r_j are commonly known as the obliquity factors. These obliquity factors are estimated by using the parameters of the ray at the particular point (angle of incidence). Thus. For prestack migration we nearly always require a starting model. This starting model is used to compute all the necessary parameters for the migration, the travel times and the obliquity factors.

Computing obliquity factors by using the forward modeling parameters, as the angle of incidence at each of the model grid point is the conventional approach. The algorithm, in this manuscript in its present form uses the semblance of the tau-p transform of the shot gathers. The most relevant difference between the conventional algorithms and the current one is that conventional schemes use to compute the r_j using the model (they are model dependent) while in the approach used in this manuscript we use the actual data to compute the obliquity factors (the algorithm is data dependent). The semblance of the tau-p transform of the shot gathers represents a measure of the reflected energy as a function of slowness (ray parameter, direction of the reflection). Therefore, these represent to some degree the obliquity factors.

Another key point in pre-stack depth migration is the generation of numerical artifacts that result in "smiling" images. This is a known issue that usually is solved by limiting the aperture in the migration algorithm. This strategy can solve the problem in subhorizontal layered models but it fails when considering complex models with vertical or dipping structures. In any case, if the fold of the data is high, the summation of complete migrated shotgathers contributes to enhance coherent signal while spurious artifacts are highly attenuated in the final image.

We coded this approach into a new pre-stack migration algorithm. In order to test the code, a synthetic model was used (Forel et al., 2005). The model consists in three layers

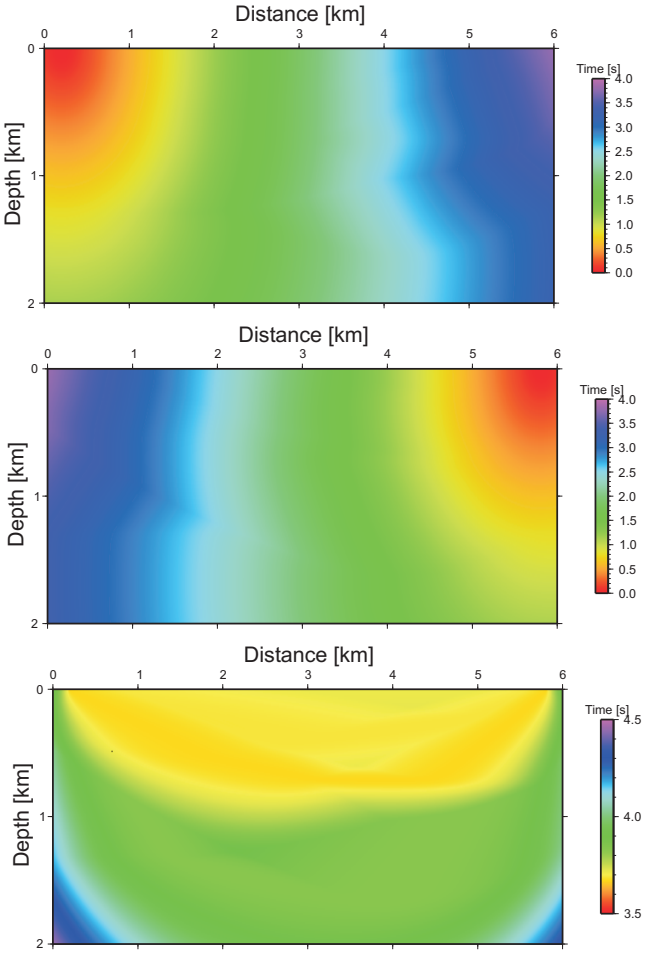

Fig. 2. Traveltime tables for the source at $x = 0.2$ km (top) for the receiver at $x = 5.8$ km (middle) and the sumation of both timetables (bottom). These traveltime tables were obtained using a finite difference solution of the eikonal equation (Hole and Zelt, 1995). The yellow and orange colors indicate the zone of minimum traveltimes. This ilustrates the fastest path from the source to the receiver within the model (the banana-kernels). This ilustrates that the scheme used is able to handle long-offsets.

and within the second one, a thin high velocity layer was included to simulate a basaltic intrusion (Fig. 1 top). Up to 40 synthetic shotgathers were calculated for this velocity model using a full waveform acoustic scheme (Fig. 1 bottom). The sources were placed on the surface every 50 m between 2 and 4 km and the receivers were also placed every 50 m at the surface using a split-spread pattern with offset ranging from -1500 m to 1500 m. For every source and every receiver, a traveltime table was calculated. Then, for every source-receiver pair, their respective traveltime tables were added to obtain a new traveltime table which represents, for each grid point, the travel time from source to receiver of a wave crossing this grid point. This new traveltime table becomes the one used in the migration (Fig. 2). Note that the

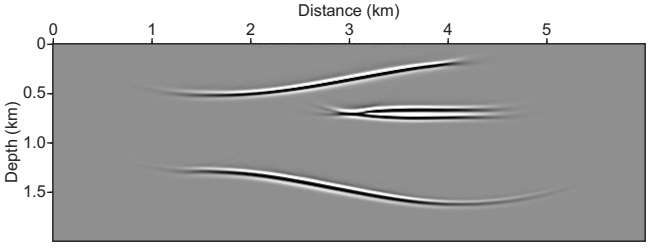

Fig. 3. Migrated image of the synthetic example.

region of minimum traveltimes (banana-kernel) in the resulting traveltime table can be used to obtain (a posteriori) the ray trajectory for first arrivals. Every shot in the dataset was migrated and stacked over every node in the model resulting in a final migrated image (Fig. 3). The resulting image reproduces reasonably well the theoretical model.

4 Real case: subbasalt imaging

Data from the survey FLO-96 over the Faroe Shelf (Fig. 4) acquired using two vessels (White et al., 1999) with multiple passes to build up a synthetic aperture of over 38 km with a receiver group spacing of 12.5 m which presents other issues associated with the geometry caused by poorly constrained cable feathering. This dataset features the conventional problems of marine seismic reflection data: multiples, peg-legs, and other reverberation; tidal and ambient noise; converted waves etc.

The lead vessel (M/V Western Cove) towed a 6 km cable and deployed a 32 sleeve-gun source array with a total volume of 3000 cu in. The second vessel (I/S Thetis) followed at variable distances and towed a 4.8 km cable and deployed a 30 sleeve-gun source array with a total volume of 5070 cu in. Data acquired using this configuration can be considered from two points of view: as a standard normal incidence experiment; or as a very dense wide-angle experiment. This combination gave an effective aperture of 16.8 km. The basic processing steps are laid out in Table 1; the philosophy was: to enhance the low frequency energy; suppress sea-bed, sediment and top-basalt multiples, peg-legs and other reverberations; suppress other low velocity energy; and stack using a velocity model based on conventional analysis. The subbasalt velocity model was determined from the occasional strong reflection event visible above the noise probably from a sill or top basement.

From the stacked image (Fig. 5 top) we can interpret the structure overlying the basalts and obtain a detailed velocity model for these sediments. We can also map the topography of the top-basalt. However, using conventional post stack imaging techniques, no laterally coherent events are identified under this high velocity layer (Fig. 5 top). In order to improve this image beneath the basalt, pre-stack depth mi-

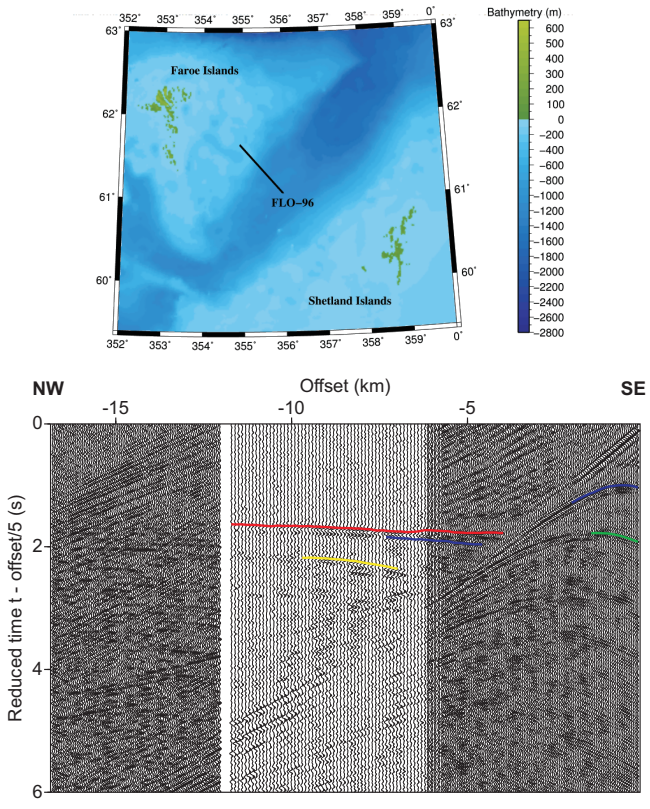

Fig. 4. Survey FLO-96. Location map of the profile (top), and shotgather (bottom). In the shot gather the NW corresponds to the left and the SE to the right The following phases are identified: sea bottom reflection (blue), top-basalt reflection (green), basalt refraction (red), base-basalt reflection (purple) and top-basement reflection (yellow). This shotgather is a composite from the two-ship experiment (see the text for an explanation).

gration was applied using the pre-stack data after SRMS and Tau-p filtering had been applied. This provides more detailed image of the subbasalt zone. While stack-based methodologies produce a section in time, pre-stack depth migration will result in a depth section which provides information for a better interpretation.

The main advantage of considering long offset streamer data is that long offset phases may be identified, providing information to perform tomographic inversions. In standard marine seismic reflection data, most of the signal and energy lie within the water-wave cone and therefore are affected by multiples and peg-leg making it very difficult to identify phases. At long offset these reflections appear as clear and isolated events and refractions can be picked as clear arrivals. The use of long offset data therefore considerably improves the accuracy and quality of the velocity model with respect to the usual velocity analysis in the CDP domain.

In the first part of the profile, refractions from basalt and reflections from the top of the basalt layer are very clear. In some shots, two hyperbolic events can be picked and

Table 1. Processing steps applied to data.

Processing step	Parameters
Source matching filter	
Assign geometry	
Bandpass filter	high-cut Ormsby 48–64 Hz
Bin	50 m receiver group/25 m CMP spacing
Create Split Spread	aperture -1 km $\rightarrow$ 16.8 km
Surface Related Multiple Suppression (SRMS)	multiple model based on sea-bed inter-sediment horizon and top-basalt picked from near-offset stack
Tau-p filter applied to both common shot and common receiver domains	Gaussian weighted filter with mean slowness of 0.075 ms m^{-1} and variance of 0.064 ms m^{-1}
Velocity analysis	Semblance, function gather and function stacks
NMO	
Mute	Outer and Inner mute
Stack	
Amplitude recovery	$t^{1.8}$
Display	

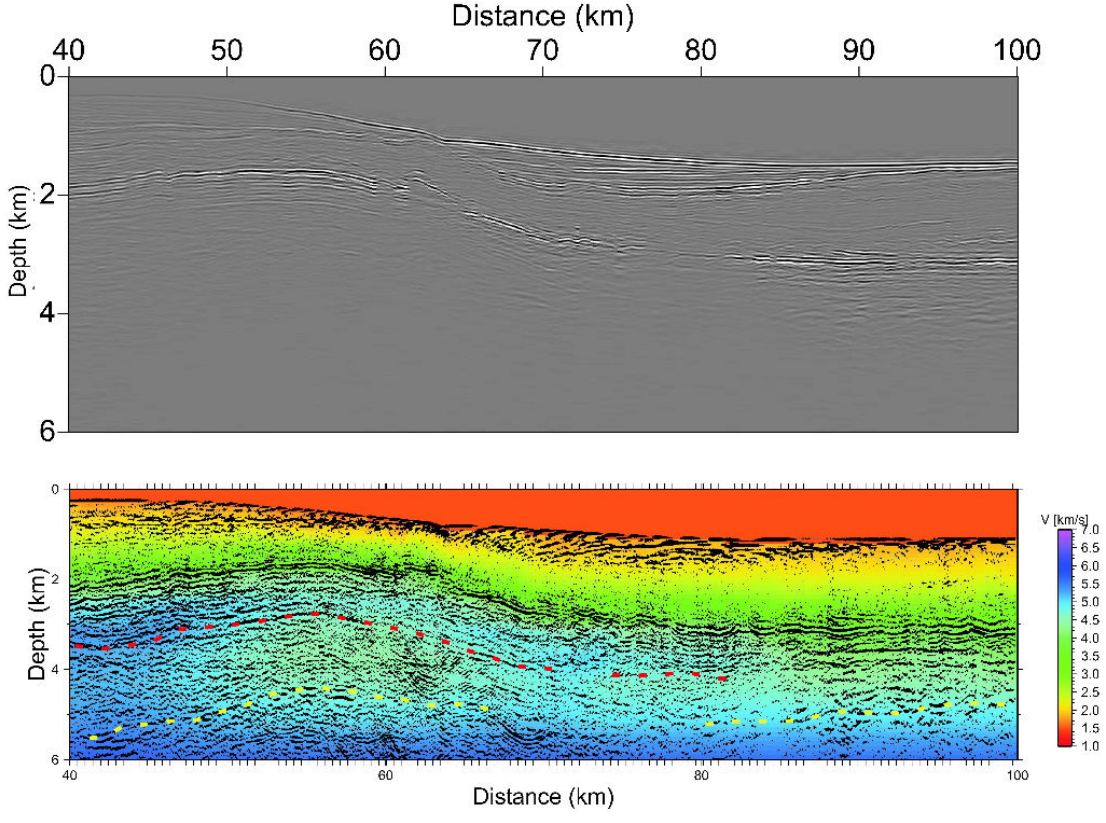

Fig. 5. Top: stacked section from the FLO-96 survey. The top of basalt is clearly delineated. At the beginning of the profile (NW) basalt is shallower (around 1.8 s) becoming deeper from kilometer 60 to kilometer 75 where it remains practically flat around 3 s until the end of the profile (SE). No coherent subbasalt events can be identified. Bottom: pre-stack depth migration of the same data set. The coloured background stands for the velocity model obtained by means of seismic tomography (Trinks et al., 2005). Dashed lines stand for interpreted base of basalt (red) and top of basement (yellow).

interpreted as the base-basalt reflection and the top-basement reflection (Fig. 4). In the last part of the profile, the top-basalt reflection could be identified while the basalt refraction completely disappeared. This is due to the thinning of the basalt layer to the SE. Also in this part, some hyperbolic events were identified in the data out of the water-wave cone, but, due to the lack of lateral continuity (events only appeared for four or five shots), these events were interpreted as sills or laminar instrusions rather than a laterally continous geological discontinuity. Inverting basalt refractions, top-basalt reflections, base-basalt reflections and basement reflections, a velocity model was obtained down to the top of the basement (coloured background in Fig. 5 bottom). The velocity model was obtained using the tomographic algorithm by Trinks et al. (2005). This algorithm is able to use diving as well as reflected waves. Therefore it recovers the velocity distribution and the topography of the reflecting structures. In this study, the reflected phases were use to increase the resolution of the velocity model. The pre-stack migration algorithm only required the distribution of velocities to generate the depth migrated image. The reflecting interfaces constrained by the tomographic algorithm were not used. The image produced correlates very closely with the interfaces constrained by the inversion algorithm.

The sedimentary cover features velocities ranging from around $2\,\mathrm{km\,s^{-1}}$ at the sea bottom to $3.5\,\mathrm{km\,s^{-1}}$ at the top of the basalt layer. A high velocity layer (4.5–$5\,\mathrm{km\,s^{-1}}$) can be identified with a decreasing thickness from 1.5 km at 40 km to 0.5 km at 100 km. The inverted model suggests that there maybe a lower velocity layer under the basalts. Nevertheless, few events were identified from under the basalt layer, suggesting velocities in this area are less constrained than in other parts of the model. The lack of events within the basement made it impossible to extend the tomographic model beyond 6 km depth. The new pre-stack depth migration scheme was used to obtain a new image using the velocity determined by the tomographic inversion (Fig. 5 bottom). This method provided an improved display under the upper basalt interface where prominent events correlate with major velocity discontinuities along the whole model. The top of the basalt is clearly delineated. The base of this layer can be estimated in some parts of the model, especially along the first 30 km. In addition, some reflectors exist between 4 and 5 km depth which may correspond to the top of the basement.

The determination of the base of the basalt layers is a key issue for exploration perspectives. Sedimentary layers can be located between the basalt intrusive and the basement. The importance of imaging these hidden sedimentary structures to gauge potential petroleum resources becomes clear.

Some authors have proposed an alternative scheme for migrating long offset reflection data (Fruehn et al., 2001; Fliedner and White, 2001, 2003; White et al., 2003). Their scheme uses only selected signal out of the water-wave cone Following this strategy a low frequency image was produced because only long offset phases were included. In the present study, all the data in every shotgather were used in the process, obtaining a more detailed image because high frequencies were also included in the migration. Migrating selected parts of the shotgathers causes final image to be highly dependent on a subjective interpretation undertaken prior to the migration. This interpretation was considered when inverting traveltimes. Migrating the whole data set has the advantge of obtaining a migrated section free of a priori interpretations. Moreover, in regions where intra-basalt and subbasalt events are weak, the reflectors are more clearly displayed using all the data as shown in the last part of the profile.

5 Conclusions

Pre-stack depth migration provided improvement in subbasalt imaging. The code developed to implement this technique takes advantage of a finitte difference algorithm that can handle sharp velocity contrasts and velocity inversions avoiding shadow zones in the traveltime tables. Synthetic simulations using a realistic model showed a good performance of the code and good recovery of the original model. The code was then used with real data from the FLO-96 survey. This processing showed that pre-stack depth migration improved the image obtained beneath the top of the basalt layer. In the final image, the base of the basalt was inferred in some parts of the model and subbasalt events were recovered. The results indicate that all offsets are required to produce a high frequency pre-stack depth migration image. The migrated section is highly dependent on the velocity model, therefore, using an accurate tomographic model is mandatory to obtain a reliable result.

Acknowledgements. Funding for this research was provided by SINDRI (Quantitative evaluation of the existing technologies for imaging within basalt-covered areas from the Faroes region), the Spanish Ministry of Science and Technology (Ref: CGL2004-04623/BTE) and Generalitat de Catalunya (Ref: 2005SGR00874). Part of this work was developed during a one month stay in Orsay financed by Université Paris-Sud. We are grateful to Immo Trinks for training in the use of the TTT code.

Edited by: T. Iwasaki

References

Fliedner, M. M. and White, R. S.: Sub-basalt imaging the Faeroe-Shetland Basin with large-offset data, First Break, 19, 247–252, 2001.

Fliedner, M. M. and White, R. S.: Depth imaging of basalt flows in the Faeroe-Shetland Basin., Geophys. J. Int., 152, 353–371, 2003.

Forel, D., Benz, T., and Pennington, W. D.: Seismic Data Processing with Seismic Un*x, Society of Exploration Geophysicists, 2005.

Fruehn, J., Fliedner, M. M., and White, R. S.: Integrated wide-angle and near-vertical subbasalt study using large-aperture seismic

data from the Faroe-Shetland region, Geophysics, 66, 1340–1348, 2001.

Hole, J. A. and Zelt, B. C.: Three-dimensional finite-difference reflection travel times, Geophys. J. Int., 121, 427–434, 1995.

Hughes, S., Barton, P. J., and Harrison, D.: Exploration in the Shetland-Faeroe Basin using densely spaced arrays of ocean-bottom seismometers., Geophysics, 63, 490–501, 1998.

Jones, I., Bloor, R. I., Biondi, B. L., and Etgen, J. T.: Prestack Depth Migration and Velocit Model Building, Society of Exploration Geophysics, Geophysics reprint series, 25, 2008.

Maresh, J. and White, R. S.: Seeing through a glass, darkly: strategies for imaging through basalt, First Break, 23, 27–33, 2005.

Martini, F. and Bean, C. J.: Interface scattering versus body scattering in subbasalt imaging and application of prestack wave equation datuming, Geophysics, 67, 1593–1601, 2002.

Noe-Nygaard, A. and Rasmussen, J.: Petrology of a 3000 metre sequence of basaltic lavas in the Faroe Islands, Lithos, 1, 286–304, 1968.

Raum, T., Mjelde, R., Berge, A. M., Paulsen, J. T., Digranes, P., Shimamura, H., Shiobara, H., Kodaira, S., Larsen, V. B., Fredsted, R., Harrison, D. J., and Johnson, M.: Sub-basalt structures east of the Faroe Islands revealed from wide-angle seismic and gravity data, Petrol. Geosci., 11, 291–308, 2005.

Richardson, K. R., White, R. S., England, R. W., and Fruehn, J.: Crustal structure east of the Faroe Islands: mapping sub-basalt sediments using wide-angle seismic data, Petrol. Geosci., 5, 161–172, 1999.

Smallwood, J. R., Towns, M. J., and White, R. S.: Thew structure of the Faeroe-Shetland Trough from integrated deep seismic and potential field modelling, J. Geol. Soc., 158, 409–412, 2001.

Sørensen, A. B.: Cenozoic basin development and stratigraphy of the Faroes area, Petrol. Geosci., 9, 189–207, 2003.

Trinks, I., Singh, S. C., Chapman, C. H., Barton, P. J., Bosch, M., and Cherrett, A.: Adaptative traveltime tomography of densely sampled seismic data, Geophys. J. Int., 160, 925–938, 2005.

White, R. S., Fruehn, J., Richardson, K. R., Cullen, E., Kirk, W., Smallwood, J. R., and Latkiewicz, C.: Faroes Large Aperture Research Experiment (FLARE): imaging through basalt, Geological Society, 1243–1252, 1999.

White, R. S., Smallwood, J. R., Fliedner, M. M., Boslaugh, B., Maresh, J., and Fruehn, J.: Imaging and regional distribution of basalt flows in the Faroe-Shetland Basin., Geophys. Prosp., 51, 215–231, 2003.

Yilmaz, O.: Seismic data processing, Society of Exploration Geophysicists, Tulsa, 1987.

Zelt, C. A. and Smith, R. B.: Seismic traveltime inversion for 2-D crustal velocity structure, Geophys. J. Int., 108, 16–34, 1992.

6. SEISMIC IMAGING AND MODELLING OF THE LITHOSPHERE OF SW-IBERIA

I. Flecha, I. Palomeras, R. Carbonell, F. Simancas, P. Ayarza, J. Matas, F. González-Lodeiro and A. Pérez-Estaún, *Tectonophysics*, 472, 148-157,2009.

Tectonophysics 472 (2009) 148–157

Contents lists available at ScienceDirect

Tectonophysics

journal homepage: www.elsevier.com/locate/tecto

Seismic imaging and modelling of the lithosphere of SW-Iberia

I. Flecha [a,*], I. Palomeras [a,1], R. Carbonell [a,1], F. Simancas [b,2], P. Ayarza [c,3], J. Matas [d,4], F. González-Lodeiro [b,2], A. Pérez-Estaún [a,1]

[a] Departament de Geofísica i Tectònica, Institut de Ciències de la Terra "Jaume, Almera"-CSIC, C/ Lluis Solé i Sabaris s/n, 08028 Barcelona, Spain
[b] Departamento de Geodinámica, Universidad de Granada, Av. Fuentenueva, s/n, 18071 Granada, Spain
[c] Departamento de Geología, Universidad de Salamanca, 37008 Salamanca, Spain
[d] Instituto Geológico Minero de España, C/ Ríos Rosas, 23, 28003 Madrid, Spain

ARTICLE INFO

Article history:
Received 21 March 2007
Received in revised form 29 April 2008
Accepted 15 May 2008
Available online 5 June 2008

Keywords:
Wide-angle stack
Mafic intrusions
Crustal heterogeneities

ABSTRACT

Data from a closely spaced wide-angle transect has been used to study the middle-to-lower crust and the Moho in SW-Iberia. A low-fold wide-angle stack image reveals a highly heterogeneous seismic signature at lower-crustal levels changing laterally along the profile. The lower crust features an irregular distribution of the reflectivity that can be explained by a heterogeneous distribution of physical properties. The Moho discontinuity also features a high variability in its seismic character that correlates with the different tectonic terranes in the area. A 2D finite difference code was used for solving the elastic wave equation and to provide synthetic wide-angle shots. Relatively simple layer cake model derived from conventional refraction interpretation generates the main events of the shot records. However, these models cannot account for the lateral variability of the seismic signature. In order to obtain more realistic simulations, the velocity model was modified introducing stochastic lensing at different levels within the crust. The Moho was modelled as a 3 km thick layered structure. The resulting average velocity models include a high velocity layer at mid-crustal depth, a highly reflective lower crust and a relatively thin horizontal Moho. This heterogeneous model can be achieved by lensing within the crust, a layered mafic intrusion and a strongly laminated lower crust and Moho.

1. Introduction

The lower crust and the Moho are major issues in deep geophysical prospecting. The knowledge about these parts of the Earth crust is limited because of the lack of direct information at this level of the lithosphere. Nevertheless, some outcrops have been identified as corresponding to lower crust materials. Good examples are the Cabo Ortegal complex (Peucat et al., 1990; Galán and Marcos, 1997; Martínez-Catalán et al., 1997; Santos-Zalduegui et al., 1997) and the Ivrea Zone (North Italy; Rutter et al., 1999). In both these cases several studies have been carried out and their crustal composition and the distribution of physical properties are well known (Holliger and Levander, 1992; Holliger et al., 1993; Levander et al., 1994b). Since the lower continental crust is not accessible for direct investigation, the main source of information about its physical properties and composition comes from indirect methods such as deep seismic surveys. Seismic vertical incidence reflection profiles provide images where geometric information about the crustal structure can be obtained and wide-angle experiments provide data about physical properties (P-wave and S-wave velocities). These physical properties can then be inverted to composition by comparing with lithologies measured in laboratories. Results from these methodologies and its correct interpretation are probably the best tools available in order to understand geological processes at lithospheric scale.

Since the early 1990's, a large research effort has been devoted to studying SW-Iberia (e.g., the EUROPROBE (Ribeiro et al., 1996) and GEODE (Blundel et al., 2005) international programmes). One of the main objectives of these programmes was the acquisition of the high resolution normal incidence deep seismic reflection transect IBERSEIS (Simancas et al., 2003; Carbonell et al., 2004). The presence of large mineral deposits in the southwestern part of the Iberian Península, within the Pyrite Belt, and surrounding areas, suggests that the crust features particular physical properties and that it underwent a singular tectonic evolution. Therefore, extensive geological and geophysical research has been undertaken in the area.

The project IBERSEIS-WA consisted in two wide-angle transects acquired in SW-Iberia. A wide-angle stack of one of the wide-angle dataset (transect B, Fig. 1) is presented in this study. The specific target of this research is the nature of the lower crust and Moho. Furthermore, synthetic seismic modelling is carried out in order to explain the

* Corresponding author. Tel.: +34 93 409 54 10; fax: +34 93 411 00 12.
E-mail addresses: iflecha@ija.csic.es (I. Flecha), ipalomer@ija.csic.es (I. Palomeras), rcarbo@ija.csic.es (R. Carbonell), simancas@ugr.es (F. Simancas), puy@usal.es (P. Ayarza), lodeiro@ugr.es (F. González-Lodeiro), andres@ija.csic.es (A. Pérez-Estaún).
[1] Tel.: +34 93 409 54 10; fax: +34 93 411 00 12.
[2] Tel.: +34 958 24 33 53; fax: +34 958 24 85 27.
[3] Tel.: +34 923 29 44 88.
[4] Tel.: +34 91 349 57 00.

0040-1951/$ – see front matter © 2008 Elsevier B.V. All rights reserved.
doi:10.1016/j.tecto.2008.05.033

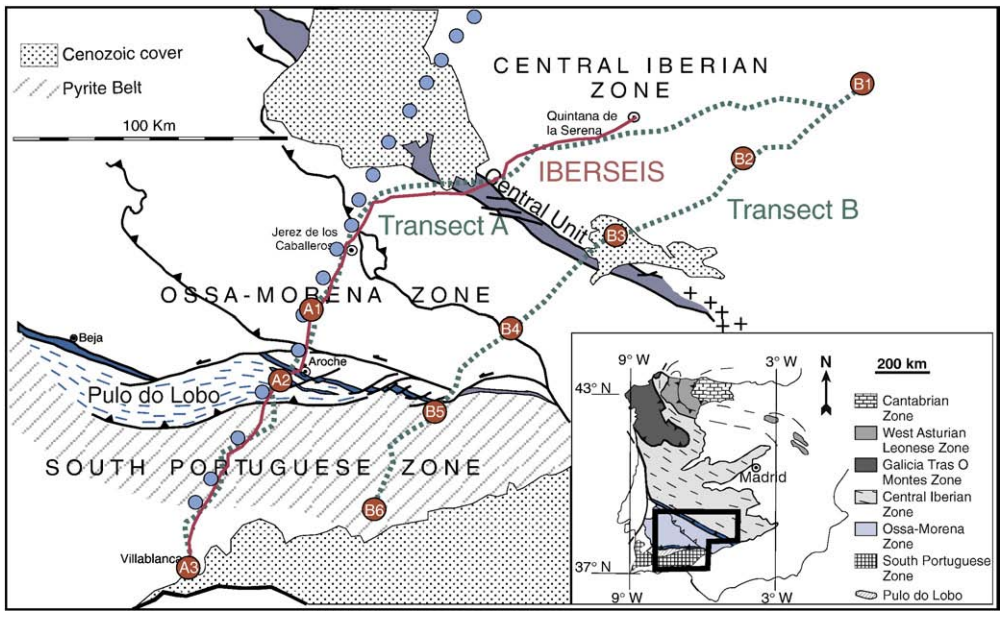

Fig. 1. Location map of the study area. The three tectonic terranes and its contacts are indicated. PL indicates Pulo du Lobo unit and CU indicates Central Unit. Dashed green lines indicate the wide-angle profiles and the red circles the shot points. Other surveys in the area are also shown: IBERSEIS deep seismic reflection transect (red line) and a magnetotelluric survey (blue circles). Data used in this work correspond to the eastern wide-angle profile, transect B. Modified from Palomeras et al. (2009).

particular characteristics of the shot-gathers and of the wide-angle stack. The main objective of the present study is to provide reliable images and geometrical models that can account for the seismic signature observed in the wide-angle dataset.

2. Geological and geophysical setting

The study area is located in the SW of the Iberian Massif, it is known to be an orogenic belt of Variscan age developed by the collision of a number of continental blocks. The area involves three tectonic terranes: South-Portuguese Zone (SPZ), Ossa-Morena Zone (OMZ), and Central-Iberian Zone (CIZ) (Fig. 1). These terranes are considered to be fragments of a Late Proterozoic mega continent which broke up in Early Paleozoic. The boundaries that limit these terranes have been interpreted as suture zones and include units of high-pressure rocks (Simancas et al., 2001).

The SPZ, which includes the Iberian Pyrite Belt, features within the upper crust a south-west vergent thrust system. The northern boundary of this zone is indicated by a series of slices of high-pressure rocks, the Beja Acebuches complex located to the north of the Pulo do Lobo Unit (Simancas et al., 2001, 2003). The surface outcrops of this contact (SPZ/OMZ) reveal fabrics that are indicative of a strike-slip component of the collision (i.e. transpression). The OMZ is mostly consistent of synforms and antiforms. This zone is limited to the north by the Central Unit (CU), and outcroping fault bounded wedge of metamorphic rocks with structural fabrics revealing strike-slip movement. Farther to the north, the CIZ features normal faults that cut recumbent folds resulting in basins of carboniferous age (Simancas et al., 2003). These structures suggest a domino-like extensional system. The surface evidences for strike-slip movement indicate that the orogen went through a strong transpression regime during its development.

A detailed geological study of the area can be found in Simancas et al. (2001) and references therein. The contribution of the IBERSEIS deep seismic reflection transect, acquired in the same area, can be found in Simancas et al. (2003) and in Carbonell et al. (2004). Finally, the crustal model derived by traveltime interpretation of the wide-angle dataset and the geologic implications on the nature of the lower crust are discussed in detail by Palomeras et al. (2009). A relevant feature within the IBERSEIS deep seismic reflection transect is the IRB (Iberian Reflective Body) reflection, a 140 km long and 4 km thick high-amplitude reflective body which has been proposed to be related to the high concentrations of mineral deposits present mainly in the OMZ (Casquet et al., 2001; Tornos et al., 2001; Carbonell et al., 2004). This anomalous body was also reported as a high velocity zone in the refraction modelling with an extended distribution over the southern part of the Iberian Variscan Belt (Palomeras et al., 2009).

3. Wide-angle data: low-fold stack

The main objective of the low-fold wide-angle stack is to obtain a simplified structural image of the deep crust to the south-east of the IBERSEIS normal incidence transects. To the northwest, the crustal structure is well constrained by the IBERSEIS normal incidence transect.

The wide-angle seismic reflection data has station spacing of 150 m on average, making it suitable for generating a low-fold wide-angle stack. Following the conventional normal incidence processing, we used the acquisition geometry to define the CMP's. Then, following Carbonell et al. (1998, 2002), we designed a hyperbolic time shift to flatten the lower crust and the Moho reflections so that these events stack constructively within a CMP. Conventional NMO can be applied to wide-angle seismic reflection data, although this is not the optimum correction as it generates large artifacts when deep events and large offsets are considered. Therefore a hyperbolic time shift was preferred. The shot records were processed to emphasize the deep reflectivity. The data was Butterworth band-pass filtered (from 1 Hz to 35 Hz) and a time-dependent gain was applied to enhance the signal from the Moho. Also, the shot-gathers were displayed using an estimate of the seismic energy (Fig. 2). This was achieved by calculating the envelope using the Hilbert transform. Since we are interested in deep events, the first arrivals were muted to avoid its influence for displaying purposes. After this pre-processing the Moho can be displayed as a flat 1–2 second thick event (Fig. 2). As in the raw

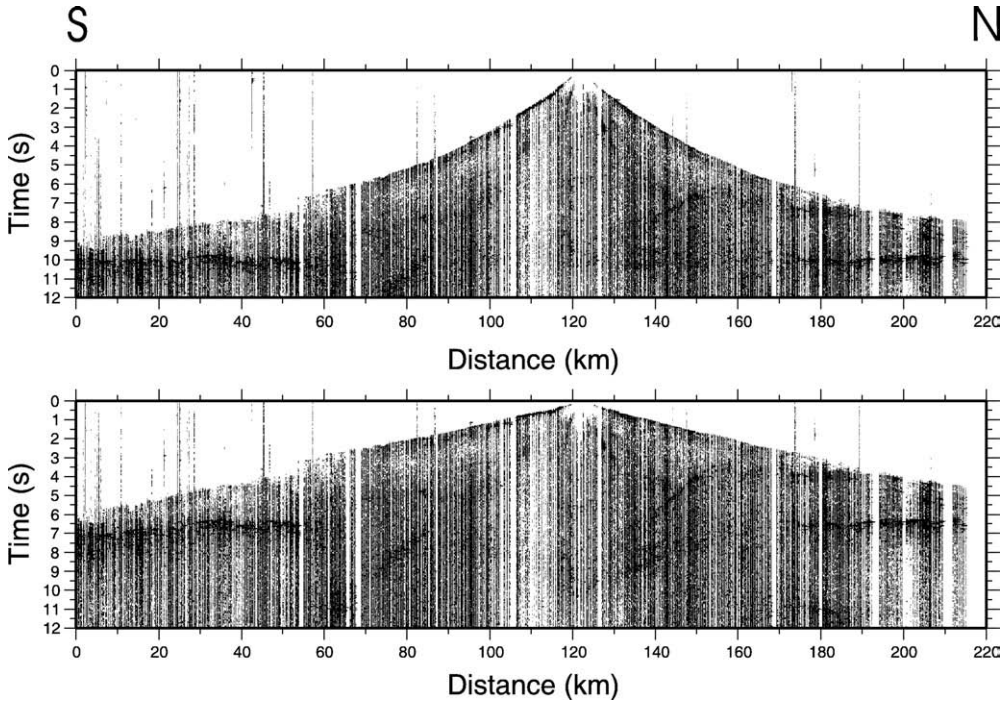

Fig. 2. Wide-angle shot-gather B3 after a hyperbolic shift using as a crustal average velocity 6.0 km/s (top) and after a linear reduction using 8.0 km/s as a reduction velocity.

data, some other coherent reflectors can be observed in the data as reflective packages at lower-crustal levels, which may image the structure in this part of the crust. The geometry of the mid-to-lower crust and the Moho reflections can be considered approximately correct with the applied time shift. An average crustal velocity deduced from Palomeras et al. (2009) was used to design this time shift.

3.1. Data description

Data after applying the hyperbolic shift are presented in Fig. 3. Shot B6 images strong reflectivity in the lower crust (6.5 to 8.5 s twtt) between 20 and 70 km. The Moho in this shot is not well resolved at short offsets (<40 km), probably because it is masked by the high-amplitude reflectors in the lower crust. At long offsets (>40 km), the Moho is imaged as a thick reflective package that slips slightly to the north. In shot B5 the Moho is imaged as a thin weak reflector at normal incidence (10 s twtt) while to the north it becomes a thicker event. Some reflectivity can be observed in the lower crust, matching the strong reflectivity exhibited by this zone in the previous shot B6. At 5.5 s twtt and normal incidence there is a prominent event, but due to the hyperbolic shift applied to the data it is difficult to determine its real geometry. Shot B4 displays strong reflectivity at lower-crustal levels, including a prominent south-dipping event between 30 and 45 km and 7.5 and 8.5 s twtt. To the north, a broad band of reflectivity (10.5 s twtt) is associated with the Moho. Shot B3 reveals a very well-defined PmP phase at 10 s twtt that delineates an almost flat Moho. The seismic signature varies significantly along this shot-gather, decreasing in thickness and complexity from south to north. A south-dipping event can be observed in the middle crust between 130 and 140 km and 6.5 and 8.5 s twtt, and is interpreted to be related to a near vertical structure because it cannot be identified in other shot-gathers. Shot B2 exhibits a clear, thick reflective package at 10 s twtt that extends laterally between 80 and 140 km. This event displays a changing characteristic along the profile. At normal incidence, the Moho is weakly imaged for positive offsets (north). In shot B1 there is large amount of reflected energy between 170 and 180 km, associated with the Moho. It can be followed to the south although it becomes diffuse. In the last 50 km to the north, the lower crust is highly reflective. Some of the events described previously are masked in the stacked image (Fig. 3) because there are reflectors that can only be imaged in single shot-gathers. However, the main features, especially the Moho, will be enhanced due by the constructive summation of seismic amplitudes. These are described below for each tectonic zone.

3.2. South Portuguese Zone (SPZ)

Within this area (0–40 km, Fig. 3) some relatively short reflectors can be observed at lower-crustal levels (between 7.5 and 8.5 s twtt). The Moho transition is identified as a thin weak reflection at 9.5 s in time (Fig. 3). Shots B5 and B6, reveal a simple event for the Moho which increases in thickness towards the east (Fig. 3). The lower crust reveals strong reflectivity that may be responsible for the back-scattered energy observed at 7–8 s twtt in the shot records. Thus, the seismic energy travelling through this structure has been noticeably decreased resulting in a weaker amplitude for deeper interfaces.

3.3. Ossa Morena Zone (OMZ)

In this part of the profile (40–110 km, Fig. 3) there are some prominent lower-crustal events in the southern part (40–60 km). To the north, this character changes and the lower crust becomes transparent. The Moho consists of a very reflective package at around 10 s twtt, with a variable thickness increasing from 1 s in the south to 2 s in the north. The change in the crust–mantle seismic signature would indicate a more complex structure compared with the SPZ.

3.4. Central Iberian Zone (CIZ)

In the second half of the profile (110–220 km, Fig. 3) the seismic energy appears as isolated packages around 10.5 s in depth. In the last part of the profile (190–210 km), some events are displayed in the lower crust at 7–8 s twtt.

4. 2D-modelling: from real data to synthetic simulations

In general, deep crust seismic data is often characterized by a high reflectivity compared to a relatively transparent upper crust (Martini

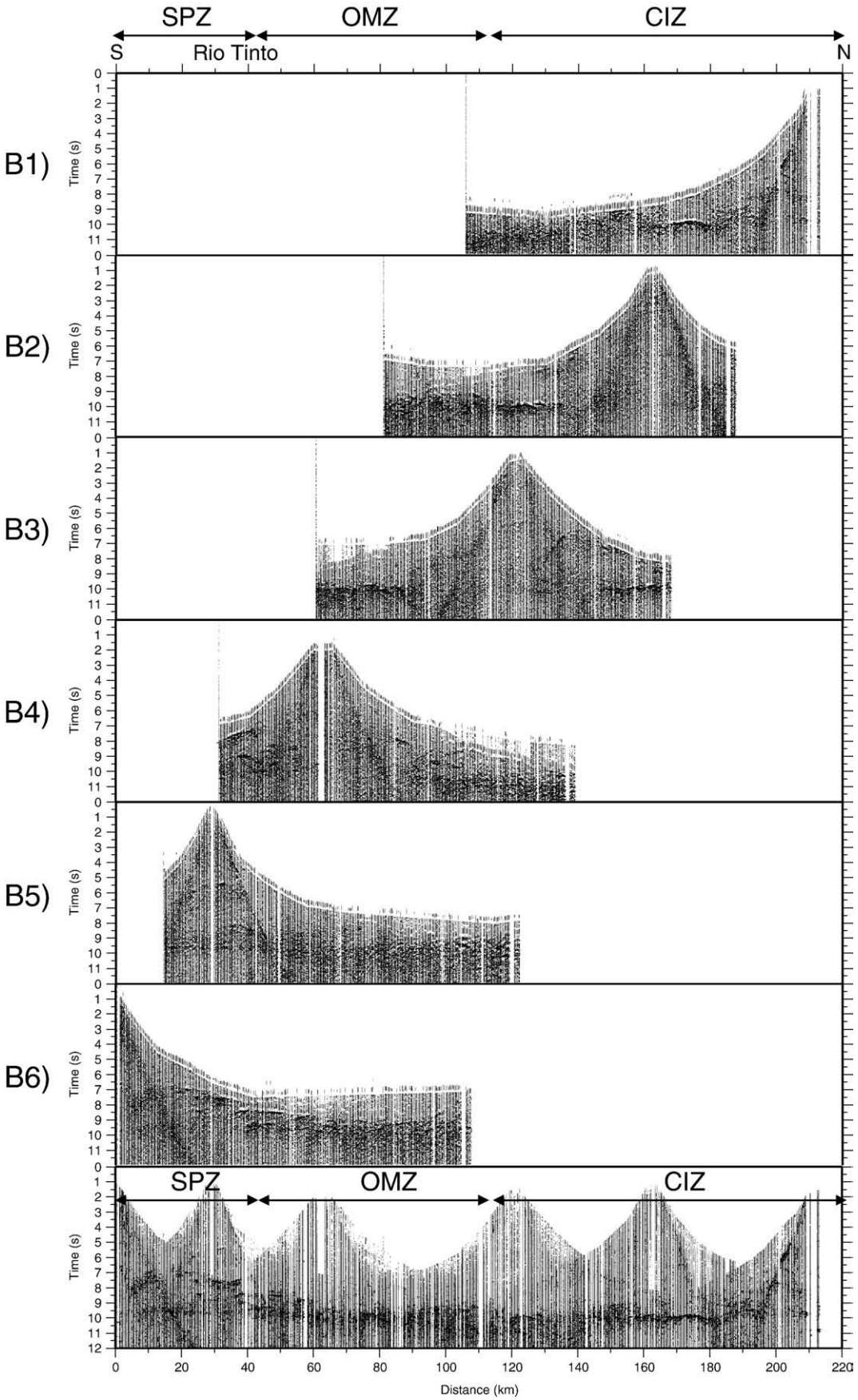

Fig. 3. From top to bottom: shot-gathers B6, B5, B4, B3, B2, B1 and stack. The shot-gathers are displayed in the CDP domain after applying a hyperbolic time shift. The three tectonic units are labelled as: SPZ (South Portuguese Zone), OMZ (Ossa Morena Zone) and CIZ (Central Iberian Zone).

et al., 2001). This reflectivity is normally composed of short, discontinuous reflections which usually appear in distinct packages confined to one or more parts of the crust (Holliger and Levander, 1992). It has been proposed that relatively small changes in composition and/or metamorphic grade, may substantially affect the reflectivity of the lower crust (Holliger et al., 1993). Otherwise, observed reflection amplitudes are often larger than the ones predicted by the reflection coefficients based on crustal composition which can be explained by the result of constructive interference between individual reflection wavelets (Hurich and Smithson, 1987). Reflection coefficients and reflection amplitudes are dependent upon the contrasts in acoustic impedance and not on bulk velocity (Deemer and Hurich, 1994), therefore a layered lower crust could be considered to justify these coefficients. This option would also account for reverberations in the data that cannot be explained by a single reflecting interface. The seismic signature featured by the acquired data can also be achieved by considering a lateral and vertical random velocity fluctuation (Gibson and Levander, 1988; Carbonell and Smithson, 1991). Isotropic random variations are consistent with models of lower-crustal petrologic processes, which may include igneous intrusions (Gibson and Levander, 1988). Hence, the most plausible scenario to satisfactorily describe the field data may consist of a random lamination or lensing coupled with random changes in rock properties. It has been shown that reflection seismic lines shot in the Variscan orogen display a strongly reflective lower crust characterized by numerous short horizontally embedded reflectors (Wenzel et al., 1987). Furthermore, field observations show that the crystalline rocks of the continental crust are often characterized by compositional variations at many scales (Hurich and Smithson, 1987) spanning at least seven orders of magnitude, from microfabrics ($\leq 10^{-3}$ m) to major crustal units ($\geq 10^{4}$ m) (Holliger et al., 1994).

Seismic theory establishes that Fresnel diameter is given by:

$$d \approx \sqrt{2z\lambda + \frac{\lambda^2}{4}} \quad (1)$$

and is the smallest resolvable feature in unmigrated seismic data, delimiting the measure of lateral resolution. Hence, crustal features smaller than Fresnel diameters are not expected to be recovered as coherent seismic events. However, fine-scale velocity fluctuations can fundamentally change the character of signals from the crust (Levander et al., 1994a). Seismic modelling has demonstrated that spatial interference is important during the formation of the reflection wavefield. Interference may result from reflecting bodies smaller than the Fresnel zone (small body diffractors), therefore constructive interference can be equally as important as compositional variation for determining reflection amplitudes (Hurich and Smithson, 1987). All these considerations must be taken into account in any model able to reproduce the crustal seismic response.

4.1. Forward modelling

The seismic velocity model (Fig. 4) obtained by Palomeras et al. (2009) indicates a maximum crustal thickness of ~33 km with a Moho characterized by a flat topography. However, the most remarkable feature from the refraction modelling is the high velocities at middle-crust levels. Velocities of 6.8 km/s to 6.9 km/s define a 70 km long lens located at 17 km in depth in the southern part of the profile. Towards the north, slightly higher P-wave seismic velocities have been modelled and can go as shallow as 12 km in the northern end of the profile (Palomeras et al., 2009).

Considering the velocity model obtained by Palomeras et al. (2009), forward modelling has been carried out using a second order finite difference solver for the elastic wave equation which includes all primary and multiple reflections (Sochacki et al., 1987, 1991). In some cases, the lower crust reflectivity patterns have been successfully modelled by using one-dimensional reflectivity codes (Wenzel et al., 1987; Carbonell et al., 2002). However, in the present study there are *a priori* reasons to think that the lower crust is a laterally inhomogeneous media (Palomeras et al., 2009). The previous IBERSEIS normal incidence experiment and the wide-angle stack are also indicative of a laterally heterogeneous media, therefore a two dimensional approach was preferred because one-dimensional modelling of wide-angle data would only result in a laterally averaged interpretation.

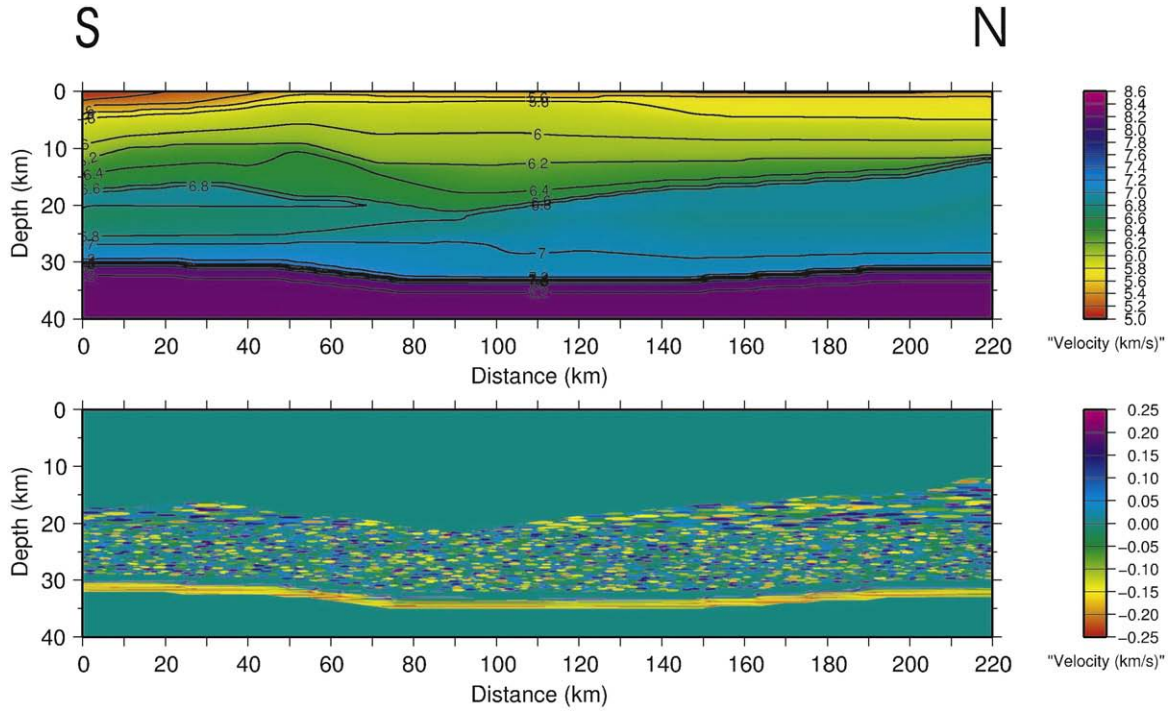

Fig. 4. Top: Velocity model obtained from refraction modelling (modified from Palomeras et al. (2009)). Bottom: Difference between refraction model and a modified velocity model to include the stochastic lensing representing mafic intrusions and lower crust as well as the layered structure of the Moho (bottom).

The P-wave velocity model derived from the refraction processing and interpretation was resampled using a 25×25 m grid which is appropriate for modelling crustal-scale seismic data. As the elastic approximation was used, also density and S-wave velocity were introduced as inputs in the code. The S-wave was calculated from the P-wave velocity using a V_p/V_s ratio of $\sqrt{3}$, and the density model was derived from V_p using the Christensen relation $\rho = 1.85 + 0.169V_p$ (Christensen and Mooney, 1995). In the resulting shot-gathers, traces were simulated in the same locations as the real receivers, the trace length was 30 s and the sampling rate was chosen to be 2 ms. With these synthetic simulations the main events in the real wide-angle shot-gathers were qualitatively well recovered (Figs. 5 and 6) because dominant reflections/refractions correlate with the boundaries of major lithological units. However, in the original shot-gathers, some events feature a complex signature consisting in a thick reflective package instead of an isolated event. The presence of these less well-defined events indicates that layering/lensing may be contributing to the seismic response. This fact forced us to consider a more sophisticated approach to model the lower crust and the mid-crustal high velocity areas.

4.2. Stochastic layering

It is well known that refraction techniques provide information about velocity, but depending on the depth (Fresnel zones), the accuracy is insufficient to assess the fine structure of the crust. Using these methodologies, major structures and discontinuities can be resolved within the crust. For the middle and the lower crust, the refraction velocity model represents an averaged background model which can fit correctly the picked traveltimes but, at small scale, it is unable to reproduce heterogeneities that feature the crustal velocity distribution. Probably the lower crust exhibits lateral heterogeneities that cannot be correctly modelled by using conventional ray tracing methods. In the recorded shot-gathers some of the phases consist of a thick reflective package instead of isolated events. This seismic signature cannot be reproduced with a simple smoothed layered model. In order to recover the observed reflectivity patterns some modifications were carried out in the velocity models to include some degree of complexity able to reproduce the seismic response recorded in the field data.

In SW-Iberia there are no outcrops of lower-crustal rocks where geological information can be obtained in order to characterize a realistic geometry and composition of this part of the crust. However, there is no seismological evidence that, apart from pressure and temperature, in situ conditions of the lower crust differ from those of its surface exposures (Wenzel et al., 1987). As the profile was acquired across Variscan terranes, we took physical properties (velocities) and geometrical information for the synthetic simulations from studies of the Variscan lower crust of Wenzel et al. (1987), Holliger and Levander (1992), Holliger et al. (1994). For the mafic intrusion, typical parameters

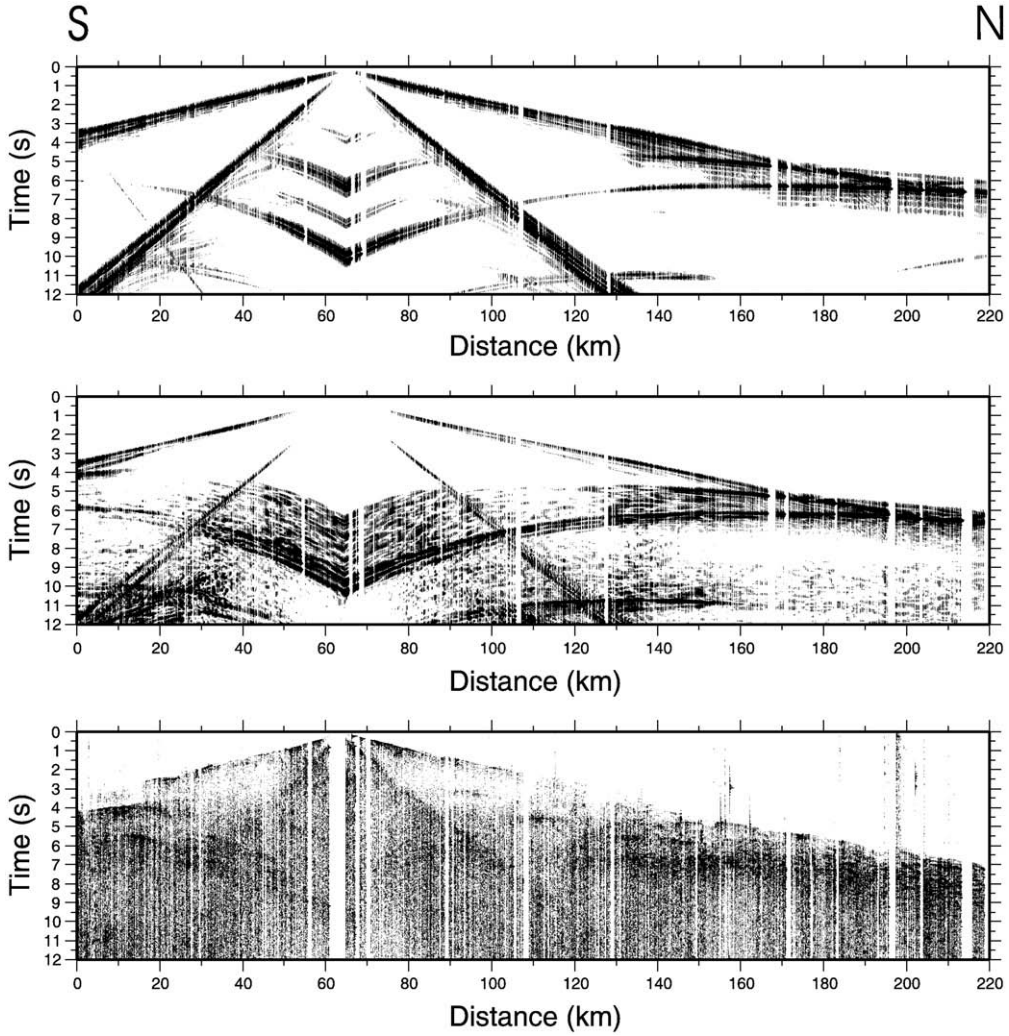

Fig. 5. Shot B4. Top: Synthetic seismic record section generated by using the homogeneous refraction velocity model. Middle: Synthetic seismic record section generated by using the heterogeneous velocity model consisting of a background velocity model which corresponds to the refraction model and the inclusion of the heterogeneities (high velocity lenses). Bottom: Real data. The synthetic sections were generated using a 2D elastic finite difference scheme.

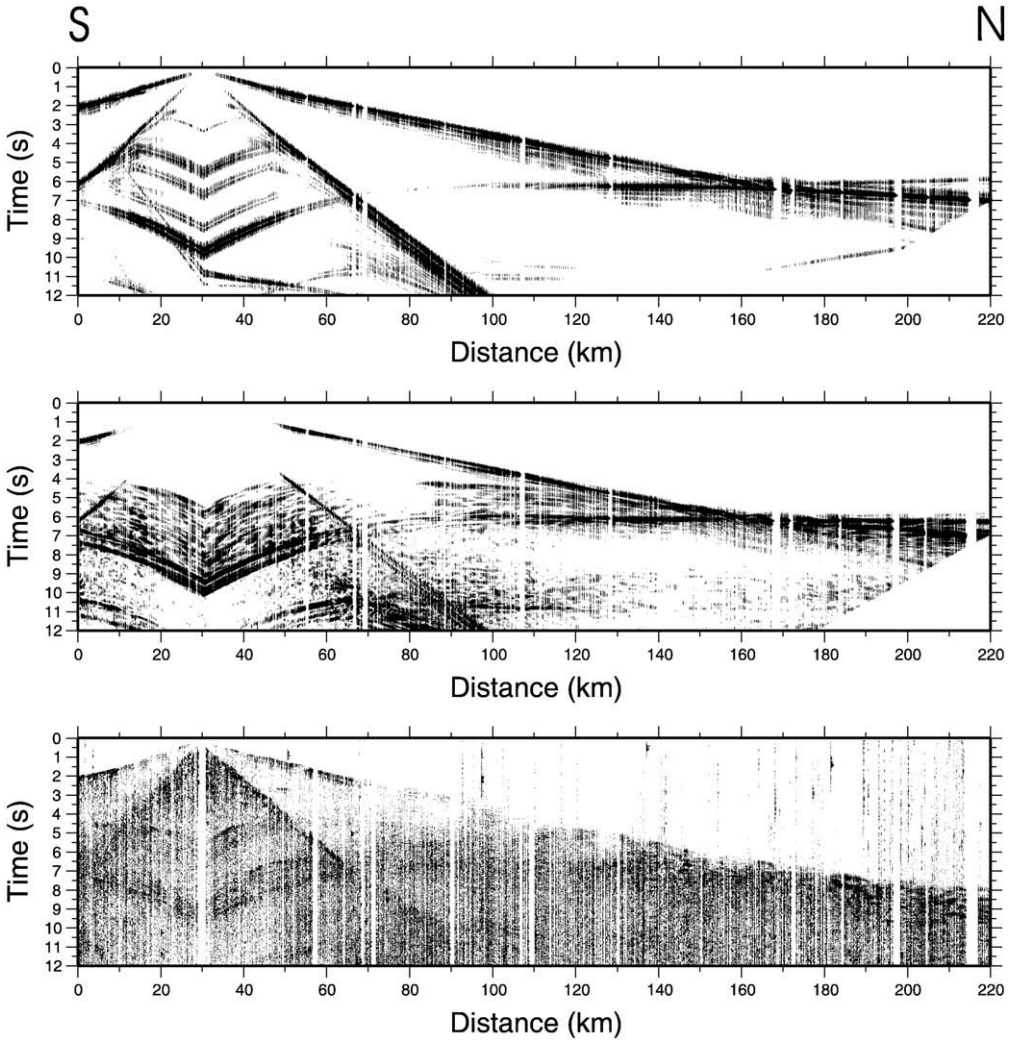

Fig. 6. Shot B5. Top, middle and bottom images correspond to the same than in Fig. 5 for the shot B4.

were taken from Deemer and Hurich (1994). At a small scale, a deterministic description of structures is unreasonable (Holliger et al., 1994), therefore a stochastic approach was applied. A new velocity model was built based on the one obtained by seismic refraction as starting point. The upper and middle crust were left unchanged whereas the high velocity layer, the lower crust and the Moho discontinuity were modified introducing lensing at different scales. The lensing was achieved by considering a set of ellipses randomly distributed along the high velocity layer and the lower crust. The center of every ellipse was chosen using a random function. The parameters defining the ellipse (semimajor axis and semiminor axis) were chosen arbitrarily ranging between a minimum and a maximum correlation length in both axes. Finally, the velocity for every ellipse was also randomly chosen considering a maximum variation of the aleatory measurements within the range of possible values of velocities for lithologies possible at this depth. The limit values for dimensions and velocities are summarized in Table 1. Both velocity models (with and without stochastic layering) are displayed in Fig. 4.

Table 1
Values used to modify the refraction velocity model in order to obtain a random layered model for the mafic intrusion, the lower crust and the Moho discontinuity.

	Mafic Intrusion	Lower crust	Moho
Bulk velocity (km/s)	6.7	7.1	7.85
Velocity variation (km/s)	±0.2	±0.2	±0.25
X dimension (km)	1–3	0.4–1.2	5–25
Z dimension (km)	0.1–0.2	0.025–0.2	0.025–0.1

Values were approximated from the literature (Wenzel et al., 1987; Holliger and Levander, 1992; Deemer and Hurich, 1994; Holliger et al., 1994).

The Moho can be identified because it features a sharp change in velocity. Classically, the Moho has been considered as a velocity discontinuity with some lateral continuity. Most authors tend to model this as a simple interface, a line avoiding any additional structure except by its topography. However, some studies have proposed a concentration of lamellae without laterally continuous velocity discontinuity to explain complex patterns in wide-angle data (Long et al., 1994). In our case, the Moho was modelled as a 3 km wide strip centered in the digitized Moho from the refraction modelling (7.85 km/s isovelocity line). Along this strip a random lensing was performed following the same stochastic process as before. Results from these simulations provide a more reflective lower crust as a result of the constructive interference between lenses. The Moho discontinuity is imaged as a 1 second reflective band which better reproduces the real data (Figs. 5 and 6).

5. Discussion

The Moho discontinuity is clearly imaged in the six shot-gathers considered in the present work (Fig. 3). In the data acquired to the south, it appears as a simple thin weak event (shots B5 and B6) around 9.5 s in twtt. Towards the north, the Moho signature changes gradually

increasing in thickness, amplitude and complexity (shots B1, B2 and B3). To the north, this seismic event seems to be slightly deeper (10 s twtt) than in the southern edge. At large scale, the Moho can be considered as a flat interface, some prominent events in the northernmost shots of the profile may indicate a variation in its topography. Other prominent events can be identified in individual shots at lower-crustal levels but its nature as well as its real geometry is difficult to assess because of the hyperbolic time correction applied. However, these reflectors are indicative of complex structures within the base of the crust. Forward seismic modelling showed that data generated using the refraction model is able to recover the main seismic events linked to major discontinuities in the velocity model but, it is insufficient to justify complex seismic patterns observed in real data. In order to better reproduce the real seismic signature, heterogeneities must be considered. Introducing lensing/layering in mafic intrusions, lower crust and Moho, more realistic simulations are achieved where interference between small diffractor bodies (lenses) can qualitatively account for the coda observed in field shot records.

The variations in the seismic signature of lower crust and Moho as well as the changes in reflectivity patterns along the profile strongly evidence a very heterogeneous crust. Although the image lacks the quality of a continuous normal incidence stack, it is possible to distinguish different areas in the lower crust based on the differences in seismic signature. Moreover, this wide-angle transect extends to the south and east, beneath the well known Iberian Pyrite Belt, the knowledge provided by the published results for the IBERSEIS profile where the Moho appears at around 10.5 s twtt (Simancas et al., 2003; Carbonell et al., 2004). The seismic data is congruent with an idealized model that consists of strongly layered high velocity intrusions in the mid-crust, a heterogeneous lower crust and a laminated Moho, thin and simple beneath the SPZ, and thicker and more complex beneath the OMZ and CIZ (Fig. 7).

Additional work would be required to better understand the distribution of acoustic properties of the lower crust as well as the detailed structure of the Moho discontinuity for instance, adding information from S-wave data.

The wide-angle stack coupled with the synthetic modelling suggests that the crust beneath the study area features strongly laminated zones at mid-crustal depths which are characterized by relatively high velocities (Fig. 4). This zones account for the relatively high frequency reflectivity at mid-crustal depth approximately at 5 to 7 s twtt (shots B1, B4, B5 and B6) and in the wide-angle stack. The velocities and the high frequency reflectivity are consistent with layered mafic intrusions (Palomeras et al., 2009). Deemer and Hurich (1994) indicated that thin layered mafic intrusions can result in high acoustic impedances. The lower crust has been modelled as a layer with a medium degree of heterogeneity and/or lamination. This result in a heterogeneous lower crust with lenses and/or deformed layering composed of gabbronorite to pyroxene quartz, some intrusives, gabbrodiorites intermixed with garnet granulites (Saleeby et al., 2003). These lithologies distributed in lense lense-like structures interfingering each other can account for the observed lower-crustal reflectivity.

The Moho has been modelled as consisting of a thinly laminated structure. The Moho is thicker in the center of the orogen where the reflectivity is higher and the band of reflectivity thicker. The reflection coefficients are also high towards the northern end of the transect. The Moho discontinuity also features lensing strongly develop and heterogeneous beneath the core of the orogen (the center of the transect beneath shot points B3 and B4) this lensing is most probably a mixture of lithologies that can include spinel peridotite layers interfingering garnet peridotite and gabbros (Saleeby et al., 2003; Palomeras et al., 2009).

The wide-angle stack does not constrain the upper crust, however it provides information on the mid-to-lower crust. The 1 to 2 s thick band of high reflectivity observed at the base of the crust in the wide-angle stack which can be accounted for by the models suggests that the lower crust and Moho are relatively young structures most probably developed in the late stages of the collision and a result of the crustal re-equilibration. After the collision and the strike-slip movements, during the late stages of the transpression tectonics, intense lithospheric processes were taking place, intense lower-crustal deformation, subcrustal erosion of the crustal orogenic root, most probably large amounts of upper mantle mafic melts intruded in the lower and middle crust and in some cases even up to the surface creating a unique tectonic evolution scenario which favored the development of the unprecedented large scale sulphide deposits observed at the surface. The mantle material also ponded at Moho level in the shape of thin lamelae. Thus, the signature of the terranes was not preserved with depth, rather the lower crust and Moho behave different than the upper crust during the transpression. The lower crust and Moho are most probably a result of the deformation and therefore the present day structure is a consequence of the re-equilibration processes during the late stages of the transpression. The transpression erased most of the characteristic features of the terranes and collision at lower crust and Moho depths.

Geologically, the mid-to-lower-crustal heterogeneities could be represented by elongated lenses featuring high seismic velocities. These are embedded into the mid-lower crust representing sills intrusions of mafic material which has been emplaced in weak zones within the crust (i.e., previous fractures). The synthetic seismic data produced by the model features interfingering domains of high-amplitude layered reflectivity. The seismic fabric and the high-amplitude reflectivity are consistent with layering caused by multiple

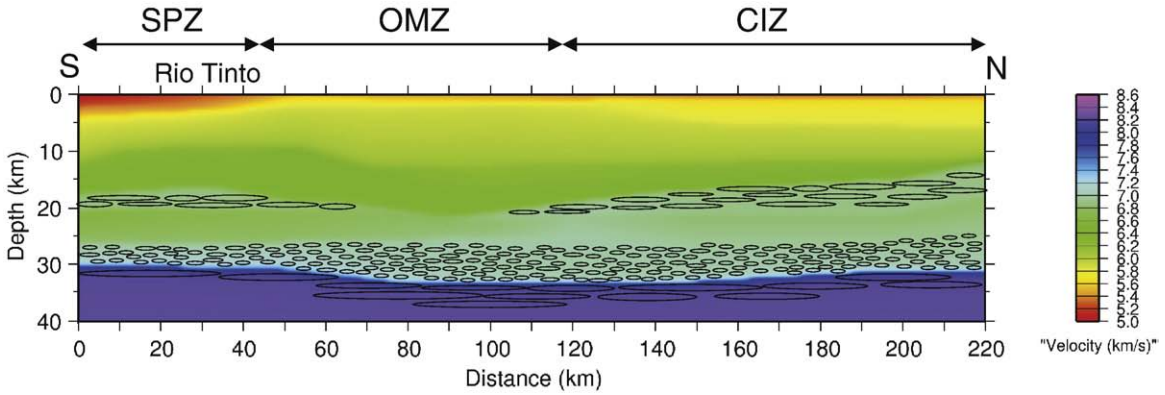

Fig. 7. Cartoon model that would account for the wide-angle data: layering/lensing in middle-crust mafic intrusions, lower crust and Moho discontinuity, across the three tectonic terranes SPZ, OMZ and CIZ.

sill lense type intrusions. The intrusion of mafic magmas in the crust assimilated part of the surrounding rocks, leaving behind relatively large amount of restites. These restites would be embedded within the lower crust resulting in more competent, higher velocity layers/lenses.

The mafic intrusion in the middle crust must have preferentially emplaced in an existing weak zones (i.e., faults, detachments). The IBERSEIS normal incidence image revealed evidences for basal detachment beneath the imbricate thrust system of the SPZ at mid-crustal depth. Which is consistent with the mid-crustal reflectivity identified in the southern end of the transect (shots B5 and B6).

Beneath the SPZ (Fig. 7) mafic layering is located at approximately 20 km depth. This layering must be simple, it most probably consist of a few relatively large sills. This structure needs to be strongly reflective because of the high-amplitude reflectivity at 7 s twtt in shots B5 and B6. Nevertheless it needs to be simple because the PMP reflection from the Moho can be identified at normal incidence offsets as a relatively thin reflection beneath this zone.

Beneath the OMZ, the band of reflectivity at the mid-to-lower crust towards the north is more transparent. Nevertheless the seismic signature of the Moho is thicker and increases slightly in depth. The thin relatively continuous PMP reflection beneath the SPZ turns into a thicker reflective band with reflection events with relatively short lateral continuity. This is qualitatively consistent with a thicker layered Moho composed of interlayering of high and low velocity lenses. This is most probably the result of the re-equilibration process, the assimilation of the root of the orogen on the OMZ which corresponds to the core of the orogen. The seismic response of the Moho discontinuity is strongly affected by the lateral dimensions of the overlying structures. These structures disperse the energy and deform the wavefront breaking up the reflection events.

Beneath the CIZ the Moho reflectivity evolves from relatively thick 0.7–1 event to a thinner and weaker event at the northern edge of the transect. This feature and the increase in reflectivity of the mid-to-lower crust have been simulated by introducing a layer of sills that increases in thickness towards the north, at 15 to 20 km in depth. This mid-crustal feature is consistent and it might represent the IRB (Iberian Reflective Body) beneath this transect. The IRB was imaged by the IBERSEIS transect which is located farther to the north-west (Fig. 1). This mid-crustal complex sill intrusion will affect the seismic signature of the Moho resulting in a weaker event.

6. Conclusions

The closely spaced wide-angle seismic dataset presented in this work, provides an image of the crust which reveals a strongly heterogeneous nature. Our results outline a picture of the Variscan lower crust as a heterogeneous media with small-scale velocity variations. Likewise, a mafic intrusion located in the middle crust features a heterogeneous layering/lensing. The full-wave forward modelling performed here shows that a simple layer cake velocity model obtained from conventional ray tracing techniques, cannot explain the lower crust reflective packages in the data. On the other hand, a qualitatively satisfactory fit of the data was accomplished when stochastic lensing was added to the refraction velocity model. This suggests that the mafic intrusion and the lower crust are strongly layered. The Moho discontinuity beneath the southern end is imaged as a thin weak reflector, accounting for a simple interface. Beneath the central part of the transect the Moho is associated to a thick high-amplitude reflective package which suggest a more complex structure. Finally, beneath the northern end, the Moho is displayed as a discontinuous interface with changing seismic signature. The wide-angle low-fold stacked section obtained from this experiment and the synthetic seismic modelling provide a new picture of the Moho discontinuity in SW-Iberia. The seismic image reveals a laterally heterogeneous Moho and a changing lower crust seismic signature along the profile. This lateral variability and the horizontality of the lower crust and Moho suggest that they are most probably the result of the re-equilibration lithospheric processes during and after the late stages of the transpression event.

Acknowledgements

Funding for this research was provided by the Spanish Ministry of Education and Science CGL200404623, TOPOIBERIA CONSOLIDER-INGENIO (CSD2006-00041), and Generalitat de Catalunya 2005SGR00874. Junta de Andalucia provided additional funds for the acquisition. This project was also supported by REPSOL-YPF.

References

Blundel, D., Arndti, N., Cobbold, P., Heinrich, C., 2005. Geodynamics and ore deposits evolution in Europe. Ore Geol. Rev. 27, 1–349.
Carbonell, R., Smithson, S.B., 1991. Large-scale anisotropy within the crust in the Basin and Range province. Geology 19, 698–701.
Carbonell, R., Lecerf, D., Itzin, M., Gallart, J., Brown, D., 1998. Mapping the Moho beneath the southern Urals with wide-angle reflections. Geophys. Res. Lett. 25, 4229–4232.
Carbonell, R., Gallart, J., Pérez-Estaún, A., 2002. Modelling and imaging the Moho transition: the case of the southern Urals. Geophys. J. Int. 149, 134–148.
Carbonell, R., Simancas, F., Juhlin, C., Pous, J., Pérez-Estaún, A., González-Lodeiro, F., Muñoz, G., Heise, W., Ayarza, P., 2004. Geophysical evidence of a mantle derived intrusion in SW Iberia. Geophys. Res. Lett. 31, L11601.
Casquet, C., Galindo, C., Tornos, F., Velasco, F., Canales, A., 2001. The Aguablanca Cuni ore deposit (Extremadura, Spain), a case of synorogenic orthomagmatic mineralization: age and isotope composition of magmas (Sr,Nd)and ore (s). Ore Geol. Rev. 18, 237–250.
Christensen, N.I., Mooney, W.D., 1995. Seismic velocity structure and composition of the continental crust: a global view. J. Geophys. Res. 100, 9761–9788.
Deemer, S.J., Hurich, C.A., 1994. The reflectivity of magmatic under-plating using the layered mafic intrusion analog. Tectonophysics 232, 239–255.
Galán, G., Marcos, A., 1997. Geochemical evolution of high pressure mafic granulites from the Bacariza formation (Cabo Ortegal complex, NW Spain): an example of a heterogeneous lower crust. Geol. Rundsch. 86, 539–555.
Gibson, B.S., Levander, A.R., 1988. Lower crustal reflectivity patterns in wide-angle seismic recordings. Geophys. Res. Lett. 15, 617–620.
Holliger, K., Levander, A.R., 1992. A stochastic view of lower crustal fabric based on evidence from the Ivrea Zone. Geophys. Res. Lett. 19, 1153–1156.
Holliger, K., Levander, A.R., Goff, J.A., 1993. Stochastic modeling of the reflective lower crust: petrophysical and geological evidence from the Ivrea Zone (northern Italy). J. Geophys. Res. 98, 11.967–11.980.
Holliger, K., Levander, A., Carbonell, R., Hobbs, R., 1994. Some attributes of wavefields scattered from Ivrea-type lower crust. Tectonophysics 232, 267–279.
Hurich, C.A., Smithson, S.B., 1987. Compositional variation and the origin of deep crustal reflections. Earth Planet. Sci. Lett. 85, 416–426.
Levander, A., England, R.W., Smith, S.K., Hobbs, R.W., Goff, J.A., Holliger, K., 1994a. Stochastic characterization and seismic response of upper and middle crustal rocks based on the Lewisian gneiss complex, Scotland. Geophys. J. Int. 119, 243–259.
Levander, A., Hobbs, R.W., Smith, S.K., England, R.W., Snyder, D.B., Holliger, K., 1994b. The crust as a heterogeneous "optical" medium, or "cocodriles in the mist". Tectonophysics 232, 281–297.
Long, R.E., Matthews, P.A., Graham, D.P., 1994. The nature of crustal boundaries: combined interpretation of wide-angle and normal-incidence seismic data. Tectonophysics 232, 309–318.
Martínez-Catalán, J.R., Arenas, R., Díaz-García, F., Abati, J., 1997. The Variscan accretionary complex of NW Iberia: involved terranes and successions of tectonothermal events. Geology 25, 1103–1106.
Martini, F., Bean, C.J., Dolan, S., Marsan, D., 2001. Seismic image quality beneath strongly scattering structures and implications for lower crustal imaging: numerical simulations. Geophys. J. Int. 145, 423–435.
Palomeras, I., Carbonell, R., Flecha, I., Simancas, F., Ayarza, P., Matas, J., Martínez Poyatos, D., Azor, A., González Lodeiro, F., Pérez-Estaún, A., 2009. Nature of the lithosphere across the Variscan Orogen of SW Iberia: Dense wide-angle seismic reflection data. J. Geophys. Res. 114, B02302.
Peucat, J.J., Bernard-Griffiths, J., Gil-Ibarguchi, J.I., Dallmeyer, R.D., Menot, R.P., Cornichet, J., de Leon, M.I.-P., 1990. Geochemical and geochronological cross section of the deep Variscan crust; the Cabo Ortegla high-pressure nappe (northwestern Spain). Tectonophysics 177, 263–292.
Ribeiro, A., Sanderson, D., Colleagues, S.I., 1996. EUROPROBE 1996 — lithosphere dynamics: origin and evolution of continents, chapter SW-Iberia. Transpressional Orogeny in the Variscides. Uppsala University, pp. 91–95.
Rutter, E.H., Khazanehdari, J., Brodie, K.H., Blundell, D.J., Waltham, D.A., 1999. Synthetic seismic reflection profile through the Ivrea Zone-Serie dei Laghi continental crustal section, northwestern italy. Geology 27, 79–82.
Saleeby, J., Ducea, M., Clemens-Knott, D., 2003. Production and loss of high-density batholitic root, southern Sierra Nevada, California. Tectonics 22, 3(1)–3(24).
Santos-Zalduegui, J.F., Schrarer, Y., Gil-Ibarguchi, J.I., Girardeau, J.J., 1997. Origin and evolution of the Paleozoic Cabo Ortegal ultramafic–mafic complex (NW-Spain). Chem. Geol. 129, 281–304.

Simancas, F., Martínez-Poyatos, D., Expósito, I., azor, A., González-Lodeiro, F., 2001. The structure of a major suture zone in the SW Iberian massif: the Ossa-Morena/Central-Iberian contact. Tectonophysics 332, 295–308.

Simancas, J.F., Carbonell, R., González-Lodeiro, F., Pérez-Estaún, A., Juhlin, C., Ayarza, P., Kashubin, A., Azor, A., Martínez-Poyatos, D., Almodóvar, G.R., Pascual, E., Sáez, R., Expósito, I., 2003. Crustal structure of the transpressional Variscan orogen of SW Iberia: SW Iberia deep seismic reflection profile (IBERSEIS). Tectonics 22, (1)-1–(1)-20.

Sochacki, J.S., Kubichek, R., George, J.H., Fletcher, W.R., Smithson, S.B., 1987. Absorbing boundary conditions and surface waves. Geophysics 52, 60–71.

Sochacki, J.S., George, J.H., Ewing, R.E., Smithson, S.B., 1991. Interface conditions for acoustic and elastic wave propagation. Geophysics 56, 168–181.

Tornos, F., Casquet, C., Galindo, C., Velasco, F., Canales, A., 2001. A new style of Ni-Cu mineralization related to magmatic breccia pipes in a transpressional magmatic arc, Aguablanca, Spain. Miner. Depos. 36, 700–706.

Wenzel, F., Sandmeier, K.-J., Wälde, W., 1987. Properties of the lower crust from modeling refraction and reflection data. J. Geophys. Res. 92, 11.575–11.583.

7. DISCUSSIÓ

7.1 "Imaging granitic plutons along the IBERSEIS profile": resultats i discussió

Les quatre àrees estudiades presenten característiques diferenciades, per tant seran tractades individualment en quant als resultats obtinguts i la seva interpretació.

7.1.1 Àrea de La Bazana

El fet més rellevant obtingut en el model tomogràfic és una zona d'alta velocitat directament associable a l'afloramen granític de la Bazana. L'anomalia presenta un gradient de velocitats que van des dels 5800 m/s en la part més interna del cos granític, fins a 5200 m/s en la zona de contacte amb la roca encaixant. Aquesta diferència en velocitats pot ser atribuïble a les diferents propietats de la roca. Les altes velocitats probablement estan associades a roca poc deformada i amb poques alteracions, mentre que les velocitats més baixes mostrarien una major alteració degut a la interacció entre el granit i la roca encaixant. La cobertura de rajos ens proporciona fiabilitat del model fins a una fondària de 700 m.

7.1.2 Àrea de La Dehesilla

En aquesta zona, s'observa una extensa anomalia d'alta velocitat que, en la seva part més superficial, és clarament identificable amb la unitat granítica de Salvatierra de Barros. Del model tomogràfic es pot deduïr que aquest complex granític té continuïtat en fondària cap al sud-oest, com a mínim fins a 900 m de profunditat, que és el màxim abast de la inversió tomogràfica per aquest cas. El valor de la velocitat és manté bastant regular al llarg de tota l'anomalia detectada, al voltant dels 5200-5300 m/s. La transició entre el que s'ha interpretat com a granit i la roca encaixant es caracteritza per un gradient decreixent i relativament suau de la velocitat, fet que segurament és causa de l'aurèola de contacte d'un kilòmetre de gruix causada per la intrusió. La imatge tomogràfica mostra algunes irregularitats pel que fa a la seva morfologia. Aquest efecte podria ser causat per: (1) la disposició poc rectilínia de fonts i receptors en aquesta zona o bé (2) per la deformació del plutó granític que es tradueix en l'aparició de zones de fractura. Amb tota probabilitat,

la imatge final és un resultat d'ambdues causes. Determinar la contribució de cadascuna requeriria d'un experiment específicament dissenyat per a tal efecte.

7.1.3 Àrea de Feria

En aquest cas, el model tomogràfic mostra una anomalia d'alta velocitat clarament delimitada. La caracterització és molt similar al cas del granit de la Bazana, amb un nucli amb velocitats de 5800 m/s i una zona perifèrica amb velocitats de 5200 m/s. La correlació d'aquesta alta velocitat amb la geologia superficial fa pensar que l'anomalia es correspon amb el plutó granític de Feria. Encara que el traçat del perfil sísmic no creua l'afloament granític, la seva proximitat (menys de 500 m al sud del perfil) fa que aquesta interpretació sigui raonable i que poguem parlar d'una prolongació en fondària del cos granític cap al nord. A més, tant el plutó de Feria com el de la Bazana són formacions carboníferes, per tant és d'esperar que tinguin característiques sísmiques comuns, com és el cas. En conseqüència, la identificació anomalia-granit queda confirmada. La cobertura de rajos arriba fins als 1200 m de profunditat, permetent una bona imatge en fondària de l'estructura del plutó granític de Feria.

7.1.4 Àrea de Villafranca

Les anomalies d'alta velocitat presents en aquesta zona no són directament correlacionables amb estructures o formacions geològiques, llevat d'una. En aquest cas, a la part més oriental d'aquesta àrea d'estudi, una anomalia superficial d'alta velocitat (6000 m/s) es correspon, tant per valors de la velocitat com per localització, amb un afloament de roques metamòrfiques d'alta pressió: amfibolites i retroeclogites. La resta d'anomalies positives requeririen d'informació addicional per tal de ser justificades. També es poden visualitzar dues discontinuïtats verticals en el model tomogràfic que es correlacionen en superfície amb la presència de dues falles. En aquest sentit, el model de velocitats permet extrapolar les falles cartografiades en fondària fins a una profunditat d'uns 1500 m, que és la màxima profunditat a la que el model proporciona resultats fiables.

7.2 "Imaging low velocity anomalies with the aid of seismic tomography": resultats i discussió

7.2.1 Estudi sintètic

L'estudi teòric mitjançant simulacions sintètiques ha permès avaluar el poder resolutiu de dos paquets de processat de tomografia de primeres arribades. Malgrat que existeixen petites diferències entre aquests dos *softwares*, la informació qualitativa que se n'extreu

dels resultats és equivalent. Tal i com era d'esperar, les limitacions teòriques existents per a la detecció d'anomalies de baixa velocitat s'han fet evidents i, en el cas sintètic, no s'ha pogut caracteritzar rigorosament l'anomalia. El model sintètic utilitzat representa segurament el pitjor dels casos per a l'aplicació de la tomografia sísmica, ja que la velocitat de l'anomalia que es pretenia caracteritzar és de 300 m/s davant d'un entorn que supera els 3000 m/s. Aquest valor tan baix és poc realista, però ha servit per tal de posar a prova el funcionament dels paquets de processat en condicions extremes.

Els resultats obtinguts en l'estudi sintètic mostren que el valor de la velocitat per a l'anomalia no es recupera estrictament en cap cas. De totes maneres, quant més favorable és el dispositiu experimental i més receptors i fonts es consideren, més s'apropa el model obtingut al model real. En qualsevol cas, els diagrames de cobertura de rajos proporcionen una informació qualitativa de gran utilitat, ja que permeten localitzar l'anomalia i fer una estimació aproximada de les seves dimensions.

En el cas plantejat, la utilització de tècniques de sísmica de reflexió proporciona informació addicional i més acurada sobre la geometria de l'anomalia, com a mínim en la part superior d'aquesta.

Malgrat tot, en situacions més realistes i davant de valors de velocitats no tan extrems, els dos codis d'inversió utilitzats proporcionen models molt més ajustats a la realitat com queda demostrat en l'aplicació de la tomografia sísmica de primeres arribades a un cas real.

7.2.2 Cas real: el plutó d'Albalà

El plutó granític d'Albalà s'ha estudiat per tal de caracteritzar-lo sísmicament. Per una banda, s'ha caracteritzat la naturalesa i l'estat de la roca mitjançant la tomografia sísmica de primeres arribades, i per altra banda s'ha obtingut informació sobre la seva estructura mitjançant la sísmica de reflexió.

Els models tomogràfics mostren un subsòl extremadament heterogeni amb alternança de zones d'alta i baixa velocitat. Les baixes velocitats s'han associat a una roca més alterada i/o fracturada. Els valors obtinguts per a les anomalies de baixa velocitat són lleugerament inferiors a 2000 m/s per a la zona més superficial. A més fondària, les anomalies de baixa velocitat mostren uns valors al voltant dels 3500 m/s, coincidint amb els registres de sondejos existents a la zona. Cal dir que els constrastos entre velocitats baixes i altes són molt menys extrems que en el cas de l'estudi sintètic, fet que permet caracteritzar aquestes zones amb fiabilitat.

La gran heterogeneïtat del subsòl poc profund de la zona d'estudi fa difícil l'aplicació d'un processat convencional de sísmica de reflexió. En aquest context, les zones de baixa velocitat provoquen un retard en l'arribada del senyal sísmic, afectant així a la continuïtat

lateral dels reflectors. L'efecte d'aquesta variabilitat en les propietats del subsòl s'ha minimitzat aplicant una correcció sobre les traces consistent amb l'equació d'ona (*wave equation datuming*). Els resultats obtinguts després d'aquesta correcció mostren una millor continuïtat lateral per a molts reflectors, aconseguint una imatge que possibilita la visualització d'una de les fractures principals de la zona: la falla Nord. La implementació d'aquest processat específic requereix d'un coneixement detallat del model de velocitats de l'àrea d'estudi, cosa que en el nostre cas ha proporcionat la tomografia sísmica.

7.3 "Limitations of wide-angle reflection/refraction methods in subbasalt imaging: investigating null space in refraction data": resultats i discussió

Mitjançant les simulacions sintètiques s'ha posat a prova un codi tomogràfic capaç de gestionar diversos events. Aquesta característica s'ha mostrat fonamental ja que els resultats obtinguts només invertint primeres arribades són molt limitats i no possibiliten la caracterització del cos basàltic ni de la capa de sediments que existeix per sota d'aquest. Incloure altres fases en l'inversió és bàsic per reproduïr amb certa fiabilitat el model utilitzat per a crear les dades sintètiques.

Els resultats de la inversió per a la primera capa de sediments són correctes quan considerem les següents fases: primeres arribades, refracció dins la primera capa de sediments i reflexions del límit superior del basalt. En aquest cas la velocitat dels sediments per sobre del basalt es reprodueix raonablement, així com el límit superior del cos basàltic.

Afegir la refracció dins el basalt al procés d'inversió és un pas crític, ja que els resultats mostren que el gruix de la capa basàltica és proporcional al màxim *offset* considerat per aquesta fase, paràmetre que és funció per una banda de la qualitat de les dades i per altra de la interpretació subjectiva de qui processa les dades. Així si es considera més offset, la capa de granit té més gruix i viceversa. Aquest fet s'explica perquè amb gruixos de basalt reduïts, la refracció dins el basalt i la reflexió de la base del basalt interfereixen en la zona exterior al con d'aigua, i per tant fan difícil una correcta interpretació/identificació de cada fase. Aquesta confusió s'elimina si el basalt presenta un gruix més gran i permet separar els events corresponents a les dues fases esmentades. Malauradament, a la conca Faroe-Shetland, la majoria d'estudis es duen a terme allà on es sospita que la capa de basalt és prima, ja que així es minimitza la influència d'aquest material sobre el senyal sísmic en els sediments subbasàltics.

Si considerem que, o bé mitjançant alguna altra metodologia geofísica o bé perforant directament, podem conèixer el gruix de la capa de basalt, llavors la inversió tomogràfica proporciona un model correcte.

Mitjançant les simulacions de Metropolis, s'ha avaluat la influència d'altres factors sobre els resultats que proporcionen les inversions tomogràfiques. L'estudi estadístic s'ha dut a terme considerant dos models (model 1 i model 2) que es diferencien en el gruix de la capa basàltica que és d'un i dos kilòmetres respectivament.

Per al model 1 i un senyal de 10 Hz s'obté un model que reprodueix aproximadament els gradients de la capa basàltica i del basament encara que prediu un gruix i una velocitat més grans per a la capa de sediments subbasàltics. En les mateixes condicions però considerant un error més baix en el procés de *picking*, el model més probable empitjora la seva predicció per a les velocitats de la capa basàltica i del basament, i a més prescindeix de la capa de baixa velocitat per sota del basalt. Aquest fet té la seva explicació en que considerant un error més gran en els temps d'arribada, les dues fases que interfereixen (refracció al basalt i reflexió de la base del basalt) es troben en el rang de temps correctes com per poder-se considerar com una refracció pura dins el basalt. Si el senyal utilitzat és de 20 Hz, el resultat millora sensiblement i el model es reprodueix raonablement.

Per al model 2 i un senyal de 10 Hz s'han diferenciat dos casos: un primer cas amb un *picking* molt conservador i un segon cas on s'han afegit *picks*. Per al primer cas, la velocitat i el gruix de la capa basàltica es reprodueix de forma satisfactòria, però no les propietats del basament. En canvi, per al segon cas, la capa que es reprodueix de forma raonable és el basament i no pas la capa de basalt. En cap dels dos casos la capa de baixa velocitat per sota del basalt es veu reflectida en el model més probable. Si augmentem la freqüència del senyal fins a 20 Hz, tant el basament com el basalt es reprodueixen correctament encara que la capa de baixa velocitat segueix sense observar-se de forma clara, segurament degut al fet de considerar més dades de les que estrictament corresponen a cada fase.

7.4 "Some improvements in subbasalt imaging using pre-stack depth migration": resultats i discussió

El nou codi utilitzat per a la implementació de la migració *pre-stack* en fondària utilitza un algoritme de diferències finites que evita l'aparició de zones d'ombra en les taules de temps de viatge. El test dut a terme amb dades sintètiques demostra que l'algoritme reprodueix de forma encertada el model teòric, malgrat la presència de la capa d'alta velocitat que tendeix a desviar bona part de l'energia que hi arriba. Per tant es pot concloure que el codi proporciona resultats satisfactoris, sempre i quan el model de velocitats utilitzat sigui correcte.

L'aplicació pràctica d'aquest nou codi s'ha dur a terme reprocessant un perfil de sísmica de reflexió adquirit a la conca Faroe-Shetland. El principal problema a resoldre per a la

caracterització tomogràfica d'aquesta zona és la presència de basalts per sobre d'una seqüència sedimentària de velocitat inferior. La zona que es troba per sobre de la capa basàltica i la topografia del límit superior d'aquesta mateixa capa es mostra perfectament en l'*stack*, mentre que per sota d'aquesta capa no es recupera cap event.

Tenint en compte els resultats previs obtinguts al capítol 4, s'han invertit les diferents fases identificades a les dades. Els resultats semblen suggerir que efectivament existeix una inversió de velocitats per sota de cert límit que s'ha interpretat com la base de la capa basàltica. Fent servir aquest model de velocitats s'ha utilitzat el codi que es presenta en aquest estudi. Fins al moment, la majoria de treballs en aquest context geològic que han implementat una migració *pre-stack* en fondària, han migrat únicament una reduïda part de les dades disponibles. Aquesta migració selectiva correspon a la zona del *shotgather* fora del con d'aigua on apareixen les refraccions del basalt, la reflexió de la base del basalt i la reflexió del basament. A més, és habitual filtrar per baixes freqüències abans d'implementar la migració. Aquesta estratègia dóna com a resultat una imatge final de baixa freqüència que, juntament amb la presència d'artefactes tipus *smiling*, fa que la interpretació dels límits geològics sigui complicada.

Com a alternativa, en el present estudi s'ha prescindit del filtratge previ de les dades i s'han migrat també les altes freqüències. Tampoc s'han limitat les dades i s'ha migrat tot el *shotgather*. Aquest processat ha proporcionat per una banda, una secció en fondària de més alta freqüència que permet una millor interpretació de la imatge final, i per altra banda, s'ha minimitzat la presència d'artefactes provinents de la migració degut a una cobertura de dades prou elevada.

La interpretació dels resultats permeten la identificació d'alguns events subbasàltics. Així en algunes parts del model es pot inferir el que seria la base del basalt i el límit superior del basament. En la primera meitat del model (entre els 40 i els 70 km) aquests límits de capa acoten una zona on la velocitat disminueix sensiblement, afavorint la hipòtesis d'una capa de sediments per sota del material basàltic. A la segona meitat de la secció migrada (entre els 70 i 100 km) es fa difícil una interpretació de la base del basalt, molt probablement perquè, en ser una zona on el basalt s'aprima, la refracció dins la capa de basalt i la reflexió de la seva base interfereixen. En canvi, l'aprimament del basalt permet una millor visualització de l'event que s'ha interpretat com el límit superior del basament.

7.5 "Seismic imaging and modelling the lithosphere of SW-Iberia": resultats i discussió

En estudis de reflexió previs el Moho es presenta, a gran escala, com una estructura bàsicament plana al voltant dels 10 s en fondària. En les dades utilitzades, es confirma

aquest fet. La gran densitat de receptors utilitzada en l'adquisició, ha permès l'obtenció d'un *stack* de baixa cobertura que possibilita una visió més detallada. Així, l'estructura del Moho és variable al llarg del perfil. La zona del sud (zona sud-portuguesa) mostra una estructura simple i amb cap relleu remarcable, mentre que les altres dues zones (zona d'Ossa-Morena i zona Centre-Ibèrica) es caracteritzen per un Moho més gruixut i amb uns patrons de reflectivitat més complexos. Aquests canvis evidencien una escorça altament heterogènia. A nivell d'escorça mitjana i escorça inferior també s'observen events sísmics diferenciats, encara que la correcció hiperbòlica utilitzada per obtenir l'*stack* fa difícil la seva interpretació.

Diverses simulacions sintètiques s'han dut a terme amb l'objectiu de reproduïr les dades adquirides. Partint d'un model de velocitats obtingut per refracció és possible recuperar els events associats a les discontinuïtats principals de l'escorça, però no és possible donar explicació a la complexitat, a nivell de reflectivitat, observada en les dades reals. Per tal de justificar els patrons de reflectivitat que es mostren a les dades adquirides, cal afegir cert grau d'heterogeneïtat al model de velocitats. Mitjançant una modificació lenticular i estocàstica del model de velocitats a nivell d'escorça inferior, es pot reproduir qualitativament l'alta reflectivitat observada en les dades de camp.

L'*stack* de gran angle, el model de velocitats i la modelització sintètica suggereixen que l'escorça en la zona d'estudi es caracteritza per zones d'alta velocitat amb una forta laminació a nivell d'escorça mitjana. Els valors de les velocitats i la reflectivitat d'alta freqüència són consistents amb intrusions estratificades de caràcter màfic.

L'alta reflectivitat de la base de l'escorça sembla suggerir que l'escorça inferior i el Moho són estructures relativament joves, segurament creades en els darrers episodis de la col·lisió com a resultat de processos de reequilibrament. Després de la col·lisió van tenir lloc diversos processos litosfèrics i tectònics, afavorint la intrusió de material magmàtic del matell superior a nivell d'escorça mitjana i escorça inferior, i en alguns casos fins i tot fins a la superfície, fet que explicaria l'anòmala concentració de dipòsits minerals que es poden observar en aquesta zona.

Geològicament, les heterogeneïtats a l'escorça inferior es poden caracteritzar per intrusions de material màfic de geometria lenticular que es van emplaçar preferentment en zones debilitades de l'escorça, per exemple aprofitant l'existència de fractures prèvies. A nivell d'escorça mitjana, la intrusió màfica es va emplaçar aprofitant falles o desenganxaments. Aquesta alternança d'intrusions i roca existent és la causant de l'alta reflectivitat observada en les dades

A la zona Sud-Portuguesa la intrusió màfica està localitzada al voltant dels 20 km de fondària. Aquesta intrusió està estratificada i probablement està formada per sills de tamany relativament gran. Aquesta estructura s'identifica en un parell de dispars com

un event de gran reflectivitat. De totes maneres ha de ser una estructura relativament simple ja que la reflexió del Moho es pot identificar en els dispars a incidència normal.

A la zona d'Ossa-Morena l'escorça inferior es mostra més transparent, mentre que el Moho es visualitza com una banda reflectiva de gruix superior si el comparem amb la zona Sud-Portuguesa. Això es pot correspondre perfectament amb un Moho estratificat format per l'alternança d'àrees lenticulars d'alta i baixa velocitat. Aquesta emprempta sísmica segurament correspon al resultat del procés de reequilibrament, l'assimilació de l'arrel de l'orogen en aquesta zona.

A la zona Centre-Ibèrica, l'event associat al Moho s'aprima i perd intensitat a mida que ens desplacem cap al nord. La intrusió que s'observa en aquesta àrea està localitzada entre els 15 i 20 km en fondària i s'ha modelitzat com una capa de sills que augmenta el seu gruix vers el nord. La presència d'aquesta estructura a nivell d'escorça mitjana modifica i limita l'energia sísmica reflectida pel Moho.

8. CONCLUSIONS

En aquest treball s'ha aplicat la tomografia sísmica a un ampli ventall de problemes i situacions, en diferents zones, en diferents contextos geològics i a diferents escales. Els algoritmes utilitzats han estat funció bàsicament de l'escala del problema. La tomografia sísmica s'ha mostrat resolutiva en la majoria dels casos i sempre que el medi estudiat presenti contrastos de velocitats apreciables. A continuació s'exposen les conclusions més rellevants de cadascun dels estudis desenvolupats en aquesta tesi.

8.1 Conclusions a "Imaging granitic plutons along the IBERSEIS profile"

Diversos plutons granítics han estat estudiats a la zona d'Ossa-Morena al sud-oest de la Península Ibèrica. Les dades utilitzades corresponen al perfil de sísmica de reflexió profunda IBERSEIS. Tot i tractar dades d'un estudi a escala cortical, l'elevada densitat de receptors utilitzats ha possibilitat dur a terme un estudi tomogràfic d'alta resolució fins fondàries properes (i en alguns casos superiors) als 1000 m. S'ha observat una dependència de la distribució de velocitats en funció de l'edat dels granits. Així, els granits del Paleozoic Inferior mostren una velocitat més o menys uniforme en tot el plutó al voltant dels 5300 m/s, en canvi els granits del Cabonífer es caracteritzen per una distribució de velocitats més irregular, d'uns 5800 m/s en el nucli del plutó i decreixent cap a la perifèria del mateix fins assolir valors d'uns 5200 m/s. Les estructures deduïdes de les imatges tomogràfiques es correlacionen a la perfecció amb la cartografia geològica de superfície, fet que demostra la idoneitat de la tomografia sísmica per a l'estudi, delimitació i caracterització de plutons granítics.

8.2 Conclusions a "Imaging low velocity anomalies with the aid of seismic tomography"

La llei d'Snell estableix que els rajos es propaguen al llarg de la trajectòria més ràpida, evitant així les zones de baixa velocitat. La tomografia de primeres arribades s'ha mostrat útil en quant a la detecció d'anomalies de baixa velocitat en el subsòl poc profund. Com

s'ha pogut apreciar en l'estudi sintètic, la bona correlació entre el model teòric i el resultat de les inversions tomogràfiques és funció, bàsicament, del dispositiu experimental utilitzat (disposició de fonts i receptors en la zona d'estudi). En el millor dels casos (cobertura màxima), es pot detectar una anomalia de baixa velocitat tot i que la morfologia i el valor de la velocitat no es corresponen exactament amb els valors teòrics. De totes maneres, pràcticament amb qualsevol dispositiu experimental, els diagrames de cobertura de rajos sempre proporcionen informació qualitativa sobre la localització i les dimensions de les anomalies de baixa velocitat. Aquesta informació es pot complementar amb la sísmica de reflexió mitjançant *stacks* i seccions d'offset comú. La combinació d'aquestes metodologies fa que l'estudi d'anomalies de baixa velocitat sigui factible.

El plutó granític d'Albalá situat al sud-oest de la Península Ibèrica ha estat estudiat amb les dues tècniques esmentades: tomografia sísmica i sísmica de reflexió. Les zones de baixa velocitat detectades es corresponen amb zones de fracturació o falles i zones associades. Aquesta correlació s'ha establert tenint en compte les dades sísmiques adquirides en sondejos que mostrejen aquestes zones. El coneixement detallat de les velocitats en la zona d'estudi proporcionat per la tomografia sísmica ha permès també implementar correccions estàtiques basades en l'equació d'ona (*wave equation datuming*) que han possibilitat una millora considerable en la visualització del sistema de falles propi de la zona.

8.3 Conclusions a "Limitations of wide-angle reflection/refraction methods in subbasalt imaging: investigating null space in refraction data"

En aquest estudi, una sèrie de simulacions sintètiques han demostrat que existeixen certes limitacions per tal d'obtenir un model de velocitats fiable per regions de l'escorça cobertes per basalts. Contràriament al que caldria esperar en conques marines, les zones cobertes per capes basàltiques primes presenten més dificultats en el seu estudi que no pas les capes de més gruix, ja que la reflexió de la base del basalt queda totalment en l'interior del con de l'ona d'aigua fent molt difícil la seva identificació a incidència normal. A grans *offsets*, aquesta fase es confon amb la refracció del basalt i per tant és susceptible de ser interpretada erròniament. De les simulacions es dedueix que una correcta identificació/interpretació d'aquestes dues fases és vital per a la determinació del gruix del basalt. També s'han avaluat altres factors subjectius que condicionen els resultats obtinguts en les inversions tomogràfiques, com ara l'*offset* màxim utilitzat en les inversions (que només és funció del criteri de qui processa les dades) o bé l'incertesa en la determinació de les fases. Pel que fa a la freqüència del senyal, els millors resultats s'han

obtingut utilitzant altes freqüències, fet que contrasta amb la tendència actual de dissenyar dispositius d'adquisició on s'afavoreixen les baixes freqüències. La caracterització d'estructures subbasàltiques està totalment condicionada per la correcta determinació del gruix i de la velocitat de la capa de basalt. Així, per tal d'assegurar una modelització correcta utilitzant dades de gran angle, caldria tenir informació complementària com ara el gruix del basalt i la distribució interna de velocitats en aquesta capa, objectius que es podrien assolir mitjançant un sondeig o bé utilitzant altres tècniques geofísiques.

8.4 Conclusions a "Some improvements in subbasalt imaging using pre-stack depth migration"

En aquest estudi s'ha utilitzat un nou codi de migració *pre-stack* en fondària. Aquest nou codi està basat en un algoritme de diferències finites apte per a tractar models amb elevats gradients de velocitats tal i com suggereix la geologia de la zona. El nou codi s'ha verificat mitjançant simulacions amb models de velocitats similars als que s'han observat en la zona d'estudi, obtenint uns resultats on es reprodueix amb precisió el model sintètic. El codi també s'ha utilitzat en el reprocessat d'un perfil de sísmica de reflexió. En aquest nou processat s'han fet algunes consideracions poc habituals fins ara en la migració d'aquest tipus de dades en aquest context geològic. Al contrari del que s'ha suggerit fins al moment, en aquest estudi s'ha utilitzat íntegrament tota la informació continguda en els dispars. Les dades utilitzades presentaven una cobertura suficient per atenuar o eliminar artefactes del tipus *smiling*, per aquest motiu no s'ha limitat l'obertura en la migració, afavorint així que les estructures no horitzontals es vegin reflexades en el resultat final. El fet de migrar els dispars complerts també ha contribuit a una imatge final de més alta freqüència i per tant més detallada. Finalment, el fet de no migrar només fragments dels dispars, elimina una subjectivitat que de ben segur afectaria al resultat de la migració. Els resultats obtinguts milloren substancialment la imatge proporcionada per la sísmica de reflexió convencional. En la imatge final s'ha deduït la base del basalt en algunes parts del model, a més d'alguns events més profunds que podrien representar el contacte dels materials subbasàltics amb el basament. Cal dir que la migració *pre-stack* en fondària té una gran dependència en el model de velocitats utilitzat en la seva implementació, per tant aquest ha de ser tan acurat com sigui possible per assegurar un bon resultat.

8.5 Conclusions a "Seismic imaging and modelling the lithosphere of SW-Iberia"

La inusual densitat de receptors amb que van ser adquirides les dades utilitzades ha permès obtenir un *stack* del perfil de gran angle. Per tal de minimitzar l'efecte de la baixa cobertura (número de traces per cdp) s'ha optat per una correcció hiperbòlica (enlloc de l'habitual *normal move out*) dissenyada per reforçar els events identificats amb el Moho i l'escorça inferior. En aquesta imatge es posa de manifest una gran heterogeneïtat en l'escorça mitja i inferior, en part atribuïda a una intrusió màfica localitzada a nivell d'escorça mitja. El model de velocitats obtingut amb tècniques de traçat de rajos aporta unes propietats (velocitats) promig que permeten dur a terme simulacions que reflecteixen les principals discontinuïtats a escala cortical, encara que no poden justificar la gran variabilitat en la resposta sísmica observada en les dades de camp. Per obtenir uns sismogrames sintètics que reprodueixin qualitativament les dades reals, s'ha realitzat una modificació estocàstica del model de velocitats introduint variacions lenticulars aleatòries basades en les observacions d'alguns afloraments d'escorça inferior. Aquests resultats porten a considerar que la intrusió màfica i l'escorça inferior són estructures que presenten laminació. El Moho consisteix en una discontinuïtat hortizontal pel que fa a la seva morfologia, variable en el gruix i extremadament heterogeni en quant a la seva resposta sísmica. La variabilitat en certes propietats es podria atribuir a les tres unitats que conformen l'àrea d'estudi, mentre que l'horitzontalitat de la discontinuitat escorça-mantell és probable que tingui el seu orígen en processos litosfèrics de "reequilibrament".

8.6 Conclusions generals

Com a resultat d'aquest treball, es pot dir que aquesta metodologia és una eina de molta utilitat en la detecció, delimitació i caracterització d'estructures que representen anomalies d'alta velocitat com ara plutons granítics o colades basàltiques. En massissos formats per un sol tipus de roca, les variacions en la velocitat han permès distingir entre els diferents estats d'aquesta roca. També ha quedat demostrada la polivalència de la tomografia sísmica en quant a la seva flexibilitat per ser utilitzada amb diferents conjunts de dades, encara que aquestes no hagin estat específicament adquirides per a la implementació d'aquesta metodologia, per exemple dades de sísmica de reflexió tant marina com terreste.

De totes maneres, aquesta tècnica no representa una solució universal per a qualsevol problema geofísic perquè, malgrat la seva versatilitat per ser aplicada a qualsevol conjunt de dades, existeixen limitacions per a la seva implementació, ja que les característiques geològiques del medi poden imposar certes restriccions. Per tant, en alguns casos serà

necessari tenir en compte certes consideracions prèvies per tal de no treure de context els resultats obtinguts. En concret, en aquesta tesi s'han desenvolupat alguns casos en que això es posa de manifest i ens porta a parlar de diferents tipus de limitacions.

La primera d'aquestes limitacions està relacionada amb el poder resolutiu de la tomografia sísmica que ve fixat pel diàmetre de Fresnel, per tant a certes fondàries és impensable reproduir amb fidelitat certes estructures de petit tamany, i com a molt podrem aspirar a obtenir propietats promig de la zona d'estudi, aquesta limitació és inherent a la física del problema i per tant insalvable.

Un altre exemple on la tomografia presenta problemes és en la detecció d'anomalies de baixa velocitat. En aquest cas el problema rau en el tipus d'algoritme utilitzat, ja que les restriccions imposades pel principi de Fermat respecte a la trajectòria dels rajos només s'haurien de considerar en tractar inversions de primeres arribades. Per tant, en teoria, utilitzant algoritmes que inverteixin diverses fases es pot resoldre el problema. Ara bé, en experiments superficials, la identificació d'altres fases que no siguin la primera arribada no resulta factible (en general) degut a la gran heterogeneïtat que caracteritza els primers metres del subsòl i per tant, encara que disposem d'algoritmes adequats i no existeixin impediments teòrics, les dades no possibilitarien una aplicació òptima de la tomografia sísmica. Ens trobariem davant d'una limitació de tipus pràctic.

Per últim, també cal esmentar la limitació que representa el fet de realitzar una interpretació de les dades prèvia a la inversió tomogràfica. En les inversions amb diverses fases s'ha demostrat que una associació errònia entre fase i estructura pot traduir-se en resultats totalment erronis o com a mínim ambigus. El fet d'identificar una fase és un acte intrínsicament subjectiu, per tant en aquests casos s'hauria d'extremar la prudència en la interpretació tant de les dades com dels models obtinguts en processar-les. Cal esmentar que per "posar a prova" la fiabilitat de la tomografia sísmica en aquests casos poc favorables han resultat imprescincibles les simulacions sintètiques, perquè seria extremadament arriscat extreure conclusions d'un experiment sense saber exactament quin és el model de subsòl que hi ha al darrera.

Malgrat les limitacions, podem concloure que s'ha demostrat la idoneïtat de la tomografia sísmica com a eina en la prospecció geofísica per tal d'estudiar estructures geològiques i obtenir-ne informació rellevant respecte a les velocitats típiques d′aquestes estructures. El coneixement de la geologia de la zona, juntament amb el model de velocitats han permès la identificació d'aquest paràmetre físic amb certes litologies, aportant així informació respecte a la seva naturalesa. A més, en certs casos la tomografia sísmica s'ha utilitzat com a metodologia auxiliar per tal d'aplicar altres tècniques de prospecció geofísica. La migració pre-stack i les correccions estàtiques són dues d'aquestes tècniques que requereixen d'un acurat model de velocitats per a la seva implementació i que en els

casos estudiats han representat una millora substancial respecte al processat previ basat en sísmica de reflexió convencional.

En els darrers anys, bàsicament com a conseqüència de l'increment de la capacitat de càlcul dels ordinadors, s'han realitzat avenços remarcables en el camp de la inversió de forma d'ona. Aquesta tècnica proporciona models de velocitats molt detallats i representa una millora notable respecte als resultats obtinguts amb la tomografia, ja que en la seva implementació es té en compte tota la informació continguda en una traça sísmica i no només els temps corresponents a certs events. És d'esperar doncs, que en els propers anys, aquesta metodologia substitueixi progressivament a la tomografia sísmica com a instrument predominant en l'obtenció de models de velocitats. Malgrat tot, la inversió de forma d'ona també requereix d'un procés iteratiu. En els algoritmes utilitzats fins al moment, el bon comportament d'aquest procés iteratiu està condicionat bàsicament pel model inicial, el qual ha de ser suficientment acurat per tal d'assegurar la convergència. Avui per avui, la millor metodologia al nostre abast per a proporcionar un model inicial satisfactori és la tomografia sísmica. Per tant, per sí mateixa o com a requisit previ per l'aplicació d'altres metodologies, sembla ser que la tomografia sísmica seguirà sent una eina de gran utilitat en el futur.

Bibliografia

Aki, K., Christoffersson, A., & Husebye, E. S. (1974). Three-dimensional seismic velocity anomalies in the crust and upper-mantle under the U.S.G.S. California seismic array (abstract). *Eos. Trans. Am. Geophys. Union*, **56**, 1145.

Aki, K., Christoffersson, A., & Husebye, E. S. (1976). Three-dimensional seismic structure of the lithosphere under Montana LASA. *Bull. Seismol. Soc. Am.*, **66**, 501–24.

Aki, K., Christoffersson, A., & Husebye, E. S. (1977). Determination of three-dimensional seismic structure of the lithosphere. *J. Geophys. Res.*, **82**, 277–97.

Aki, K. & Lee, W. H. K. (1976). Determination of three-dimensional velocity anomalies under a seismic array using first P-arrival time from local earthquakes, 1. A homogeneus initial model. *J. Geophys. Res.*, **81**, 4381–99.

Benz, H., Chouet, B., Dawson, P., Lahr, J., Page, R., & Hole, J. (1996). Three dimensional P and S wave velocity structure of Redout Volcano, Alaska. *J. Geophys. Res.*, **101**, 8111–8128.

Berryman, J. G. (1991). *Lecture Notes on: Nonlinear Inversion and Tomography: I.Borehole Seismic Tomography.*

Carbonell, R., Simancas, F., Juhlin, C., Pous, J., Pérez-Estaún, A., González-Lodeiro, F., Muñoz, G., Heise, W., & Ayarza, P. (2004). Geophysical evidence of a mantle derived intrusion in SW Iberia. *Geophysical Res. Lett.*, **31**, L11601.

Carmichael, R. S. (1982). *Handbook of Physical Properties of rocks, vol II.* CSC Press.

Chalmers, J. A. & Waagstein, R. (2006). Scientific results from the deepened Lopra-1 borehole, Faroe Islands. *Geological survey of Denmark and Greenland bulletin*, **9**.

Christensen, N. I. & Mooney, W. D. (1995). Seismic velocity structure and composition of the continental crust: A global view. *J. Geophys. Res.*, **100**, 9761–9788.

Clayton, R. & Comer, R. (1983). A tomographic analysis of mantle heterogeneities from body wave travel time (abstract). *Eos. Trans. Am. Geophys. Union*, **64**, 776.

Escuder-Viruete, J., Carbonell, R., Martí, D., Jurado, M. J., & Pérez-Estaún, A. (2003). Architecture of fault zones determined from outcrop, cores, 3-D seismic tomography and geoestatistical modeling: example from the Albalá Granitic Pluton, SW Iberian Variscan Massif. *Tectonophysics*, **361**, 97–120.

Flecha, I., Martí, D., Carbonell, R., Escuder-Viruete, J., & Pérez-Estaún, A. (2004). Imaging low velocity anomalies with the aid of seismic tomography. *Tectonophysics*, **388**, 225–238.

Fliedner, M. M. & White, R. S. (2003). Depth imaging of basalt flows in the Faeroe-Shetland Basin. *Geophys. J. Int.*, **152**, 353–371.

Hole, J. A. & Zelt, B. C. (1995). Three-dimensional finite-difference reflection travel times. *Geophys. J. Int.*, **121**, 427–434.

Hughes, S., Barton, P. J., & Harrison, D. (1998). Exploration in the Shetland-Faeroe Basin using densely spaced arrays of ocean-bottom seismometers. *Geophysics*, **63**, 490–501.

Jegen-Kulcsar, M. & Hobbs, R. (2005). Outline of a joint inversion of gravity, MT and seismic data. *Annales Societatis Scientiarum Færoensis*, **43**, 163–167.

Korenaga, J., Holbrook, W. S., Kent, G. M., Kelemen, P. B., Detrick, R. S., Larsen, H. C., Hopper, J. R., & Dahl-Jensen, T. (2000). Crustal structure of the South-east Greeenland margin from joint refraction and reflection seismic tomography. *J. Geophys. Res.*, **105**, 21.591–21.614.

Martini, F. & Bean, C. J. (2002). Interface scattering versus body scattering in subbasalt imaging and application of prestack wave equation datuming. *Geophysics*, **67**, 1593–1601.

Martini, F., Bean, C. J., Dolan, S., & Marsan, D. (2001). Seismic image quality beneath strongly scattering structures and implications for lower crustal imaging: numerical simulations. *Geophys. J. Int.*, **145**, 423–435.

Martí, D., Carbonell, R., Trygsvason, A., Escuder, J., & Pérez-Estaún, A. (2002). Mapping brittle fractures zones in 3 dimensions: high resolution travel time seismic tomography in a granitic pluton. *Geophys. J. Int.*, **149**, 134–148.

McMehan, G. A. (1983). Seismic tomography in boreholes. *Geophys. J. R. Astron. Soc.*, **74**, 637–48.

Metropolis, N., Rosenbluth, A. W., Rosenbluth, M. N., & Teller, A. H. (1953). Equation of state calculations by fast computing machines. *Journal of Chemical Physics*, **21(6)**, 1087–1092.

Neumann-Denzau, G. & Behrens, J. (1984). Inversion of seismic data using tomographic reconstruction techniques for investigation of laterally inhomogeneus media. *Geophys. J. R. Astron. Soc.*, **79**, 305–16.

Nolet, G. (1983). Inversion and resolution of linear tomographic systems (abstract). *Eos. Trans. Am. Geophys. Union*, **64**, 775–6.

Paige, C. C. & Saunders, M. A. (1982). LSQR: An algorithm for sparse linear equations ands sparse least squares. *ACM Trans. Math. Software*, **8**, 43–71.

Palomeras, I., Carbonell, R., Flecha, I., Simancas, F., Ayarza, P., Matas, J., Martínez Poyatos, D., Azor, A., González-Lodeiro, F., & Pérez-Estaún, A. (2008). The nature of the lithosphere across the Variscan Orogen of SW-Iberia: Dense wide-angle seismic reflection data. *J. Geophys. Res.*, .

Pearse, S. (2002). *Inversion and modelling of seismic data to assess the evolution of the Rockall Trough*. PhD thesis, Cambridge University.

Podvin, P. & Lecomte, I. (1991). Finite-difference computation of traveltimes in very contrasted velocity models: a massively parallel approach and its associated tools. *Geophys. J. Int.*, **105**, 271–284.

Pratt, R. G., Song, Z. M., Williamson, P., & Warner, M. (1996). Two-dimensional velocity models from wide-angle seismic data by wavefield inversion. *Geophys. J. Int.*, **124**, 323–340.

Raum, T., Mjelde, R., Berge, A. M., Paulsen, J. T., Digranes, P., Shimamura, H., Shiobara, H., Kodaira, S., Larsen, V. B., Fredsted, R., Harrison, D. J., & Johnson, M. (2005). Sub-basalt structures east of the Faroe Islands revealed from wide-angle seismic and gravity data. *Petroleum Geoscience*, **11**, 291–308.

Richardson, K. R., Smallwood, J. R., White, R. S., Snyder, D. B., & Maguire, P. K. H. (1998). Crustal structure beneath the Faroe Islands and the Faroe-Iceland Ridge. *Tectonophysics*, **300**, 159–180.

Richardson, K. R., White, R. S., England, R. W., & Fruehn, J. (1999). Crustal structure east of the Faroe Islands: mapping sub-basalt sediments using wide-angle seismic data. *Petroleum Geoscience*, **5**, 161–172.

Rousseau, J. H. L., Calandra, H., & de Hoop, M. V. (2003). Three-dimensional depth imaging with generalized screens: A salt body case study. *Geophysics*, **68**, 1132–1139.

Sallarès, V., Charvis, P., Flueh, E. R., & Bialas, J. (2003). Seismic structure of Cocos and Malpelo Ridges and implications for hot spot-ridge interaction. *J. Geophys. Res.*, **108**, 5(1)–5(21).

Sava, P. & Biondi, B. (2004). Wave-equation migration velocity analysis. II. Subsalt imaging examples. *Geophys. Prosp.*, **52**, 607–623.

Simancas, F., Martínez-Poyatos, D., Expósito, I., Azor, A., & González-Lodeiro, F. (2001). The structure of a major suture zone in the SW Iberian Massif: the Ossa-Morena/Central-Iberian contact. *Tectonophysics*, **332**, 295–308.

Simancas, J. F., Carbonell, R., González-Lodeiro, F., Pérez-Estaún, A., Juhlin, C., Ayarza, P., Kashubin, A., Azor, A., Martínez-Poyatos, D., Almodóvar, G. R., Pascual, E., Sáez, R., & Expósito, I. (2003). Crustal structure of the transpressional Variscan orogen of SW Iberia: SW Iberia deep seismic reflection profile (IBERSEIS). *Tectonics*, **22**, 1–1–1–19.

Smallwood, J. R., Towns, M. J., & White, R. S. (2001). Thew structure of the Faeroe-Shetland Trough from integrated deep seismic and potential field modelling. *J. Geol. Soc.*, **158**, 409–412.

Sochacki, J. S., George, J. H., Ewing, R. E., & Smithson, S. B. (1991). Interface conditions for acoustic and elastic wave propagation. *Geophysics*, **56**, 168–181.

Sochacki, J. S., Kubichek, R., George, J. H., Fletcher, W. R., & Smithson, S. B. (1987). Absorbing boundary conditions and surface waves. *Geophysics*, **52**, 60–71.

Sørensen, A. B. (2003). Cenozoic basin development and stratigraphy of the Faroes area. *Petroleum Geoscience*, **9**, 189–207.

Staples, R. K., Hobbs, R. W., & White, R. S. (1999). A comparison between airguns and explosives as wide-angle seismic sources. *Geophys. Prosp.*, **47**, 313–339.

Tarantola, A. (1987). *Inverse proble theory.* Elsevier, Amsterdam.

Trinks, I., Singh, S. C., Chapman, C. H., Barton, P. J., Bosch, M., & Cherrett, A. (2005). Adaptative traveltime tomography of densely sampled seismic data. *Geophys. J. Int.*, **160**, 925–938.

Vidale, J. E. (1988). Finite-difference traveltime calculation. *Bull. Seismol. Soc. Am.*, **78**, 2062–2076.

Vidale, J. E. (1990). Finite-difference calculation of traveltimes in three dimensions. *Geophysics*, **55**, 521–526.

White, R. S., Christie, P. A. F., Kusznir, N. J., Roberts, A., Davies, A., Hurst, N., Lunnon, Z., Parkin, C. J., Roberts, A. W., Smith, L. K., Spitzer, R., Surendra, A., & Tymms, V. (2002). iSIMM pushes frontiers of marine seismic acquisition. *First Break*, **20**, 782–786.

White, R. S., Smallwood, J. R., Fliedner, M. M., Boslaugh, B., Maresh, J., & Fruehn, J. (2003). Imaging and regional distribution of basalt flows in the Faroe-Shetland Basin. *Geophys. Prosp.*, **51**, 215–231.

Williamson, P. (2003). Introduction. *Geophys. Prosp.*, **53**, 167–168.

Zahradnik, J., O'Leary, P., & Sochacki, J. (1994). Finite-difference schemes for elastic waves based on the integration approach. *Geophysics*, **59**, 928–937.

Zelt, C. A. & Barton, P. J. (1998). Three-dimensional seismic refraction tomography: A comparison of two methods applied to data from the Faeroe Basin. *J. Geophys. Res.*, **103**, 7187–7210.

Zelt, C. A. & Smith, R. B. (1992). Seismic traveltime inversion for 2-D crustal velocity structure. *Geophys. J. Int.*, **108**, 16–34.

Ziolkowski, A., Hanssen, P., Gatliff, R., Jakubowicz, H., Dobson, A., Hampson, G., Li, X.-Y., & Liu, E. (2003). Use of low frequencies for sub-basalt imaging. *Geophys. Prosp.*, **51**, 169–182.